MASTER THESIS

INFLUENCE OF LARGE WOOD TRANSPORT ON STRUCTURING PROCESSES OF DYNAMIC RAMPS

AUTHOR:	CLARA STREULE, CLARA.STREULE@EPFL.CH
INSTITUTION:	SECTION OF ENVIRONMENTAL SCIENCES AND ENGINEERING (SIE), ECOLE POLYTECHNIQUE FEDERALE DE LAUSANNE (EPFL), LAUSANNE, SWITZERLAND
EXTERNAL SUPERVISOR:	DR. CHRISTIAN TOGNACCA LABORATORIUM^{3D} SAGL BIASCA, SWITZERLAND
ACADEMIC SUPERVISOR:	DR. GIOVANNI DE CESARE PLATFORM OF HYDRAULIC CONSTRUCTIONS PL-LCH LAUSANNE, SWITZERLAND

MARCH 2022

Acknowledgements

This thesis was written as a master project in enterprise, during my employment at the Laboratorium^{3D} Sagl in Biasca, TI with academic supervision at the the Platform of Hydraulic Constructions (PL-LCH) at EPFL in Lausanne, VD. The project was funded by the Giovanni Lombardi Foundation. I like to acknowledge Dr. Giovanni De Cesare, the academic supervisor, for his visits in Biasca, bringing along cheerfulness and valuable input. A warm thank you to all collaborators of the Laboratorium^{3D} for the cooperative working atmosphere, which has motivated me and led me to enjoy my work. I would like to thank Dr. Christian Tognacca, the external supervisor, for his continuous support, the helpful discussions and review of this thesis. Laboratory assistance provided by Chiara Benedetti and Enea Toschini, as well support for the particle image velocimetry analysis by Viriginia Rossi are highly appreciated.

Summary

Contents

1 Introduction

1.1 Motivation

Large wood (LW) is an integral part of alpine rivers and an important component of flood events. If LW accumulates, it alters the flow field (Gippel, 1995; Schalko et al., 2021), which in turn can have a significant impact on river morphology and sediment dynamics (Ruiz-Villanueva, Piégay, et al., 2016; E. Wohl and Scott, 2017). It is thus important to understand where LW will deposit, how long it will remain, and what its effect on bed morphology will be. Large boulders have been shown to influence the transport of LW by trapping key pieces, leading to the formation of wood deposits (Nakamura and Swanson, 1994, Faustini and Jones, 2003, Bocchiola et al., 2008, Figure 1.1). Nevertheless, local obstructions are not considered in common indexes that describe the factors controlling LW deposition in a river.

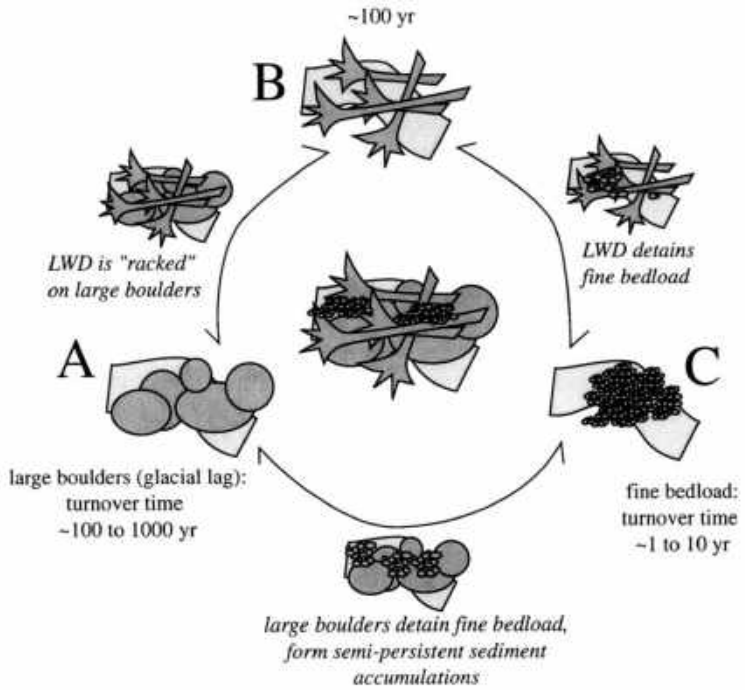

Figure 1.1: Conceptual model for persistent features affecting sediment storage and turnover in supply-limited mountain stream channels. Sediment storage and transfer is a function of three kinds of interactions among large boulders (A), large wood (B), and bed load (C). Stream channels lacking in LW may store and release fine bed load over shorter periods, whereas streams with LW may store and release bed load over longer periods (Faustini and Jones, 2003).

Protruding boulders are naturally present in rivers, but are also artificially placed in river engineering structures, such as block ramps. In the effort to implement ecologically valuable bed stabilization measures, several types of ramps relying on dispersed configurations of block clusters have been developed. They are referred to as “block cluster” type block ramps (Tamagni et al., 2010). Block ramps are engineering structures that can fulfill both hydraulic

engineering (bed stabilization through concentrated energy conversion) and ecological (passability) functions. Therefore, the performance of these structures are evaluated not only according to their stability behavior, but also according to their ecological behavior (DWA, 2009). Little is known about the effect on block ramp performance of LW that might deposit around the stabilizing blocks.

1.2 Background

Dynamic ramps are block ramps of the "block cluster" type, using material with a widely graded grain size distribution ranging from fine material to large blocks. The material is installed as a plane bed with a higher slope, so that a stable, natural structure with the sizing slope will form upon sizing runoff (Weichert et al., 2007). Beffa Tognacca Sagl. proposed a practical implementation of dynamic ramps for the stabilization and environmental upgrading of several watercourses in the canton of Ticino. The flow conditions on these rough and inhomogeneous beds are very complex and difficult to be described mathematically. Since there was no empirical basis or reliable theoretical approach for the dimensioning of dynamic ramps, tests were performed on a physical model in the Laboratorium^{3D} (C. Tognacca et al., 2019, C. Tognacca et al., 2021). Experiments on a physical model were part of the design phase of the following three works: ramp on the river Ticino at Lodrino, ramp on the river Tresa at Madonna del Piano and ramp on the river Ticino at Ronco Bedretto (Figure 1.2). The average slopes of the tested structures are around 2-3% for Lodrino and Madonna del Piano, respectively around 9-10% for Ronco. The specific discharges for the first two cases are high, while for the third case, with high slopes, the determining specific discharges are relatively low. Upon LW loading, significant deposits formed for the experiments on the ramp in Ronco, while LW was transported across the ramp in Lodrino without interaction with the channel bed. The LW deposits on the ramp in Ronco did not prove to compromise the performance of the engineering structure.

Figure 1.2: Dynamic ramp on the Ticino at Ronco Bedretto in the physical model at Laboratorium^{3D} (left) and after realization (right) (C. Tognacca et al., 2021).

1.3 Objectives

To better assess the behavior of dynamic ramps over the whole range of possible slopes between about 2 and 10%, it was necessary to complete the experiments with physical model test of a structure with an intermediate slope. The present work aims to analyze the structuring processes under the influence of LW of a dynamic ramp with a target slope of 6%, and determining discharge of HQ_{100} = 300 m^3/s. Both sizes lie between those of the works in Lodrino and Ronco Bedretto.

2 Literature review

2.1 Wood in river ecosystems

Trees or parts of trees (including rootstocks, roots, crowns, trunks, branches, and twigs) that are carried into a fluvial corridor, are referred to as large wood (LW). In the literature, LW is commonly defined as single logs with a diameter ≥ 0.1 m and a length ≥ 1.0 m (Keller and Swanson, 1979 Nakamura and Swanson, 1994, E. Wohl and Jaeger, 2009, Ruiz-Villanueva, Piégay, et al., 2016). The available LW volume in a fluvial system can be estimated by a quantitative analysis of the recruitment processes of a specific catchment area, or by using empirical formulas (Schalko, 2018).

2.1.1 LW potential and recruitment

LW recruitment processes have been shown to include tree death and subsequent felling or uprooting, tree toppling due to high winds or fires, bank erosion, and LW delivery from surrounding hillslopes by debris flows, landslides and avalanches (Keller and Swanson, 1979, Benda and Sias, 2003, Reeves et al., 2003). The identification of potential process areas commonly relies on geographical information systems (GIS), remote sensing tools, field examinations, or a combination of these (Mazzorana et al., 2009, Bertoldi et al., 2013, Ruiz-Villanueva et al., 2014). Identified process areas are intersected with forest areas and the water network to obtain the potential LW volume V_{pot}, the stock of wood in the catchment area that can theoretically collect into the river. During a flood, not all of the potentially available wood enters the waterbody and is transported. The effective LW volume V_{eff} can be estimated based on recorded LW volumes in similar catchment areas of past floods.
Based on surveyed LW volumes during the floods of 1987 and 1993 in Switzerland and floods in Germany and Japan, Rickenmann, 1997 derived empirical formulas to estimate V_{pot} and V_{eff}. He investigated relations of the LW volume to the following catchment area or flood characteristics: Size of the catchment area A_c, discharge volume V_d, Sediment load SL, forested catchment area $A_{c,f}$ and forested stream length L_f. Steeb et al., 2019 expanded the results to include LW volumes from the 2005 flood in Switzerland and found significant correlations to the following parameters in addition to those studied by Rickenmann: Stream length L, peak discharge $Q_{\max}$ and precipitation volume V_p. The best goodness of fit was found in the following empirical formulas:

$$V_{eff} = 38 A_c^{0.54} \tag{2.1}$$

$$V_{eff} = 0.2 SL^{0.65} \tag{2.2}$$

$$V_{eff} = 5.7 Q_{\max}^{0.91} \tag{2.3}$$

$$V_{eff} = 0.2 A_c^{0.23} SL^{0.6} \tag{2.4}$$

2.1.2 Transport and deposition

LW transport usually begins when a certain discharge is reached. It then gradually increases until it reaches a certain discharge, which is usually higher than the discharge capacity of the channel, and then levels off again. Braudrick et al., 1997, identified three distinct LW transport regimes: Uncongested, congested, and semicongested. During uncongested transport, logs move without much, if any interaction between pieces and occupy less than 10 per cent of the channel surface area. In congested transport, in contrast, the logs move together as a single mass and occupy more than 33 per cent of the channel area. Semi-congested transport is an intermediate regime, in which some pieces move individually while others interact. Ruiz-Villanueva et al., 2019 extended the classification with another regime, hypercongested transport (Figure 2.1 a). This regime describes a downstream moving log mass with several layers of wood, occupying the entire channel area. Figure 2.1 b) shows the relationship of the LW transport regimes and the flood hydrograph. The hypercongested phase forms on the rising limb. Just before or during the flood peak, transport occurs in the saturated regime. After the flood crest LW is transported uncongestedly. LW transport rates are thus characterized by hysteresis, with more wood transported during the rising limb of the flood hydrograph than during the falling limb Ruiz-Villanueva, Wyżga, et al., 2016.

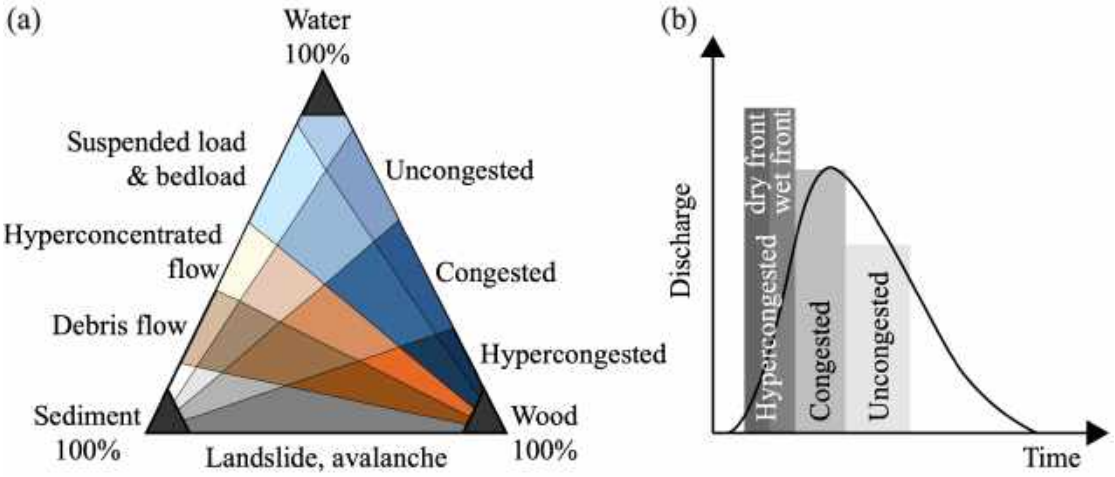

Figure 2.1: (a) Flow classification according to the content of sediment, water and wood. (b) Conceptual model for the relationship between the discharge hydrograph and LW transport regimes (adapted from Ruiz-Villanueva et al., 2019).

Nakamura and Swanson, 1994 identified channel width and sinuosity to be the main factors that control the formation of LW deposits. The predominant trapping sites were identified to be (1) the entrance of secondary channels, (2) within secondary channels, (3) outside of bends, and (4) behind or between large boulders. These factors lead to relatively high abundances of LW deposits in wide, sinuous geomorphic channels. Narrow, straight beds lack secondary channels, but may have other trapping sites, such as very large boulders. Braudrick and Grant, 2001 introduced the so-called debris roughness that describes the factors promoting

LW deposition in a river. This dimensionless index characterizes a stream reach in a similar way to hydraulic roughness, incorporating the ratios of LW piece length to mean channel width L_L/w_m, LW piece length to channel radius of curvature L_L/R_c and LW buoyant depth to channel depth d_b/h_m. The debris roughness DR is defined as

$$\mathrm{DR} \propto \left(a_1 \frac{L_L}{w_m} + a_2 \frac{L_L}{R_c} + a_3 \frac{d_b}{h_m}\right) \tag{2.5}$$

where a_1, a_2 and a_3 are coefficients that vary according to the relative importance of each variable. The DR thus accounts for the large scale geomorphic features, but does not consider local obstructions. Bocchiola et al., 2006b investigated the transport of large woody debris in the presence of obstacles. The distance traveled is assumed to be a function of the characteristic distance between obstacles L_0, of the LW piece length L_L and of the force applied by the flow. The regression analysis based on dimensionless groups of these variables showed a high statistical significance.

2.1.3 Effect of LW deposits

LW deposits in the channel alter the flow field, leading to geomorphological changes. The altered flow resistance, sediment dynamics, and bedforms affect ecological processes in the stream. A summary of the effects of the presence of LW in water courses is presented in Table 2.1.

Table 2.1: In-channel effects of LW.

Type of effect	Description	Studies
Geomorphic effects	Flow resistance: Wood is a roughness element and leads to steps	MacFarlane and Wohl, 2003, Comiti et al., 2008
	Sediment dynamics: The presence of wood promotes sediment storage, patches of finer sediment, and alluvial channel segments	Faustini and Jones, 2003, Osei et al., 2015, E. Wohl and Scott, 2017
	Bedforms: Wood influences channel anabranching and the formation of bars and pools	Abbe and Montgomery, 2003, Baillie and Davies, 2002
Ecological effects	Habitat diversity: Wood enhances habitat diversity	Collins et al., 2012, Gurnell et al., 2012
	Nutrient retention: Wood can increase the retention of organic matter	Guyette et al., 2002, Beckman and Wohl, 2014

2.1.4 Physical modeling of LW processes

In the context of river engineering, physical modeling in the laboratory has long been used to link knowledge gained from field observations to theoretical and computational concepts (Thomas et al., 2014, Friedrich et al., 2022). As such, physical modeling has also been applied by many scientists in the study of LW processes relevant to river management. Combined with rare but detailed observations of the complex interactions of LW in the field, the simplification of LW and river channels in the laboratory becomes justifiable Ruiz-Villanueva, Wyżga, et al., 2016. Friedrich et al., 2022 presented a detailed review of the state-of-the-art physical modeling for the investigation of (1) LW transport dynamics and effects on channel morphology, (2) LW-flow-sediment interactions at bridge piers and (3) LW–flow–sediment interactions at retention racks. Since neither bridge piers nor retention racks are of relevance in the present study, model experiments of the latter two categories are not discussed here.
Table 2.2 summarizes selected physical model studies that aim to analyze LW recruitment, transport and deposition. In these works, both movable and fixed beds at slopes of around 1% were investigated. The model sediment applied was fine, without larger roughness elements such as blocks. In most studies, the length of the modeled LW was smaller than half of the channel width. The studies investigating morphological effects of LW, summarized in Table 2.3, relied on similar experimental conditions with respect to slope, LW size and grain size. The fine bed material was installed as movable bed to allow studying erosion. Figure 2.2 shows a photo of such a model flume. The studies investigating higher slopes and gravel beds address exclusively the effect of LW on flow resistance (Table 2.4). In these surveys the maximum log length of the modeled LW was for the most part higher than the channel width. Under these conditions, logs are integrated in step structures and increase flow resistance.

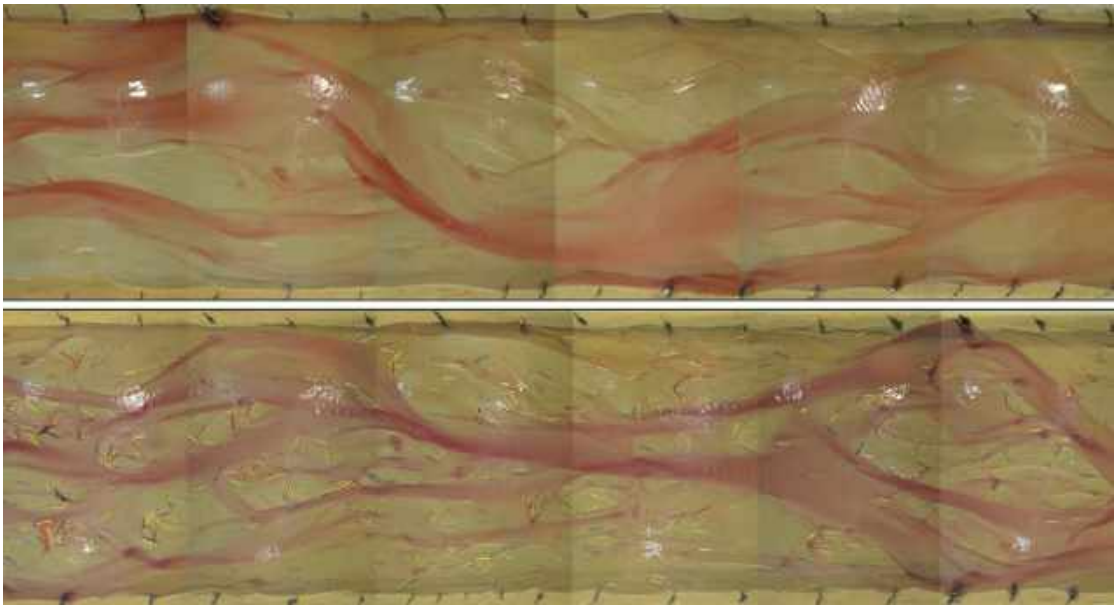

Figure 2.2: Photo of a model flume with a width of 1.3 m, used to investigate the influence of 0.08 m long LW logs on the topographic characteristics (Mao et al., 2020).

Table 2.2: Summary of selected studies employing physical modeling to investigate LW recruitment, transport and deposition.

Physical process	**Flume dimensions: length, width, depth [m]**	**Slope [%]**	**Flow conditions [m^3/s]**	**Bed type; D_{50} [mm]**	**Model LW shape and composition**	**LW dimensions: diameter, length [m]**	**Studies**
Dynamics of LW transport	15, 1, NA	Constant (NA)	Stationary (0.0045-0.012)	Movable bed; 1	Wooden dowels, trunks	0.02-0.04, 0.2-0.4	Braudrick et al., 1997
Thresholds for LW movement	9.14, 1.22, NA	Constant (1)	Stationary (NA)	NA, 8	Wooden dowels, trunks	0.025-0.038, 0.30-0.60	Braudrick and Grant, 2000
Transport distance and deposition of LW	9.14, 1.22, NA	Constant (1)	Stationary (NA)	Movable bed; 8	Wooden dowels, trunks	0.025-0.038, 0.30-0.60	Braudrick and Grant, 2001
LW entrainment	30, 1, NA	Constant (0.6)	Stationary (NA)	Fixed bed; 2 and 5	Wooden dowels, trunks	0.03-0.1, 0.25-0.5	Bocchiola et al., 2006a
Transport distance and deposition of LW	30, 1, NA	Constant (0.6)	Stationary (NA)	Fixed bed; 2	Wooden dowels, trunks	0.014, 0.05-0.25	Bocchiola et al., 2006b
Transport distance and deposition of LW	30, 1, NA	Constant (0.6)	Stationary (0.0028-0.0159)	Fixed bed; 2	Wooden dowels, trunks	0.014, 0.66-0.94	Bocchiola et al., 2008
LW deposition patters	25, 3, NA	Constant (1)	Stationary (0.0018)	Movable bed, 1.03	Wooden dowels, trunks	0.002-0.006, 0.04-0.12	Welber et al., 2013
Deposition and remobilization of LW	11, 1.7, NA	Constant (1.3)	Stationary (0.00126)	Movable bed, 0.73	Wooden dowels, trunks	0.003, 0.08	Bertoldi et al., 2014

Table 2.3: Summary of selected studies employing physical modeling to investigate the effect of LW on bed morphology.

Physical process	**Flume dimensions: length, width, depth [m]**	**Slope [%]**	**Flow conditions [m^3/s]**	**Bed type; D_{50} [mm]**	**Model LW shape and composition**	**LW dimensions: diameter, length [m]**	**Studies**
Effect on scour size and depth	10, 0.123, 0.6	Constant (0)	Stationary (0.001-0.027)	Movable bed, 5.4	Metal cylindar, trunk	0.06-0.2, NA	Beschta, 1983
Effect on scour size and depth	10, 0.63, NA	Constant (0.7)	Stationary (NA)	Movable bed, 0.4	Wooden dowels, trunk	0.063, 0.582	Beebe, 2000
Effect on bed scour, bank erosion and bedforms	10, 0.63, 0.61	Constant (0.22)	Stationary (0.0033)	Movable bed, 0.8	Aluminum cylinder, trunk	0.19, 0.07-0.3	Wallerstein et al., 2001
Effect on bed scour	9, 2.7, 0.2	Constant (NA)	Stationary (NA)	Movable bed, 8	Wooden dowels, trunk and rootwad	0.091-0.183, 1.4	Svoboda and Russell, 2011
Effect on bedforms	NA, 0.34, NA	Constant (NA)	Stationary (0.0018)	Movable bed, 1.4	Wooden dowels, trunk	NA, 0.1-0.4	Davidson and Eaton, 2013
Erosion around LW deposits	7, 1.9, 0.5	Constant (0.05 - 0.06)	Stationary (0.00268)	Fixed bed; NA, movable bed; 0.8	Wooden dowels, trunk	0.033, 0.401	Gallisdorfer et al., 2014
Effect on bedforms	10, 1.7, NA	Constant (1.3)	Stationary (0.00126)	Movable bed, 0.73	Wooden dowels, trunks	0.003, 0.08	Mao et al., 2020

Table 2.4: Summary of selected studies employing physical modeling to investigate the effect of LW on flow resistance.

Physical process	**Flume dimensions: length, width, depth [m]**	**Slope [%]**	**Flow conditions [m^3/s]**	**Bed type; D_{50} [mm]**	**Model LW shape and composition**	**LW dimensions: diameter, length [m]**	**Studies**
Effect on flow resistance	118, 12, 0.6	Variable (3.6, 4.4, 3.7, 5.6, 3.8)	Gradually increasing stationary (0.1-4)	Heavy clay soil, NA	Cylindars, trunk	NA	Dudley et al., 1998
Effect on flow resistance	2, 0.6,2	NA	NA	NA	PVC cylindars and wooden dowels, trunk	0.0254-0.0755, 0.33-1	Shields and Gippel, 1995
Effect on flow resistance	9, 0.6, NA	Variable (5, 10, 14)	Gradually increasing stationary (0.094-0.064)	Fixed bed, 15	PVC cylindars, trunk	0.025, 0.3 -0.Wilcox and Wohl, 2006	
Effect on flow resistance	106, 0.99, NA	Constant (NA)	Stationary (NA)	Mobile bed D_{16} = 0.27, D_{84} = 0.62,	Wooden dowels, trunks	0.01-0.2, 0.3-2	Mutz et al., 2007

2.2 Dynamic ramps

2.2.1 Concept and design of dynamic ramps

In the effort to implement ecologically valuable bed stabilization measures, several types of block ramps relying on dispersed configurations of block clusters have been developed (Lange, 2007, Tamagni et al., 2010). Inspired by the self-stabilizing potential of natural channels, Weichert et al., 2007 introduced one type of such engineering structure, the so-called dynamic ramp. Weichert et al., 2009 described processes in steep open channels at discharges that exceed the bed stability on different geomorphological scales (Figure 2.3). They described the micro-scale as being dominated by individual bed particles, the meso-scale by a succession of steps and pools. Laterally, the macro-scale describes the fluvial morphologies straight, meandering, alternate bars and braided. Longitudinally, bedforms such as riffles and pools are exhibited. In the reach scale, the geomorphic features refer to landforms rather than bedforms. At the micro-scale the self-stabilizing corresponds to the selective erosion leading to a coarsening of the surface layer, protecting the underlying finer bed material. This so-called armoring process thus leads to an increase of the mean grain size of the armor layer upon increasing discharge. At the meso-scale, the self-stabilizing mechanism corresponds to the optimization of the roughness geometry. The channel responds to the exceeding of stability by reconfiguring itself towards a step-pool geometry. At the macro-scale the self-stabilization occurs due to an assimilation of the bed structures to riffles and pools resulting in alternate bar structres. Self-stabilization in the reach-scale is thought to occur due to the reduction of slope (Weichert et al., 2009).

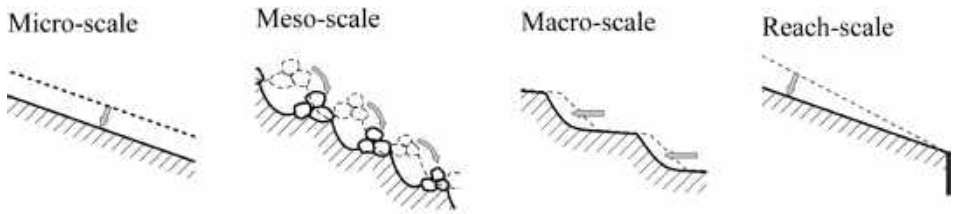

Figure 2.3: Self-stabilizing processes in different geomorphological scales (Weichert et al., 2009).

Based on these observations, Weichert et al., 2007 proposed the design of dynamic ramps, imitating the structure of natural water courses. These are characterized by a course structured surface layer featuring a sequence of steps and pools. Instead of constructing this structure artificially, the river is left to its own resources to form a stable bed configuration. To achieve this, bed material with a highly graded grain size distribution is installed as a plane bed at an increased slope. The development of an armor layer and the formation steps by the grouping of coarse blocks into bars across the channel width occurs naturally due to hydraulic loading of the riverbed. The initial slope is chosen so that upon a certain dimensioning discharge, a stable bed configuration with dimensioning slope will form.
The dimensioning procedure proposed by Weichert et al., 2007 initiate at the final condition by the determination of the dimensioning discharge q_{dim} and the dimensioning slope S_{dim}.

Aberle, 2000 derived a stability approach relating the critical discharge q_c to the roughness and the slope of the channel. The roughness is described by the standard deviation of the bed elevations σ_z and the slope by $\sin\alpha$ where α is the angle of the channel bed against the horizontal:

$$q_c = 0.20 \cdot \sin\alpha^{-1.30} \cdot \sqrt{g\sigma_z^3} \tag{2.6}$$

Since the differences between $\sin\alpha$ and the slope S are negligible, Equation 2.6 can be rewritten to find the roughness as a function of q and S:

$$\sigma_z = 2.92 \cdot q^{0.67} \cdot S^{0.87} \cdot g^{-0.33} \tag{2.7}$$

By doing this, the final bed roughness of the dimensioning condition $\sigma_{z,dim}$ can be determined. This dimensioning roughness is decisive for the size of the largest blocks necessary. Weichert et al., 2007 proposed to use the widely graded grainsize distribution given in Table 2.5 and a maximum block diameter of $d_{\max} = 4 \cdot \sigma_{z,dim}$. In the initial condition, where this material is homogeneously placed, the roughness can be estimated to be $\sigma_{z,dim} = 0.62 \cdot d_m$. The necessary slope of this initial condition is estimated by calculating σ_z for successively lower discharges and slopes until the initial $\sigma_{z,0}$ is reached.

$d_{16}/d_{\max}$	$d_{50}/d_{\max}$	$d_{84}/d_{\max}$	$d_{90}/d_{\max}$	$d_m/d_{\max}$
0.044	0.133	0.422	0.578	0.230

Table 2.5: Grain size distribution of bed material proposed by Weichert et al., 2007.

S. Tognacca et al., 2021 reported on the application of the above-mentioned concept in a river engineering structure of $S_{dim} = 2-3\%$. For practical reasons, the grain size distribution proposed by Weichert et al., 2007 was divided into a fine and a coarse fraction as base material and stabilizing blocks. The stabilizing blocks were modeled in three block classes. The largest class consisted of blocks with weights of 11.1 t and equivalent spherical diameters of 2 m, which is inferior to $d_{\max}$ proposed by Weichert et al., 2007. S. Tognacca et al., 2021did not install the material homogeneously but in a structured way. The largest block class was installed to protrude from the base material, while the two smaller classes were fully embedded (Figure 2.4). Due to the protruding blocks, the initial roughness of the bed thus differed from $\sigma_{z,0}$ derived by Weichert et al., 2007. Upon hydraulic loading, exposure of the smaller rocks was exhibited due to the erosion of the base material. This, which begins to occur at relatively low discharges, led to a further, gradual increase in bed roughness.

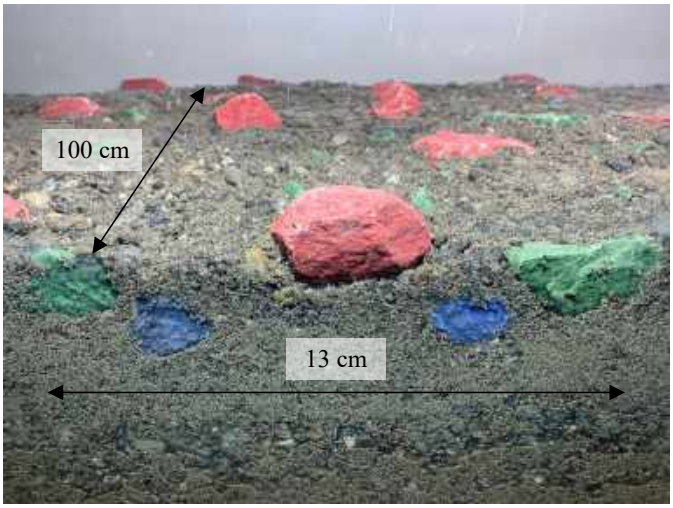

Figure 2.4: Dynamic ramp structure with the large structuring elements installed in layers as proposed by S. Tognacca et al., 2021.

2.2.2 Stability design criteria

One way to quantify the stability of an open channel is through flow resistance, which relates bed topography (slope, roughness and bedforms) to flow velocity and unit discharge. High flow resistance implies high energy dissipation, and thus reduces the capability of the flow to mobilize and transport sediment. Flow resistance is expressed as the ratio of the mean velocity U of the flow to the shear velocity U^* of the bed. The mean velocity U is traditionally expressed using the Darcy-Weisbach equation which originally considered the turbulent flow in pipes:

$$h_f = f \frac{L_p}{d_0} \frac{U^2}{2g} \tag{2.8}$$

where h_f is the friction loss, f denotes the Darcy-Weisbach friction factor, U denotes the mean velocity of the flow, L_p is the length of the pipe, and d_0 the diameter of the pipe. The energy gradient $S_e = h_f / L_p$ can be approximated with the bed slope S. Since $d_0 = 4R$, with R being the hydraulic radius, which for a wide channel can be approximated by the flow depth h, the equation can be rewritten for the mean flow velocity:

$$U = \sqrt{\frac{8ghS}{f}} \tag{2.9}$$

With the shear velocty $U^* = \sqrt{ghS}$ the ratio is thus given by:

$$\frac{U}{U^*} = \sqrt{\frac{8}{f}} \tag{2.10}$$

The term $\sqrt{8/f}$ is usually expressed as a function of the relative flow depth h/k, where k is a measure for the bed roughness height. Commonly, a characteristic grain size is used as descrip-

tor of k, in steep open channels the grain diameter for which 84% of the bed surface grains are smaller d_{84} is claimed to be most adequate (Rickenmann and Recking, 2011, Hohermuth and Weitbrecht, 2018). Aberle and Smart, 2003, however, argue that a characteristic percentile of the grain size distribution does not sufficiently describe the structure of gravel-bed profiles, due to their irregular nature. They suggest that the standard deviation of the bed elevations, σ_z describes the bed roughness more adequately. Chen et al., 2020 analyzed a large data set of measurements with a wide range of channel morphologies and flow conditions to test the performance of d_{84} or σ_z. They found that σ_z consistently outperformed d_{84}.
The modified logarithmic law, introduced by Hey, 1979, is used typically as flow resistance equation.

$$\sqrt{8/f} = a_1 + a_2 \cdot \log(a_3 \cdot h/k) \tag{2.11}$$

a_1, a_2, and a_3 are coefficients that have been calibrated e.g. by J. C. Bathurst, 1985, Rickenmann and Recking, 2011, Hohermuth and Weitbrecht, 2018 or Chen et al., 2020. Smart and Jaeggi, 1983 introduced an additional slope variable in their modified equation.
Various researchers (Bray, 1979, Griffiths, 1981, J. Bathurst, 2002) applied a power law

$$\sqrt{8/f} = a_1 (h/k)^{a_2} \tag{2.12}$$

Ferguson, 2007 introduced the variable power equation (VPE), which is linear for small and a power law for high relative flow depths h/k. It is defined as

$$(8/f)^{0.5} = \frac{a_1 a_2 \cdot (h/k)}{(a_1^2 + a_2^2 \cdot (h/k)^{5/3})^{0.5}} \tag{2.13}$$

In both Equation 2.12 and Equation 2.13, a_1 and a_2 are calibrated coefficients.
Rickenmann and Recking, 2011 tested various flow resistance equations against a large field data set, and found the VPE to perform best. Hohermuth and Weitbrecht, 2018 came to the same conclusion, analyzing flume experiments with step-pool channels.
Another way to evaluate the stability is the determination of a critical specific discharge q_c, for which a channel is stable at a certain structure and slope. Aberle, 2000 derived a stability approach, where the standard deviation of the bed elevations σ_z accounts for the structure of the slope:

$$q_c = 0.20 \cdot \sin\alpha^{-1.30} \cdot \sqrt{g\sigma_z^3} \tag{2.14}$$

where α is is the angle of the channel bed against the horizontal, and g is acceleration due to gravity.
In the context of river engineering structures that protect against bed erosion, the stability criteria is often defined as a certain slope S that shall be maintained at a defined critical discharge q_c (eg. Weichert et al., 2007, Tamagni, 2013, Maager et al., 2019).

2.2.3 Ecological and landscape criteria

The implementation of a dynamic ramp can not only be seen as flood protection, but also as a river restoration measure. River restoration measures are defined by their common goal of improving hydrologic, geomorphic, and ecological processes within a degraded watershed and replacing lost, damaged, or compromised elements of the natural system (E. Wohl et al., 2005). To evaluate the benefit of such measures, it is necessary to define its goals, and to identify quantifiable sizes to evaluate the reaching of these (Gostner et al., 2013).
E. Wohl et al., 2015 summarized common goals of river restoration with the categories defined in Table 2.6. From an ecological point of view, the implementation of a dynamic ramp is primarily aimed at improving fish passage and esthetics of river sections where a major elevation difference has to be overcome locally (Weichert et al., 2007 S. Tognacca et al., 2021). The alteration of the channel geometry generated by this measure leads to a higher variability of flow depths and velocities. The goals of channel reconfiguration and instream habitat improvement can thus also be met through the implementation of this measure.

Goal	Description
Esthetics/recreation/education	Activities that increase community value: use, appearance, access, safety, and knowledge
Bank stabilization	Practices designed to reduce or eliminate erosion or slumping of bank material into the river channel
Channel reconfiguration	Alteration of channel geometry, planform, and/or longitudinal profile and/or daylighting; includes meander restoration and in-channel structures that alter the thalweg
Dam removal/retrofit	Removal of dams and weirs or modifications/retrofits to existing dams to reduce negative impacts
Fish passage	Removal of barriers to upstream/downstream migration of fishes
Floodplain reconnection	Practices that increase the inundation frequency, magnitude, or duration of floodplain areas and/or promote fluxes of organisms and materials between channels and floodplain areas
Flow modification	Practices that alter the timing and delivery of water quantity
Instream habitat improvement	Altering structural complexity to increase habitat availability and diversity for target organisms and provision of breeding habitat and refugia from disturbance and predation
Instream species management	Practices that directly alter aquatic native species distribution and abundance through the addition (stocking) or translocation of animal and plant species and/or removal of exotic species
Land acquisition	Practices that obtain lease for streamside land for the explicit purpose of preservation or removal of impacting agents and/or to facilitate future restoration projects

Table 2.6: Definition of common river restoration goals (adapted from E. Wohl et al., 2015).

The facilitation of fish passage can be evaluated by identifying migratory corridors. The suitability of the flow conditions for fish migration is determined by the maximum acceptable flow velocity U_c and the minimum required flow depth $h_{\min}$. The flow velocity is compared to the swimming velocity and the flow depth to the size of a target species (Tamagni et al., 2014).

Those fish species whose habitat corresponds to the natural river state are considered as target species. Table 2.7 lists channel characteristics that correspond to the zones of different species. The ecological effectiveness does not have to be guaranteed for all flow conditions, but only in a certain range of discharges (DWA, 2009). Fish migration should be assured for a period of at least 300 days per year, i.e. between Q_{30} and Q_{330} (Tamagni et al., 2014).

	Slope [%] for water course width of		
	[1-5 m]	**[5-25 m]**	**[25-100 m]**
Trout-zone	2.50-0.75	1.75-0.60	1.25-0.45
Grayling-zone	0.75-0.30	0.60-0.20	0.45-0.13
Barbus-zone	0.30-0.10	0.20-0.05	0.13-0.03
Bream-zone	0.10-0.00	0.05-0.00	0.03-0.00

Table 2.7: Typical slopes S [%] of the piscicultural zones of water courses in temperate Western Europe (adapted from Huet, 1949).

For the assessment of the improving ecomorphological status in intream habitats, a number of methods exist. In Switzerland, the modular stepwise procedure (Liechti et al., 1998) is commonly used. In the USA, the rapid bioassessment protocols (Barbour et al., 1999) are applied. Gostner et al., 2013 introduced the hydro-morphological index of diversity, HMID, a metric for quantifying the variability of a stream section. The HMID is determined by the coefficient of variation, CV, of the two variables flow velocity v and water depth h. Partial diversity $V(i)$ of each variable was expressed as

$$V(i) = 1 + CV_i = (1 + \sigma_i / \mu_i) \tag{2.15}$$

with σ_i the variance and μ_i the average of the variable i. The HMID is defined as the multiplication of the squared values of partial diversity:

$$\text{HMID} = V(v)^2 \cdot V(h)^2 \tag{2.16}$$

2.3 Summary and research gaps

Despite the progress made in recent years, current understanding of the interactions between LW and channel morphodynamics is still limited. Physical model experiments have been applied to investigate recruitment, transport and deposition of LW. These previous studies have mainly focused on low gradient flumes without local obstructions. The influence of LW deposits on erosion processes was mainly studied in wide channels with gentle slopes. The role of LW in steep gravel beds is usually associated in the literature with the formation of steps leading to an increase in flow resistance. Due to their task of overcoming a steep section, dynamic ramps have channel characteristics that are not sufficiently represented in the above-mentioned studies. The steepness and roughness structure of these structures correspond to that of steep mountain streams with step-pool structures. However, unlike in mountain streams, the width of dynamic ramps is significantly greater than the longest expected LW pieces. Therefore, the findings of studies on the effect of LW on steep mountain streams cannot entirely be transferred to dynamic ramps. Even independent of LW, the structuring processes of dynamic ramps are poorly studied. Physical modeling is still necessary for the design of these engineering structures. For practical implementations, the behavior of dynamic ramps at slopes around 2-3% and 9-10% under the influence of LW have been studied. For a structure at a slope on the intermediate range, the following research questions shall therefore be treated:

- Structuring processes of dynamic ramps
  How does the structure of the dynamic ramp adapt to progressively increasing hydraulic loading? To what extend does the structuring correspond to the processes described by Weichert et al., 2009?

- Effect of LW on the structuring processes
  Under which conditions do LW deposits form? What direct influence do LW deposits have on bedload dynamics? What is the effect of LW on both stability and ecological performance of the ramp?

- Contextualization: Effect of hydraulic load type
  To what extent do the structuring processes differ when the ramp is hydraulically loaded stationary or with a hydrograph?

3 Methods

The research questions formulated here-above are investigated by means of physical modeling. Channel geometry, hydrology and LW quantities of the test setup are loosely based on a 1:35 Froude-scaled model of the Ticino River, in the municipality of Osco between the confluences with the tributaries Foss and Piumogna. In the following physical model, the experimental procedure and the measurement techniques are described.

3.1 Physical model

The experimental flume provided in the Laboratorium^{3D} has a length of 8.5 m, and a width of 1.0 m and a depth 0.5 m. The upper part of the channel, which has a length of 6 m could be inclined to 6%. The side walls were equipped with a roughness structure. Figure 3.1 shows a photo of the model flume at the initial condition.

Figure 3.1: Photo of the model flume situated at Labroatorium^{3D} in the initial condition. Water will be run through flowing from left to right.

3.1.1 Similarity and scale effects

The physical model is built at a geometrical scale of 1:35. To maintain the constant ratios of velocity, time and force a scaling law was applied. This was done to ensure geometrical, kinematic and dynamic similarity. In open-channel flow, the common scaling law is according to Froude, with inertia as the retaining and gravity as the driving force. The Froude number is defined as

$$Fr = \sqrt{\frac{\text{Gravity}}{\text{Intertia}}} = \sqrt{\frac{U}{gL}} \tag{3.1}$$

with U the flow velocity, g the gravitational acceleration, and L a characteristic length. The similarity requires Froude numbers to be identical in the model and in the prototype. From this condition, the scale factors given in Table 3.1 can be derived.
The use of natural wood dowels as model LW leads to an overestimation of their strength properties (tensile, bending and flexural) and their Young's modulus. Consequently, fracture and deformation behavior as of the prototype cannot be adequately reproduced in the model. Deposited logs in the prototype can break into smaller pieces, increasing the compactness of the deposit Schalko, 2018. The scale effects due to cohesion can be neglected if mean grain size diameter of the model is above the limit of 0.22 mm Zarn, 1992.

Table 3.1: Scale factors according to Froude similitude.

Parameter	Scale factor
Length	λ
Area	λ^2
Volume	λ^3
Time	$\lambda^{1/2}$
Velocity	$\lambda^{1/2}$
Discharge	$\lambda^{5/2}$
Force	λ^3

3.1.2 Channel geometry

The model flume was equipped with a movable bed at variable slope. Upstream, a 1.00 m long inlet section with larger stable roughness elements at a slope of 3% was installed in order to gain a fully developed turbulent flow. The buffer zone had a length of 2.25 m and a slope of 3%, the ramp a length of 3.75 m at an initial slope of 7%. Downstream of the ramp the model had a length of 1.50 m where the movable bed was also installed at a slope of 3% as outlet section. A coordinate system was used with x measured along the flume length, y across the flume centered on the flume axis, and z as elevation. The geometry of the movable bed is provided in Figure 3.2 as a schematic drawing.

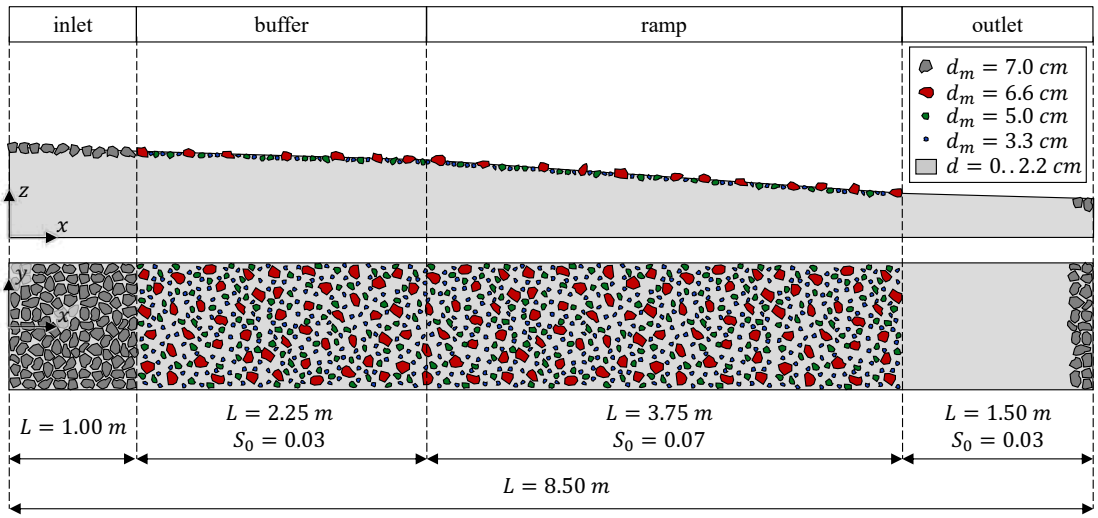

Figure 3.2: Schematic drawing of the model flume, length profile and plan view.

3.1.3 Model sediment

As implemented by S. Tognacca et al., 2021, the widespread grain size distribution proposed by Weichert et al., 2007 was divided in a base material and larger blocks. The characteristic parameters of the base material in model scale are provided in Table 3.2. The blocks that lined the buffer zone and the ramp were divided into three classes of different sizes that were marked with different colors. The equivalent spherical diameters D of the classes in model (M) and prototype (P) scale, as well as their mass m in prototype scale are summarized in Table 3.3.

Table 3.2: Characteristic parameters of the grain size distribution of the base material in model scale.

d_m [mm]	d_{10} [mm]	d_{16} [mm]	d_{60} [mm]	d_{84} [mm]	d_{90} [mm]
9.2	0.4	0.6	8.8	15.3	17.7

Table 3.3 also states the number of blocks of each class per unit area N_A. The blocks were placed on the base material with a resulting block placement density $\Lambda_0 = N_A \cdot \pi(D/2)^2$ (Figure 3.3 a). Then they were inserted into the base material, so that the blue and green class were fully embedded and the red class was semi embedded (Figure 3.3 b). The resulting protrusion P of the block classes in the initial condition are provided in Table 3.3. The block density Λ, defined as the proportion of the armor layer surface covered by blocks of each class was determined by processing the orthomosaics.

Table 3.3: Definition and characteristics of the block classes.

color	m_P [t]	D_P [m]	D_M [cm]	N_A [m^{-2}]	Λ_0 [%]	P [cm]
blue	2.1	1.2	3.3	1210	17.6	0
green	7.4	1.8	5.0	248	8.1	0
red	16.9	2.3	6.6	129	7.5	3.3

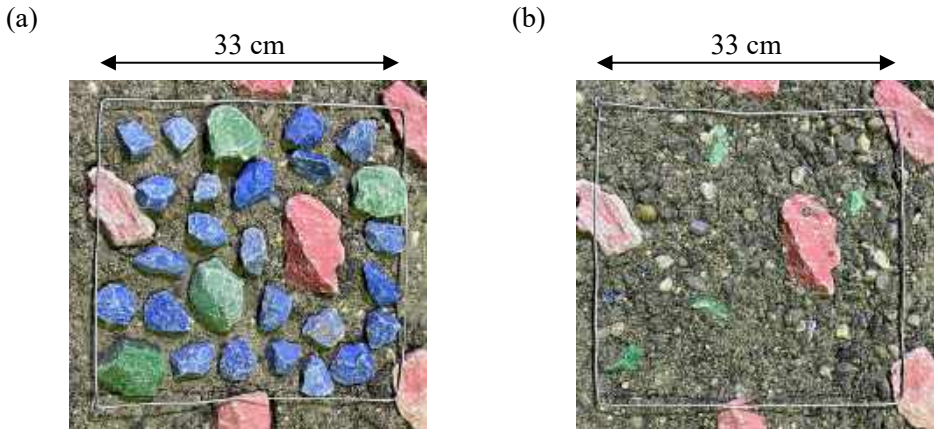

Figure 3.3: Block placement (a) and block position in initial condition, after insertion into the base material (b).

3.1.4 Model LW

The model LW, consisting of natural wooden dowels without branches, is shown in Figure 3.4. The size distribution was derived from the distributions provided in BAFU, 2019 that were based on the analysis of LW deposits on watersheds in Switzerland (Figure 3.5). The largest pieces, in the upper quartile of the size distribution, were modeled in five classes, with relative fractions by number N_i/N_{tot} derived from the length distribution (Figure 3.5 b). Table 3.4 summarizes the definition and characteristics of the LW classes.

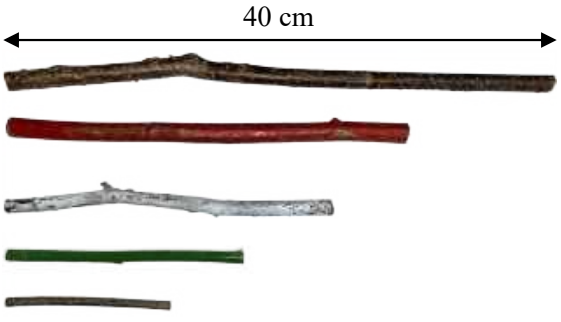

Figure 3.4: Model LW consisting of five classes of wooden dowels.

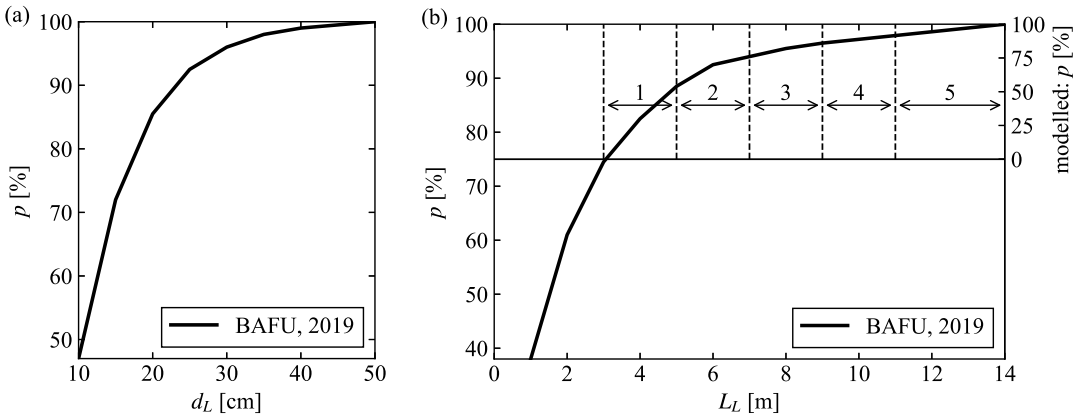

Figure 3.5: Typical diameter (a) and length (b) distribution by number of logs of wood deposits in Swiss water courses (BAFU, 2019). The modeled LW accounts for the 25% largest pieces in five classes as indicated in (b).

Table 3.4: Definition and characteristics of the LW classes.

class	$d_{L,\mathrm{P}}$ [m]	$L_{L,\mathrm{P}}$ [m]	$d_{L,\mathrm{M}}$ [cm]	$L_{L,\mathrm{M}}$ [cm]	color	N_i/N_{tot} [%]	V/V_{tot} [%]
1	0.2	4.0	0.6	11	brown	55	15
2	0.3	6.0	0.9	17	green	22	20
3	0.3	8.0	0.9	23	white	10	12
4	0.4	10.0	1.1	29	red	7	19
5	0.5	14.0	1.4	40	brown	6	35

3.2 Experimental procedure

A total of 4 experiment series were conducted. Experiment series S1-S3 served to investigate the influence of LW by comparing erosion processes upon loading without LW (experiment series S1) to those including LW (experiment series S2). A series including LW was repeated (experiment series S3) to test reproducibility. The three series S1, S2, and S3 consisted of a set of runs with incrementing stationary discharges that were run through the flume until sediment transport had ceased, and a stable channel configuration was formed. Experiment series S4 aimed to investigate the overestimation of erosion induced by this stationary hydraulic loading. This was done by loading the flume with a flood hydrograph. The duration of the run was not limited by morphological equilibrium, but by the total water volume acting on the ramp. This volume was determined corresponding to typical flood volumes at the prototype site in Piumogna. Table 3.5 summarizes the experiment series.

Table 3.5: Summary of the experiment series.

Series	Hydraulic loading	LW loading
S1	stationary	
S2	stationary	x
S3	stationary	x
S4	hydrograph	

3.2.1 Hydraulic loading

The hydraulic loading was based on the peak discharge Q_{max} of the characteristic floods of the river Ticino between the confluences with the tributaries Foss and Piumogna: HQ_{30} = 253 m^3/s, HQ_{100} = 301 m^3/s, HQ_{300} = 346 m^3/s and EHQ = 452 m^3/s. Additional discharges were defined so that the increments between the runs were around 7 l/s in model scale. The return period of these additional floods was determined with a logarithmic relationship (Figure 3.6 a). All investigated peak discharges and their return period are given in Figure 3.6.

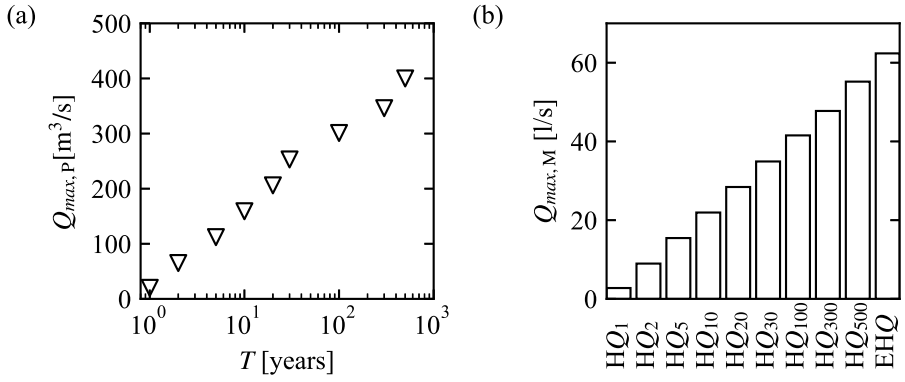

Figure 3.6: Return period of the investigated peak discharges.

The hydrograph was derived based on a parametrization of a flood hydrograph of the Ticino registered at the hydrological gauging station Piotta. The station is situated immediately upstream of the inflow of the tributary Foss. The flood of August 25 1987, corresponding to a return period of >150 years, was parametrized (Figure 3.7 a). The total duration of the flood t_{HQ} was defined as $t_{HQ} = 4t_{tp}$ with t_{tp} the time to peak. The time of peak flow was defined as t_{peak} = 30 min. The extrapolation of the hydrograph to the peak discharges was reached by an extrapolation of the rising limb, so that the slope was identical for floods of all return periods (Figure 3.7 b).

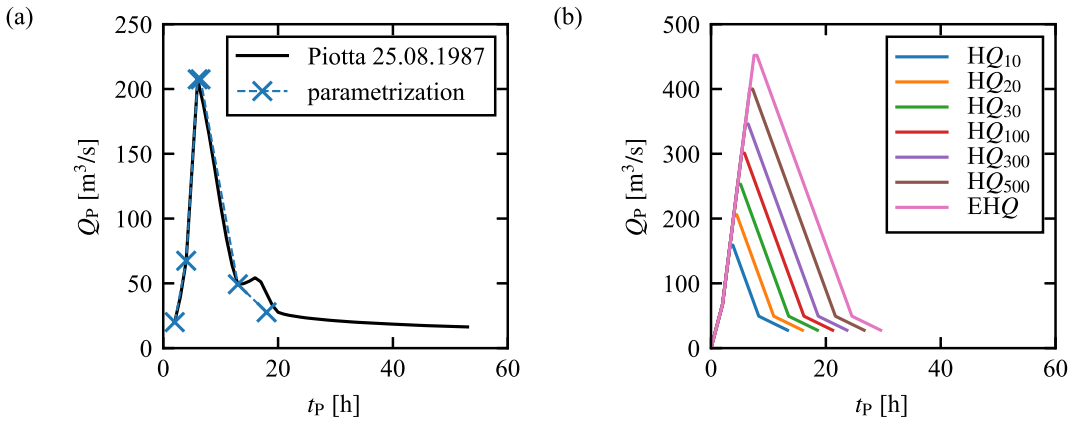

Figure 3.7: Derivation of the flood hydrographs.

In the first run, the channel was loaded with the entire derived flood hydrograph. To avoid repeating the rising and the falling limb in the subsequent runs, which would result in an overestimation of the total water volume acting on the ramp, only the additional volume of the incremented peak was considered. This led to the modeled hydrographs given in Figure 3.8.

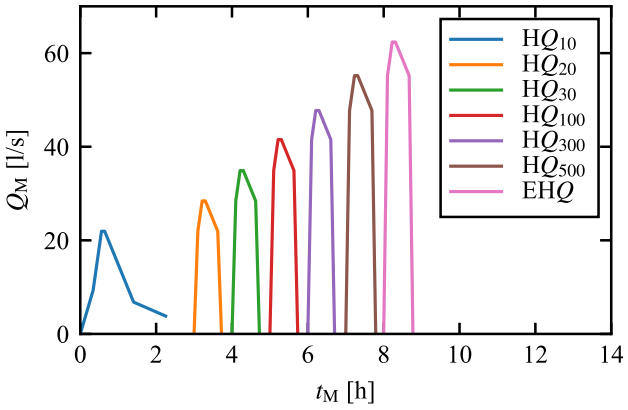

Figure 3.8: Modeled hydrographs.

3.2.2 LW loading

LW was loaded in series S2 and S3 at time intervals of 5 min in packages with the size distribution given in Table 3.4. The volume of the packages, V_p, was increased linearly with peak discharge as given in Figure 3.9. The wood pieces of each package, were introduced individually into the top of the flume, randomly oriented and distributed over the channel width. In series S2 packages were introduced until morphological equilibrium was reached. To test reproducibility in series S3 the same amount of packages were introduced.

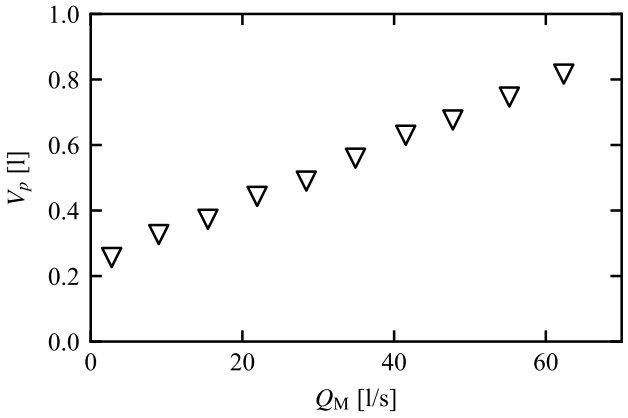

Figure 3.9: Volume of the LW packages.

3.3 Measurement techniques

3.3.1 Photographic documentation

The experiments were photographically registered with a stable camera, automatically recording an image every minute. This allowed for a time lapse sequence to be generated. Relevant details were filmed and/or photographed additionally. Furthermore, the channel was systematically photographed at morphological equilibrium during the run and after the run from a side view in a series covering the entire channel length.

3.3.2 Manual survey

Elevations of the bed were measure with a laser rangefinde at the initial condition and after each run. This was done at intervals of 0.25 m in the x direction and 0.10 m in the y direction with a laser rangefinder. In the series with stationary hydraulic loading (S1, S2, S3) the water level at morphological equilibrium was measured on the same measuring grid with a ruler. Furthermore, the position and class of each deposited log was registered in the two series including LW (S2, S3). When larger deposits were formed, the position of the corresponding logs was simplified to the position of the cluster center.

3.3.3 Photogrammetric survey

The bed topography was captured with a high resolution camera (type: Canon EOS 90D, resolution: 6960 x 4640 px, Focal length: 24 mm) on a mobile crane above the channel. A total of 20 to 50 photographs was registered on two axes along the x direction, resulting in an overlap over nine images on the channel surface. The images were aligned using the the Agisoft software Metashape.
19 ground control points (GCP) were defined, of which 14 were situated on the top edge of the channel sidewalls and 5 around the channel on the floor, around 0.5 m beneath. The elevation of all GCP was determined by means of a theodolite. The x and y position of the

GCP on the channel edge was determined by a series of distance measurements between the points. The Excel solver add-in was used to minimize the total error of the GCP coordinates and to distribute it evenly among the points. The square sum of the error of the GCP locations could be optimized to 6 mm.

3.3.4 Particle image velocimetry

In series S2 and S3, particle image velocimetry (PIV) was applied to analyze flow velocities on the ramp. For this, the flow field was homogeneously seeded with confetti (typical size 3-4 mm). The images of the tracer particles were recorded with a fixed camera (type: GoPro HERO9, spacial resolution: 3840 x 2160 px (4K), temporal resolution: 20 fps) above the channel. The field of view covered the full width of the channel and the range x = [3,8]m. Both protruding blocks and wood deposits lead to confetti blockages. PIV was therefore only applicable when the blocks in the wetted channel were fully submerged and LW deposits had resolved. A PIV algorithm developed at the Laboratorium^{3D} was used to process the captured images to obtain velocity vector fields.

4 Results and discussion

4.1 Qualitative observations

4.1.1 Series S1 - stationary, without LW

In the first runs, with relatively low specific discharges, the base material was mobilized revealing the blue and green blocks. This can be interpreted as the channel's response to the exceeding of stability being the armoring of the surface layer. The process was not revealed homogeneously over the entire channel. The wake of the red blocks emerged as a calmed zone where fine material was deposited. Furthermore, the armoring process was more pronounced on the ramp than on the buffer zone. This can be explained by the higher slope on the ramp, reflected by higher shear forces allowing the mobilization of larger grains. A mobilization of the blue blocks was first observed upon the specific discharge of q = 15 l/(sm), red and green blocks started to move at q = 22 l/(sm). At this discharge, and mainly also at q = 28 l/(sm) an increased meso-scale structuring was observed. Clustering of the blocks, initiated from the bottom of the ramp, was observed mainly on the central strip (Figure 4.1 a).

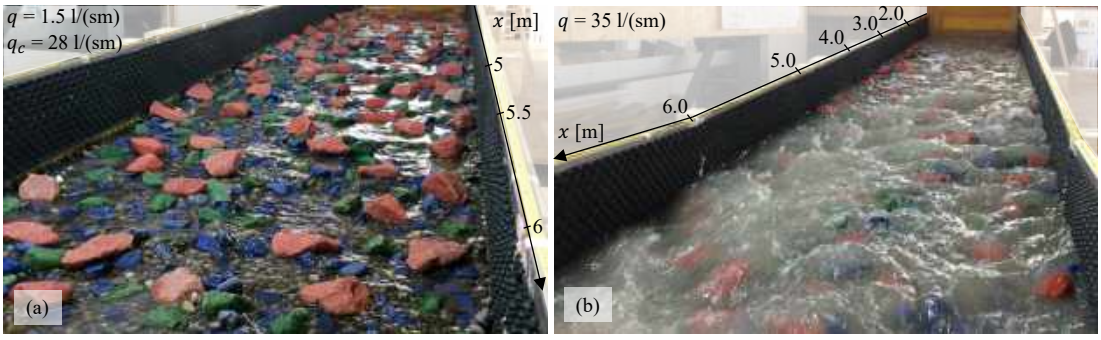

Figure 4.1: Impressions of series S1. (a) Bed formed by the critical discharge q_c = 28 l/(sm), loaded with q = 1.5 l/(sm). Meso-scale structuring has led to the formation of steps and pools. (b) Formation of bar features upon q = 35 l/(sm). Between x = 2 m and x = 4.5 m a bar feature has formed on the right side.

Upon q = 35 l/(sm) the flow concentrated on the left side at the ramp head and on the right side at the ramp foot. At stable bed conditions, a bar structure had formed on the right side of the ramp head. On this bar feature the flow depth was low and the red blocks were not submerged (Figure 4.1 b). The formation of this bar feature is understood as a macro-scale response to the exceeding of the bed stability. The relatively low flow velocity on the bar structure allowed for the deposition of fine material (Figure 4.2). However, since no sediment was supplied, the structural formation of the macro-scale structures was less so due to the deposition of incoming material, and more so due to the effects of erosion. A large volume of sediment, including roughly 300 blue blocks and 20 green blocks, were transported out of the channel. The resulting rotational erosion led to a lowering of the ramp head of 7.5 cm on average. The channel responded to the exceeding of stability, also on the reach scale by a decrease in slope. The roughness elements at the inlet section were mobilized, so that the

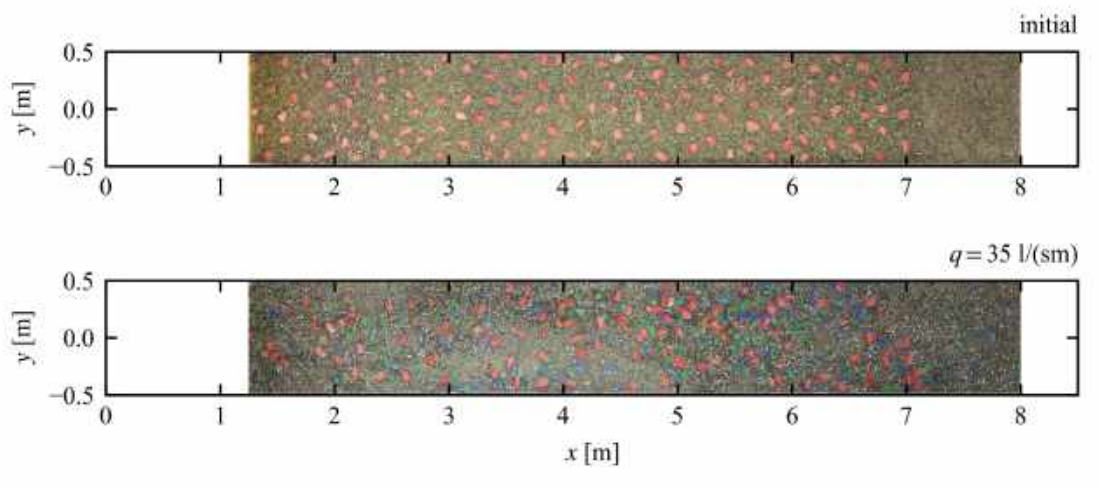

Figure 4.2: Selected orthomosaics of series S1. The top image shows the ramp at its initial condition, the bottom image after significant structuring on all morphological scales.

development of the flow was no longer guaranteed. The inlet section was econstructed before the following run.
The further increase of the specific discharge led to a gradual erosion of the bar structure from upstream. Already at stable conditions upon q = 42 l/(sm), the red blocks on the bar feature were fully submerged. After loading with q = 48 l/(sm), the stable bed was more or less plane. The gradual decrease in slope continued upon increased loading. Morphological equilibrium could not be attained in the last run with q = 62 l/(sm), since the maximum erosion of 15 cm at the inlet was reached. The processes on different morphological scales as described by Weichert et al., 2009 were observed. Processes on the macro- and reach scale, however, were only observed at discharges of $q > 30$ l/(sm).

4.1.2 Series S2 - stationary, with LW

As described in Chapter 3, LW LW pieces were loaded individually, with their orientation randomized. At discharges between q = 3 l/(sm) and q = 22 l/(sm) the individual logs moved by rolling, sliding, or floating, with no dominant bias towards a particular orientation. At higher discharges, when the red blocks were fully submerged, flotation was the most common mode of transport observed. The collision of moving pieces with stable pieces were observed to lead to (a) redirection of the moving piece, (b) trapping of the moving piece in front of the stable piece, or (c) mobilization of the stable piece. Therefore, although the logs were supplied uncongestedly, the mobilization of larger deposited clusters ocasionally led to semi-congested transport. The time to morphological equilibrium was determinant for the number of LW packages supplied. The number of packages supplied during each run N_p, the resulting cumulative number of logs supplied $N_{L,tot}$, and the number of logs that remained stable on the channel $N_{L,\text{stable}}$ are provided in Table 4.1. Since no more interaction between channel bed and LW pieces could be observed at specific discharges $q > 22$ l/(sm), the addition of wood

was ceased from a discharge $q > 35$ l/(sm).

Table 4.1: LW budget during the runs of S2. At runs with discharges $q > 35$ l/(sm) the addition of wood was omitted.

q [l/(sm)]	N_p [-]	$N_{L,tot}$ [-]	$N_{L,\text{stable}}$ [-]
3	2	46	24
9	6	220	71
15	12	628	62
22	15	1228	2
28	18	2056	0
35	21	3127	0

In the first run, all LW pieces deposited, most of them at the inlet section. These logs were removed after the run. The 24 pieces that remained stable on the ramp were mainly deposited individually. In the second run, a total of 71 logs was deposited, both individually and in three larger clusters, located around $x = 1.25$ m, $x = 1.75$ m (buffer zone) and $x = 5.5$ m (ramp). 51 of the 62 deposited logs in the following run ($q = 15$ l/(sm)) were clustered in a large deposit on the left side of the buffer zone ($x = 1.5$ m). Figure 4.3 shows the deposited LW pieces on a scatter plot and on the orthomosaic. In the following run at $q = 22$ l/(sm), the red blocks were fully submerged and the existing LW deposits dissolved. Two pieces remained on the ramp. Additional orthomosaics are given in Figure A.2 in Appendix A and Figure B.1 in Appendix B summarizes the number and position of logs deposited during the runs of S2.

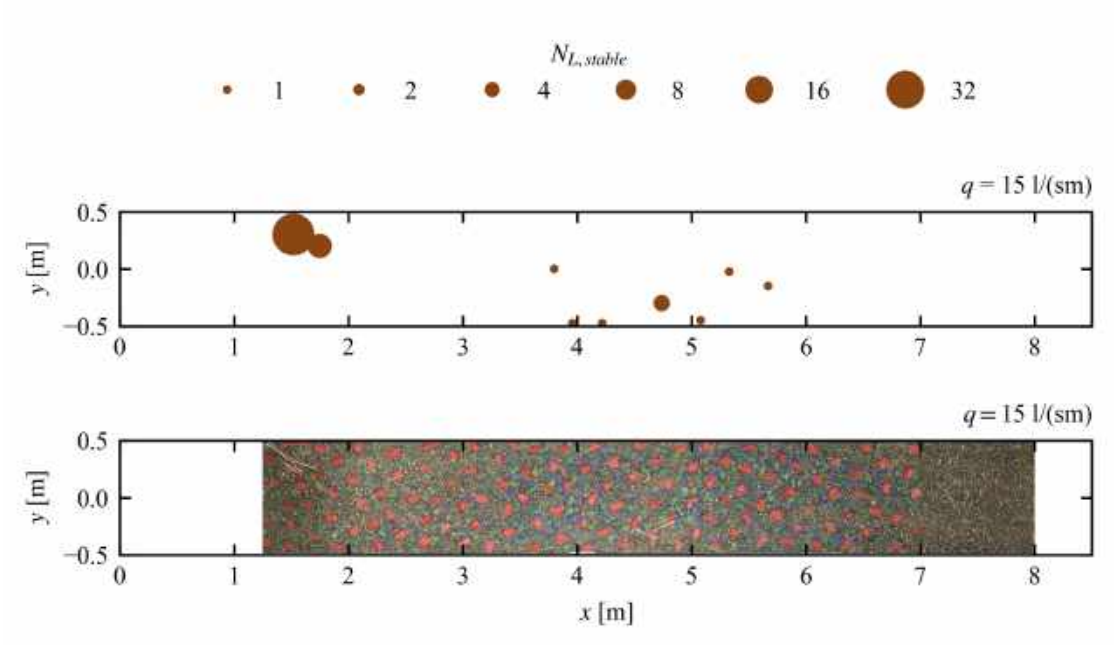

Figure 4.3: LW deposits that formed upon $q = 15$ l/(sm) as scatter plot and visible on the orthomosaic.

The first runs of S2, up to q = 28 l/(sm), were marked by structuring processes on the micro- and the meso-scale. The armoring process (micro-scale structuring) was influenced by the heterogeneous flow conditions on the channels. During this run they were not only driven by roughness elements and differences in slope, but also by deposited LW pieces. Around the LW deposits, a redirection of the flow leading to increased erosion was observed (eg. Figure 4.4). The mobilization of blue blocks was first observed at q = 9 l/(sm), mobilization and clustering of all block classes (meso-scale structuring) was observed at q = 15 l/(sm). At q = 28 l/(sm) a deepening of the central axis at the ramp head occured, leading to pronounced step features. Upon q = 35 l/(sm) pronounced alternate bar features formed on the left side of the ramp head and on the right side on the outlet section. The dry bar around x = 3.5 m was up to 25 cm wide in the y direction and extended over 2.5 m in the x direction. As in series S1, deposition of fine material on the bar structure could also be observed. The bar feature was also gradually transported downstream upon incremented discharge. However, at q = 48 l/(sm) the bar feature was still not fully submerged (Figure 4.4). After q = 55 l/(sm) the maximum erosion of the inlet of 15 cm was reached and the run with q = 62 l/(sm) was dispensed with.

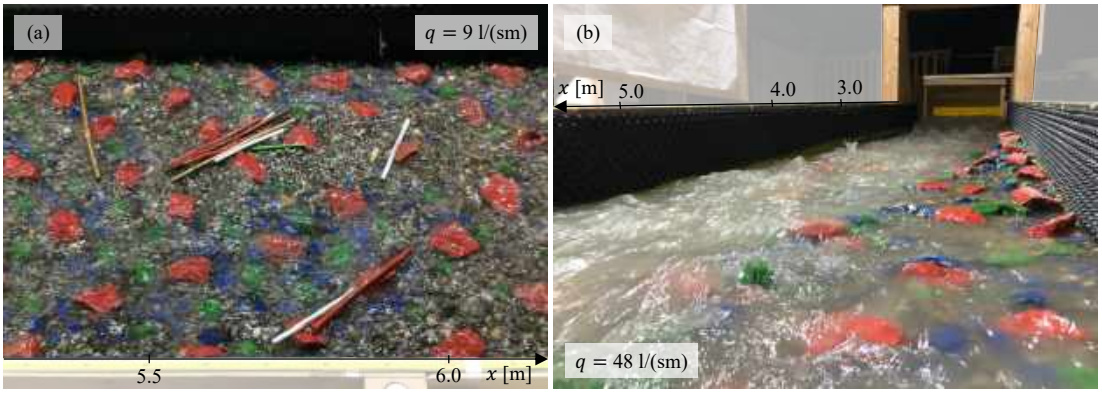

Figure 4.4: Impressions of series S2. a) Heterogeneous armoring process around LW deposits. b) Persisting bar feature at q = 48 l/(sm).

4.1.3 Series S3 - stationary, with LW (reproducibility)

The LW transport processes observed in S3 were consistent with those observed in S2. Table 4.2 summarized the LW budget for this series. In the first two runs, LW was deposited in a rather dispersed manner over the entire width and length of the buffer zone and the ramp. Upon q = 15 l/(sm) the deposits concentrated on the right side of the channel, where the mobilization of the base material was observed to be reduced. Deposits of over 20 logs remained stable on the right bank even upon q = 28 l/(sm), when elsewhere the red blocks were fully submerged. Figure B.2 in Appendix B summarizes the number and position of logs deposited during the runs of S3.

Table 4.2: LW budget during the runs of S3. The LW supplied was kept equal to that of S2, at runs with discharges $q > 35$ l/(sm) the addition of wood was omitted.

q [l/(sm)]	N_p [-]	$N_{L,tot}$ [-]	$N_{L,\text{stable}}$ [-]
3	2	46	19
9	6	220	46
15	12	628	70
22	15	1228	28
28	18	2056	1
35	21	3127	0

At the micro scale, the structuring was increased on the left side next to the deposits (Figure 4.4 a). Macro- and reach-scale structuring initiated at $q = 35$ l/(sm), with the formation of a bar feature on the right channel side around $x = 3.5$ m. A length of roughly 2.5 m in x and a maximum width of 0.4 m in y was unwetted. An alternate bar structure formed on the right side of the outlet around $x = 8$ m. Figure 4.6 shows the bar feature and a high density of red blocks around $x = 6$-7 m. This clustering of red blocks downstream of the highly eroded zone can also be observed in series S1 (Figure 4.2). However, in this run the red blocks were stabilized higher up around $x = 5$ m. Upon increasing loading, the bar structure was eroded from upstream, but it remained partially dry for two more runs. Figure 4.5 b) shows the bar structure at equilibrium after $q = 42$ l/(sm).

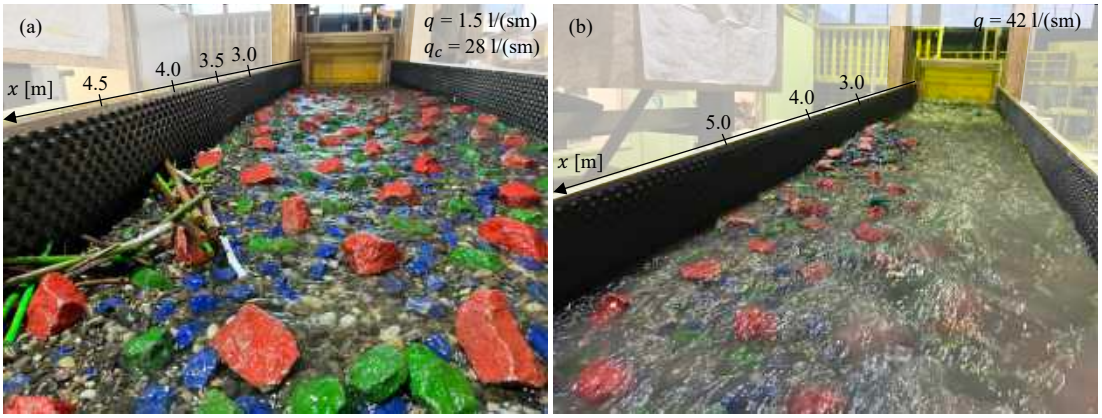

Figure 4.5: Impressions of series S3: a) LW deposit that remained stable upon the bedforming discharge $q_c = 22$ l/(sm). The channel is loaded with $q = 1.5$ l/(sm) revealing meso-scale structures. b) Macro-scale structure of the stable bed upon $q = 42$ l/(sm).

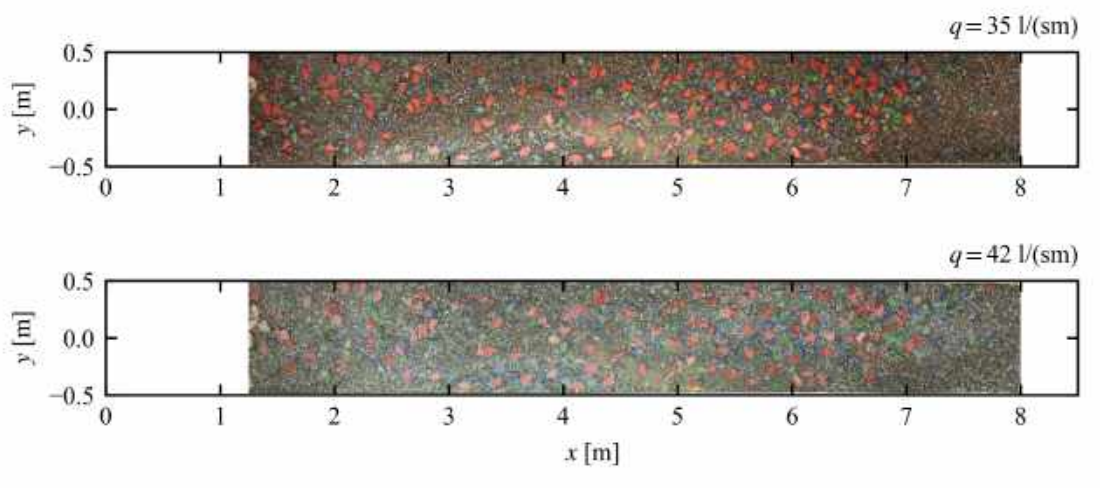

Figure 4.6: Series S3: Orthomosaics of the bed structure with pronounced bar features. Note the high density of red blocks between x = 6-7 m.

4.1.4 Series S4 - hydrograph, without LW

In series S4, where flood hydrographs were tested, the moment of grain mobilization, and the behavior of the ramp during the rising and falling limb could be observed in more detail. During the first run with a peak discharge of q_{max} = 22 l/(sm), a mobilization of the bed matrix could be observed at q = 7.5 l/(sm), a mobilization of the blue blocks at q = 12.5 l/(sm), and of the red blocks at q = 21 l/(sm). Isolated LW pieces of all classes were supplied at peak discharge, revealing no interaction with the channel bed. During the falling a displacement was observed among some of the blue blocks.
Morphological action was observed in the following run, when the previous peak discharge was exceeded. At peak discharge several red blocks were mobilized and deposited upstream of another red block, forming stable structures consisting of two blocks. The erosion was observed to be stronger on the right bank of the ramp and a slight aggradation of the bed was observed on the right side of the outlet zone. During the peak of the following run (q_{max} = 35 l/(sm)) a high mobilization of the blocks was observed, especially on the ramp foot. The morphological equilibrium was not attained at the end of the peak and many green blocks, occasionally even red blocks, were moving during the falling limb. The structure of the bedforms after the run showed a high variability. The flow depths and velocities established with a specific discharge of q = 1.5 l(sm) were noticeably diverse and step-pool structures could be recognized (Figure 4.8 a))
The following run, with a peak discharge of q_{max} = 42 l/(sm), was marked by a strong erosion at the right side of the ramp head. A considerable fraction of the mobilized material was deposited on the same side of the outlet section. However, a significant transport of sediment out of the channel, including many blue and green blocks, was observed. At the end of the peak, the erosion was still quite strong. But only a few stabilizing blocks were transported out. An alternate bar structure was identified at the end of the run with bar features on the right

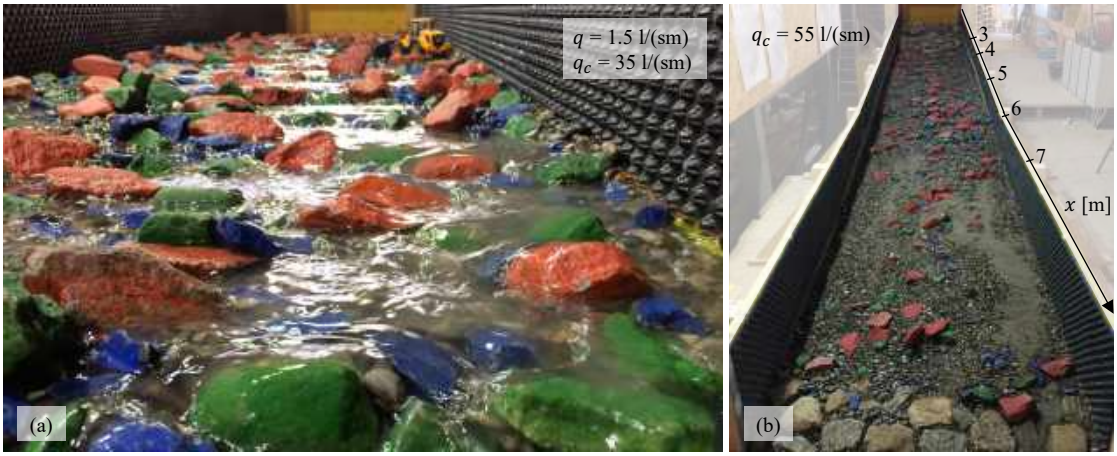

Figure 4.8: Impressions of series S4. a) Stable bed after a bedforming discharge of q_c = 35 l/(sm). Step and pool structure with high variability in flow conditions at a discharge of q = 1.5 l/(sm). The excavator in the background is at scale. b) Stable bed after a bedforming discharge of q_c = 55 l/(sm). The fine material deposits lie on the aggradation.

side around x = 3.5 m and on the left side around x = 7.5 m. The features were accentuated in the following run with a peak discharge of $q_{\max}$ = 48 l/(sm).
The last two runs, with peak discharges of q = 55 l/(sm) and q = 62 l/(sm), resulted in the dissolution of the bar features towards a more plane bed structure. A portion of the material which had eroded on the left side deposited on the left side of the outlet zone. This resulted in an aggradation upon which also fine material remained stable (Figure 4.8 b) and Figure 4.6). More orthomosaics of series S4 are provided in Figure A.4 in Appendix A.

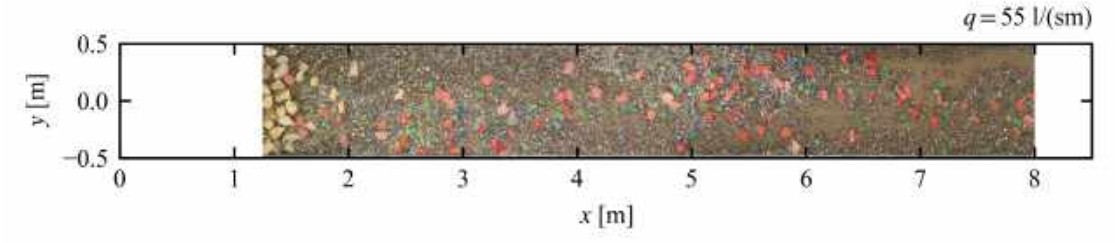

Figure 4.7: S4: Orthomosaic of the structured bed. Deposits on the outlet zone can be recognized.

4.2 Quantitative observations

4.2.1 Bed elevation

At the resolution of the bed elevation measurements, macro- and reach-scale structures could be identified. The total erosion, dz, was determined as the difference between the elevation of the bed at morphological equilibrium and the the initial bed elevation. Contour plots of dz after each run are presented in Figures C.1 - C.4 in Appendix C. The averaging of the bed elevations over each cross section results in the longitudinal profiles provided in Figure 4.9. The longitudinal profiles of S1 reveal the first strong erosion at q = 35 l/(sm), as observed and described in Section 4.1. The bed elevation then further decreases in a gradual manner, initially on the upper part of the ramp and in the last two runs also around the ramp toe. The erosion at q = 35 l/(sm) is more significant in series S2 and S3 than in S1. The decrease in bed elevation is only minor in the following runs. S2 show an significant decrease in mean bed elevation already at q = 28 l/(sm). The decrease in mean bed elevation is more gradual in S4. Lateral variability in bed elevations is presented with three cross sections on the ramp head, in the middle of the ramp, and on the ramp toe, in Figures C.5 - C.7 in Appendix C. Upon q = 35 l/(sm), when strong changes in the longitudinal profile can be detected, the lateral variability also increases. Especially in series S2 and S3, the bed at the ramp head was strongly deepened on one bank, while hardly any erosion occurred on the other bank. This gradient in bed elevation along the cross section was also present in the middle of the ramp, although less pronounced. The deviation from the mean bed elevation is furthermore presented in a condensed way as the elevation of the talweg, defined as the minimum bed elevation in each cross section, in Figure C.8 in Appendix C.
By a linear regression of the mean bed elevation on each cross section on the ramp, the ramp slope S was derived. Figure 4.10 shows the stability diagram, in which this stable slope is plotted against the specific discharge. In all series, a decrease in slope is observed around q = 30 l/(sm). In series S2, a decrease in slope is already identified at q = 28 l/(sm). In series S4, the decrease upon q = 35 l/(sm) is only minor compared to the other series. At the discharge, where the decrease in slope initiated, a change in morphological structuring regime could be observed. Although processes on the micro- and the meso-scale still take place after this threshold, macro- and reach-scale processes dominate.

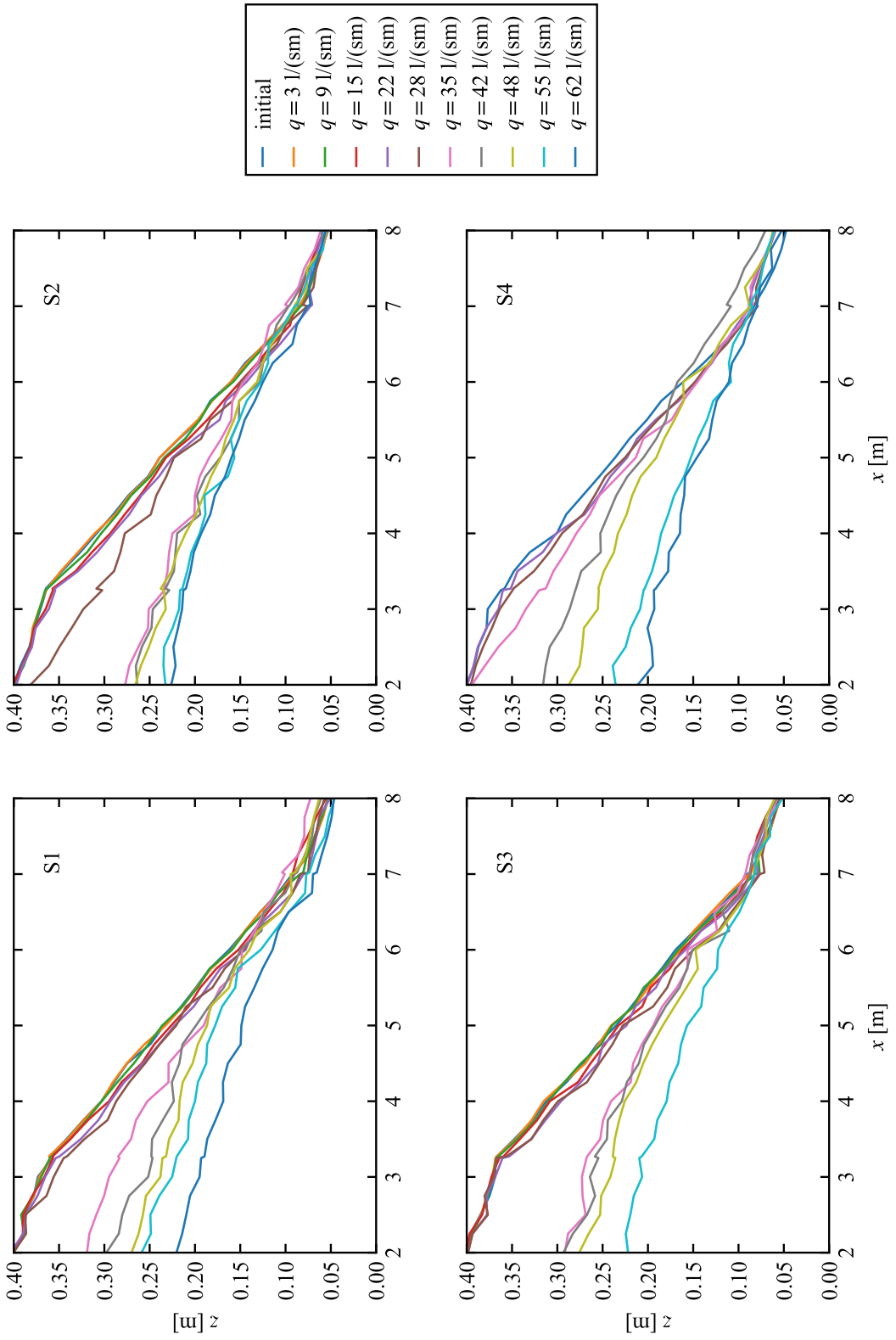

Figure 4.9: Longitudinal profiles of the mean bed elevation.

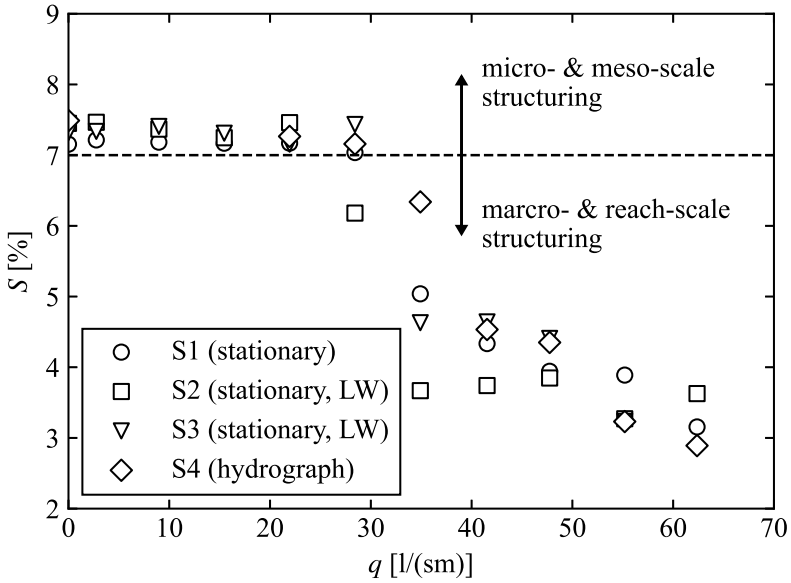

Figure 4.10: Stability diagram of the four experiment series. The decrease in slope is considered at reach-scale structuring process. Upon the same hydraulic loading time macro-scale structuring was observed (Chapter 4.1). At lower discharges, the channel was observed to react to increased hydraulic loading with morphological processes on the micro- and meso-scale.

The given structuring, by the installation of the stabilizing blocks in layers, allows the stability of the bed slope up to a substantial hydraulic load to be sustained. Morphological processes on the micro- and macro-scale produced structures that were perceived as diverse and natural. For a site with the hydrology of the Ticino River in the municipality of Osco, however, the proposed geometry cannot guarantee a stable ramp slope of 6% after loading with the hundred-year flood. If such a structure was planned, it would be necessary to consider an additional stabilization of the bed, for example, through the application of a deeper layer of stabilizing blocks. It is important to mention that with the test series, only the structuring induced by flood events was considered. Even though the constant, lower load acting most of the time influences the river morphology, it can be assumed that the gross structural changes become prominent during large flood events (Weichert, 2006).

4.2.2 Water level

The water level at morphological equilibrium could be measured in the series with stationary hydraulic loading (S1 - S3). The flow depth was derived through a point by point subtraction of the bed elevation from the water level. Figures D.1 to D.3 in Appendix D show the contour plots of the calculated flow depths. The flow depth was averaged over the ramp, over the buffer zone, and over the entire channel for comparison (Figure 4.11 a) - c)). In series S1, the flow depth averaged on the ramp and on the entire channel increase in a approximately linear manner with specific discharge. The mean flow depth on the buffer zone is increased

at q = 35 l/(sm), when the bar features formed. In series S2, the mean flow depth increases progressively without large variations between the sampling areas. The mean flow depth in series S3 reveals a drastic increase in all sampling areas at q = 35 l/(sm). The comparison between the series shows most significant differences at q = 28 l/(sm) and q = 35 l/(sm). At q = 28 l/(sm) the flow depth established in series S2 is higher than in the other runs. This is in line with the stronger erosion that was observed in the series at this run. At q = 35 l/(sm) the stronger increase in flow depth at q = 35 l/(sm) on the buffer zone in series S1 and on all sample areas in series S3 can attributed to the stronger erosion (Figure 4.10). However, in series S1 the flow depth on the ramp did not increase disproportionately. This can be explained by the bar feature, that, unlike in series S2 and S3, in series S1 was fully submerged. The low flow depth on the feature reduces the mean flow depth on the ramp. In series S2 and S3, in contrast, a considerable fraction of the bar feature remained dry and was not reflected in the flow depth.

From the average flow, the relative submergence of the red blocks, defined as the ratio between flow depth and block protrusion h/P, can be quantified. The size is only meaningful in plane bed configurations, thus up to q = 28 l/(sm) in the conducted series. The protrusion of the red blocks is assumed to correspond to the initial value of P = 3.3 cm in these runs. Figure 4.11 b) shows the resulting relative submergence. The red blocks were fully submerged at q > 20 l/(sm). The flow depth was averaged over the entire channel was denoted by h.

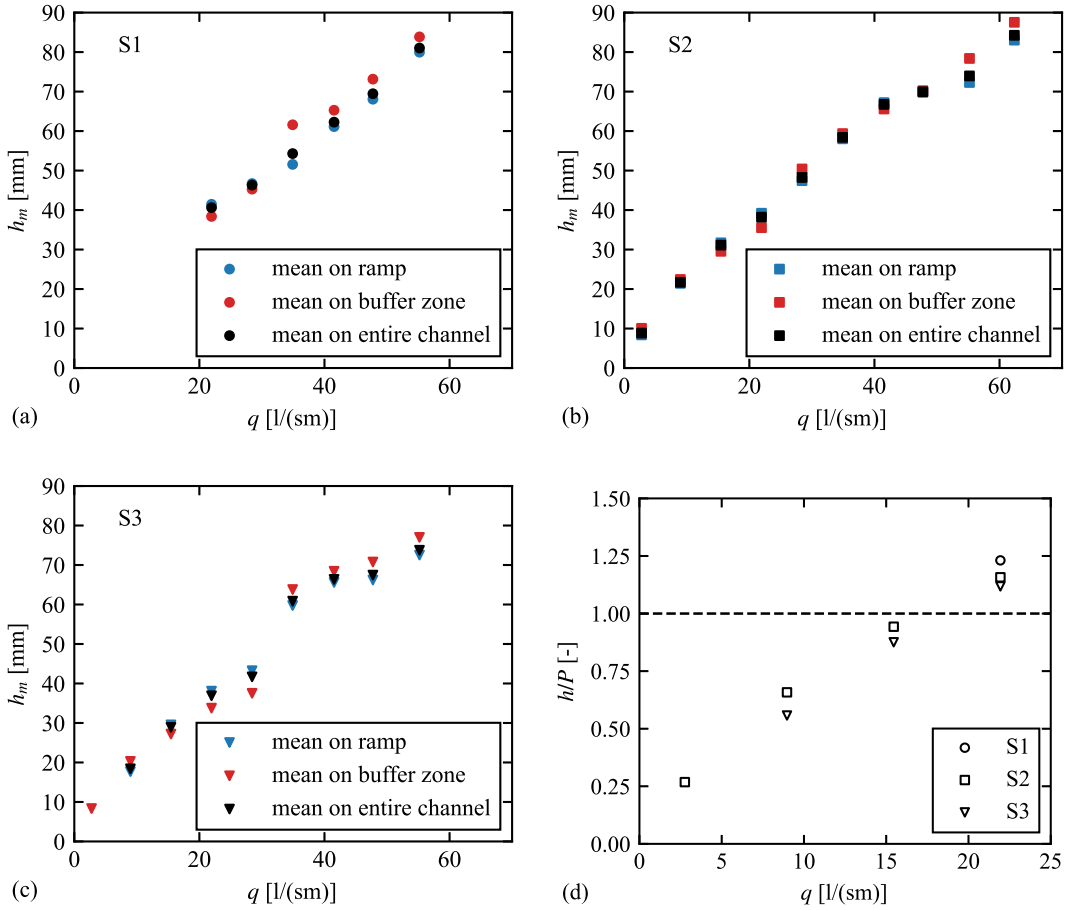

Figure 4.11: a) - c) Flow depth h averaged on three different sections: ramp, buffer zone and entire channel. d) Relative submergence h/P of the red blocks calculated with the flow depth averaged over the entire channel. The red blocks are fully submerged at dischages $q > 20\,\mathrm{l/(sm)}$.

4.2.3 Flow velocity

Based on the manual surveys of the bed elevation and the water level (measured in series S1, S2 and S3), the mean velocity v_m on each cross section was derived according to the continuity law. The cross-sectional area was determined as the area between the linear interpolation of the measuring points. Figure 4.12 shows the derived velocity as mean on the ramp plotted against the specific discharge.

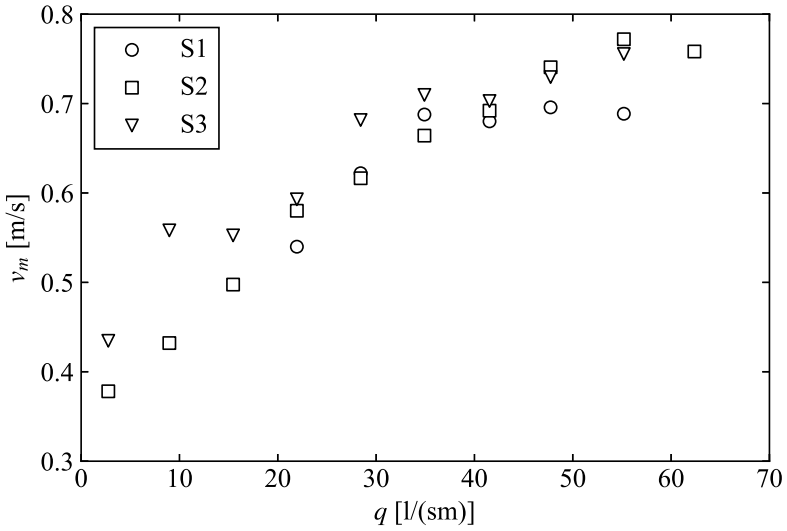

Figure 4.12: Averaged flow velocity determined based on the water level measurements according to the continuity law on the cross sections of the ramp.

In series S3 and S4, the flow velocity at the surface was additionally investigated for selected discharges by means of a PIV analysis. This allowed the flow velocities to be additionally examined as a two-dimensional velocity field. Figure 4.13 shows such velocity fields by the example of S4, figure E.1 in Appendix E for series S3. For illustration purposes, the flow depths are also presented. It can be seen that with the formation of macro features, a diversification of surface flow velocities occurs. Elevated flow velocities develop in the talweg, while velocities around the bar features are low. Figure 4.13 furthermore shows the mean velocities on the cross sections. The velocity calculated using the water level measurements is compared with the surface velocity determined by the PIV analysis. The magnitude of the two metrics is comparable, however, the high resolution of the PIV analysis allows allows the variabilitiy flow velocity to be investigated at a smaller scale, In more plane bed configurations, as developed at q = 28 l/(sm) or q = 55 l/(sm), a surface velocity with a lower variability was identified, in contrast to the runs with the dominant bar features (q = 35 l/(sm) - q = 48 l/(sm).

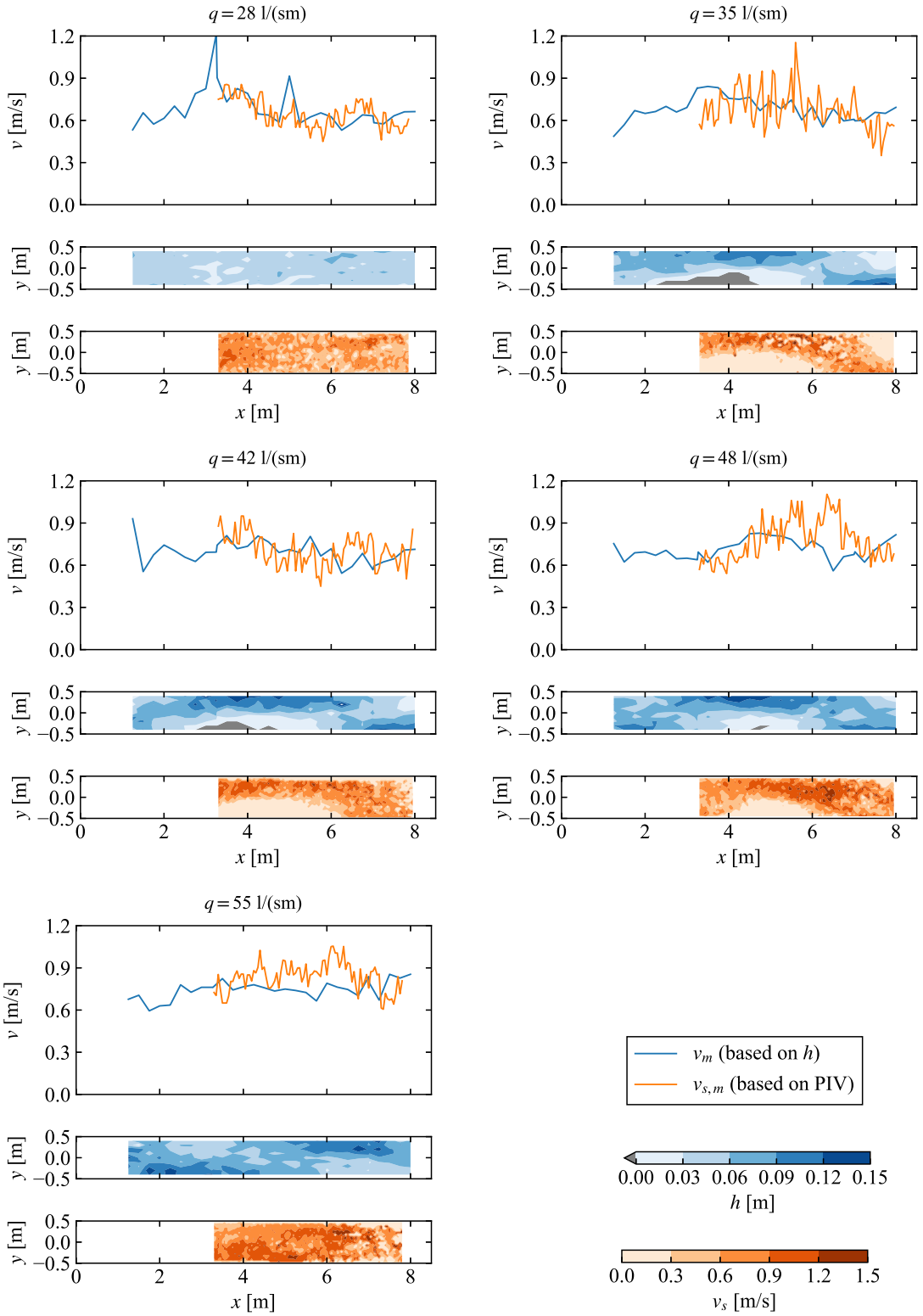

Figure 4.13: Series S4: Flow depth h based on the manual survey and surface flow velocity v_s based on the PIV analysis. Based on these sizes the mean velocity v_m and the mean surface velocity $v_{s,m}$ was determined. PIV was not applicable on runs with lower specific discharges.

4.3 Effect of LW loading

In both runs with LW, deposits grew up to a specific discharge of q = 15 l/(sm) and were then dissolved. At the same threshold, the relative submergence of the red blocks passed one, indicating that the red blocks were fully submerged. A direct relation between the submergence of the plane bed and the LW deposition probability can thus be assumed. As soon as the relative submergence of the red blocks exceeded the threshold value of 1, LW deposits were dissolved and the LW budget was negative. This is consistent with the literature, as submerged blocks do not interact with LW. Blocks that protruded from the water because they were situated on a bar feature were not effective in stopping the LW. In fact, the logs were moving along the valley path, or along the path with maximum flow velocity. This contradicts to some extent the thesis of increased deposition probability with increased sinuosity as described by Braudrick and Grant, 2001. This could be attributed to methodological differences or that effect of sinuosity on the trapping probability might be reduced during strong flood events associated with high flow velocities.
An analysis of the orthomosaic after the critical loading of 15 l/(sm) was conducted in order to examine the direct impact of LW deposits on micro-scale structuring processes. Since the blue blocks were initially fully embedded, their visibility indicates enhanced micro-scale structuring through erosion of the base material. The blue blocks were identified with a color filter (Figure A.5 in Appendix A). The proportion of their visible surface in the uppermost layer of the bed, the block density Λ, is presented in Figure 4.14. In all three experiments series, Λ was higher on the ramp than on the buffer zone. In S2, a dominant LW deposit formed on the buffer zone at x = 1.5 m on the left side. Downstream of this deposit (x = 2-3 m), the right side shows an increased density of visible blue blocks, while on the left side almost no blue blocks are visible. Also in the wake of the deposits on the right side of the ramp around x = 4 m, Λ is reduced. In S3, multiple LW deposits were formed on the right channel side. A gradient of Λ in y can be observed with higher visibility of blue blocks on the left side of the ramp with respect to the right side.

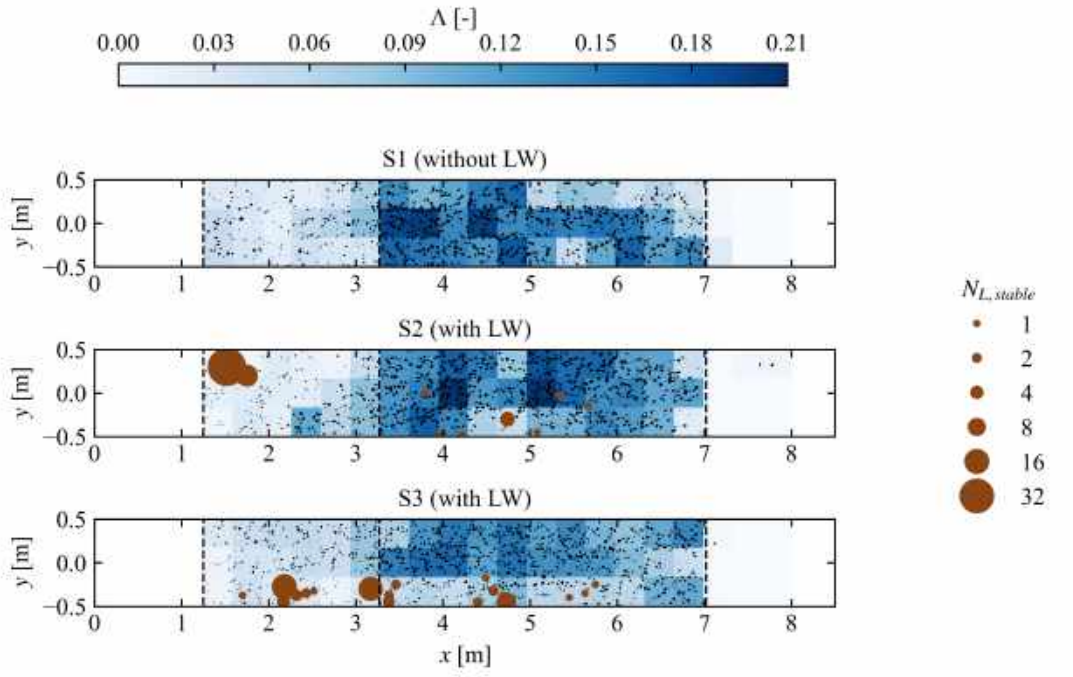

Figure 4.14: Analysis of the orthomosaic of the model flume at the morphological equilibrium after q = 15 l/(sm), flow from left to right. The black dots represent visible blue blocks. The density of these blocks is presented in a raster of 33x33 cm^2 large cells. The brown dots indicate LW deposits with their size corresponding to the number of logs in the cluster. The limits of the buffer zone (S_0= 3%) and the initial ramp (S_0= 7%) are indicated by dashed lines.

The difference in blue block density between the ramp and the buffer zone can be explained by their difference in slope. The higher slope on the ramp is reflected by higher shear forces allowing for the mobilization of larger sediment grains. By changing the flow field, LW deposits influence the shear forces. On the one hand, this can be shown by the fact that the concentration of the flow leads to increased shear forces and consequently greater mobilization of the fine fraction on the side opposite to the LW deposit. This was observed on the buffer zone in series S2. On the other hand, the shear forces in the protected zone in the downstream of the wood deposits are lower so that the fine fraction remains stable at a higher hydraulic load. This was observed on the ramp in both series.
In the runs where macro- and reach-scale structuring processes were observed, i.e. around q = 30 l/(sm), the LW deposits had already been dissolved. Nevertheless, some differences in the processes on these scales were observed between the runs with and without LW. In S2 (with LW), the decrease in slope was more rapid and pronounced than in S1 (Figure 4.10). LW thus might lead to an acceleration of the structuring processes on the reach scale. The behavior was not reproduced in the second run with LW (S3).
During the morphologically strongly active specific discharges around 30 l/(sm), macro-scale structuring lead to the development of an alternate bar structure in all three experiment series. The flow depths that were established in the two runs, with q = 35 l/(sm) and q = 48 l/(sm),

illustrate this (Figure 4.15). The bar feature formed at $q = 35$ l/(sm) was almost fully submerged in series S1, while in series S2 and S3 a significant area was dry. After two runs, at $q = 48$ l/(sm), the bar structure was eroded in series S1, while it persisted and was even enhanced in series S2 and S3. It should be noted that in the following runs the bar features developed on the respective side of the dominant LW deposits in both series. The increased erosion adjacent to the LW deposits appear to have continued after their dissolution. The bar features that formed as a result of this asymmetric erosion were more pronounced than those that formed in the series without LW and therefore persisted at higher specific discharges.

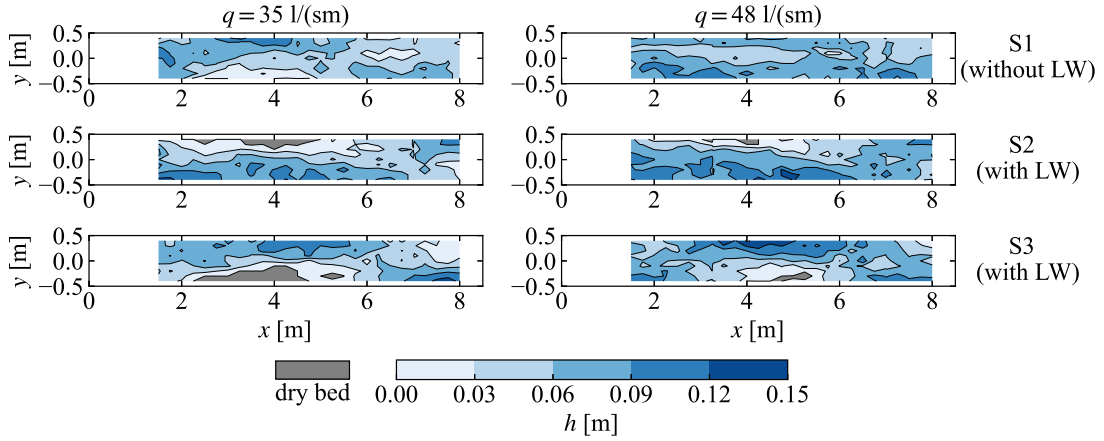

Figure 4.15: Flow depth h for two selected runs in the series without LW versus the series with LW.

On an individual cross section, a high variation of measured bed elevations is an indicator for a non-plane bed. This is because measuring intervals of 0.10 m do not capture the meso- and micro-scale roughness. As a reach-scale indicator for the variability of bed elevation, the standard deviations of the bed elevations of each cross section were averaged over the ramp:

$$\sigma_{z,m} = \frac{1}{n} \sum_{i=1}^{n} \sigma_{z,i} \tag{4.1}$$

where n is the number of cross sections on the ramp and $\sigma_{z,i}$ the standard deviation of the bed elevations z on the cross section i. This size is presented in Figure 4.16. Upon specific discharges between 35 and 50 l/(sm) $\sigma_{z,m}$ was 50% higher in the series with LW loading. In both series, the bars were situated on the side, where dominant LW deposits were formed in the previous runs with lower specific discharge (see Figure 4.15). The effects of LW deposits on bed elevation diversity tends to dissapear at higher discharges compared to series S1. These remarks suggest that wood affects the variability of flow depths, which according to Chapter 2 can be considered positive from an ecological point of view. For example, an increase in the variability of flow depths can be expected to have a positive effect on HMID.

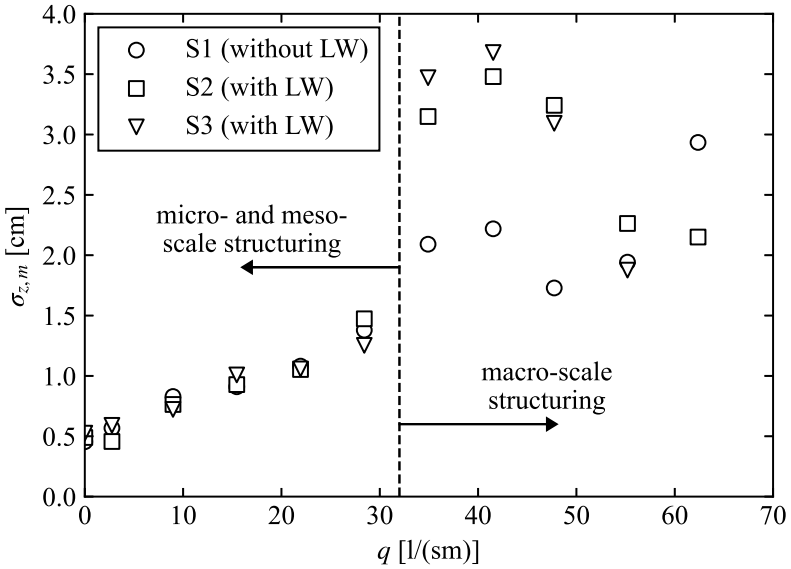

Figure 4.16: Mean standard deviation of the bed elevations on the cross sections $\sigma_{z,m}$ as an indicator for bar features.

4.4 Effect of hydraulic load type

The general structuring processes were observed to be similar in the experiment series with stationary (S1) and hydrograph (S4) loading. At low specific discharges micro- and meso-scale structuring processes dominated. At specific discharges above q = 30 l/(sm) macro- and reach-scale processes took over, leading to the formation of bar features and to a decrease in slope. In this regime, it was observed that the morphological equilibrium was not reached in the runs with hydrograph loading after the peak duration.

The bar features upon hydrograph loading formed more gently but remained stable at higher specific discharges than those formed upon stationary hydraulic loading. The standard deviation of the bed elevations of each cross section averaged over the ramp, $\sigma_{z,m}$, reflects this development (Figure 4.17 a)). $\sigma_{z,m}$ increases linearly at discharges between q = 28 l/(sm) and q = 48 l/(sm) and only decreases upon higher loading. On the reach-scale, a more gradual decrease in slope was observed (Figure 4.17 b)). While the slope decreased in a roughly linear manner in series S4, the decrease in slope in series S1 resembled an exponential decay.

Compared to the experiment series with stationary loading, the experiment with hydrograph loading resulted in larger sedimentations on the outlet zone. This is exemplified by the deviation from the initial bed elevation, the total erosion dz, after the runs with q = 42 l/(sm) and q = 55 l/(sm) shown in Figure 4.18. Also the maximum height of the sediment deposits differed: In series S1 the $dz_{\max}$ was 5 cm, in series S4 7.5 cm.

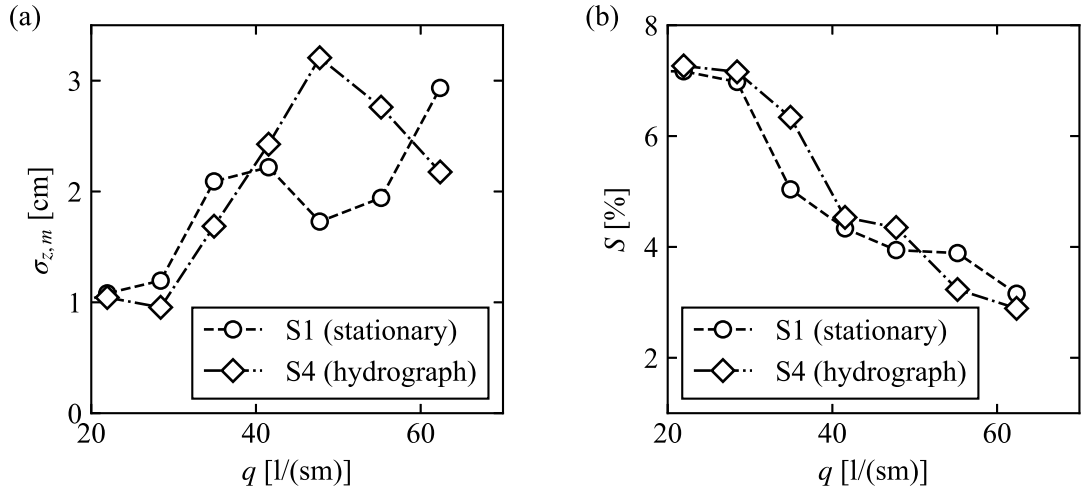

Figure 4.17: Comparison of the structuring processes upon stationary and hydrograph loading. a) Mean standard deviation of the bed elevations on the cross sections $\sigma_{z,m}$ as an indicator for the macro-scale process of bar formation. b) The decrease in slope as indicator for the reach-scale process of rotational erosion.

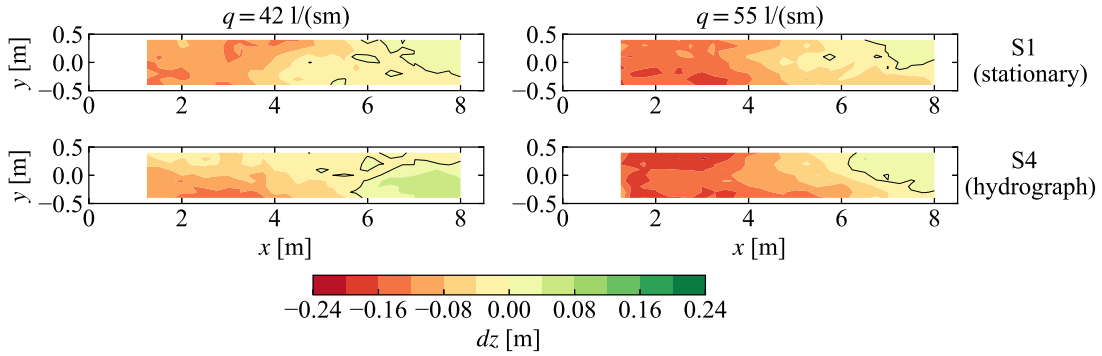

Figure 4.18: Deviation from the initial bed elevation *dz* for two exemplary runs, showing larger sediment deposits on the outlet zone in the series with hydrograph loading with respect to the series with stationary loading.

The structuring processes that in nature develop under the load of a flood hydrograph can thus be reproduced well with stationary loading. In both series, the morphological processes start at comparable hydraulic loads. Their intensity, however, was not observed to be quite identical. The reason for this is that the peak discharge duration is overestimated in the case of stationary loading. As a result, both macro- and reach-scale structuring occur more gradually upon hydrograph loading. The sedimentation on the outlet zone probably increased in volume during the falling limb, which is not replicated in the stationary tests.

5 Conclusions and outlook

5.1 Conclusions

Hydraulic model tests were conducted to study the structuring processes that develop on a dynamic ramp with an initial slope of 7% under the influence of LW transport. This thesis investigates the structuring processes of dynamic ramps and the effects of LW and hydraulic load type on these mechanisms.

(1) Structuring processes of dynamic ramps (base case)
The objective of this part was to gain an understanding of the bed morphology and stability of a dynamic ramp with a slope in a yet unstudied range. For this purpose, an experiment series with gradually increasing, stationary hydraulic load was conducted as a base case. The observed processes were described and compared to those found in literature. Structuring processes can be understood as the ramps response to loading that exceeds the bed stability. According to Weichert et al., 2009, these self-stabilizing mechanisms occur at different morphological scales. Observed processes are summarized below and visualized in Figure 5.1.

- Micro-scale: Armoring process
  At the micro-scale the self-stabilizing corresponds to the selective erosion leading to a coarsening of the surface layer, protecting the underlying finer bed material. This so-called armoring process leads to an increase of the mean grain size of the armor layer upon increasing discharge. This phenomenon was observed during experimental runs with relatively low hydraulic loading. Since the blue blocks were initially fully embedded in the base material, their visibility indicates enhanced micro-scale structuring. Figure 5.1 a) shows the armoring processes, revealed by visible blue blocks on the orthomosaic.

- Meso-scale: Formation of steps and pools
  At the meso-scale the self-stabilizing corresponds to the optimization of the roughness geometry. The channel responds to the exceeding of stability by reconfiguring itself towards a step-pool geometry. In the experiments, the formation of steps and pools could be identified by stable clusters of the large blocks. The block clusters acted as a fixed points allowing bedload to be deposited upstream to locally reduce the bed slope. However, they remained dynamic and reconfigured regularly with increased hydraulic load. Clusters of red, green and blue blocks building steps can be identified on the orthomosaic presented in Figure 5.1 b).

- Macro-scale: Alteration of the bedforms
  At the macro-scale the self-stabilization occurs due to an assimilation of the bed structures to riffles and pools resulting in alternate bar structures. Such structures were very distinctly observed in the experiments. They formed rather abruptly and were gradually eroded from upstream as hydraulic load increased. Figure 5.1 c) shows the flow depth on a bedform strongly marked by an alternate bar structures.

- Reach-scale: Reduction of the bed slope
  Self-stabilization at the reach-scale is thought to occur due to the reduction of slope. A reduction of the slope through rotational erosion was observed and quantified based on the bed elevation measurements. Figure 5.1 d) shows the strong erosion on the ramp head reflected in a decreased ramp slope.

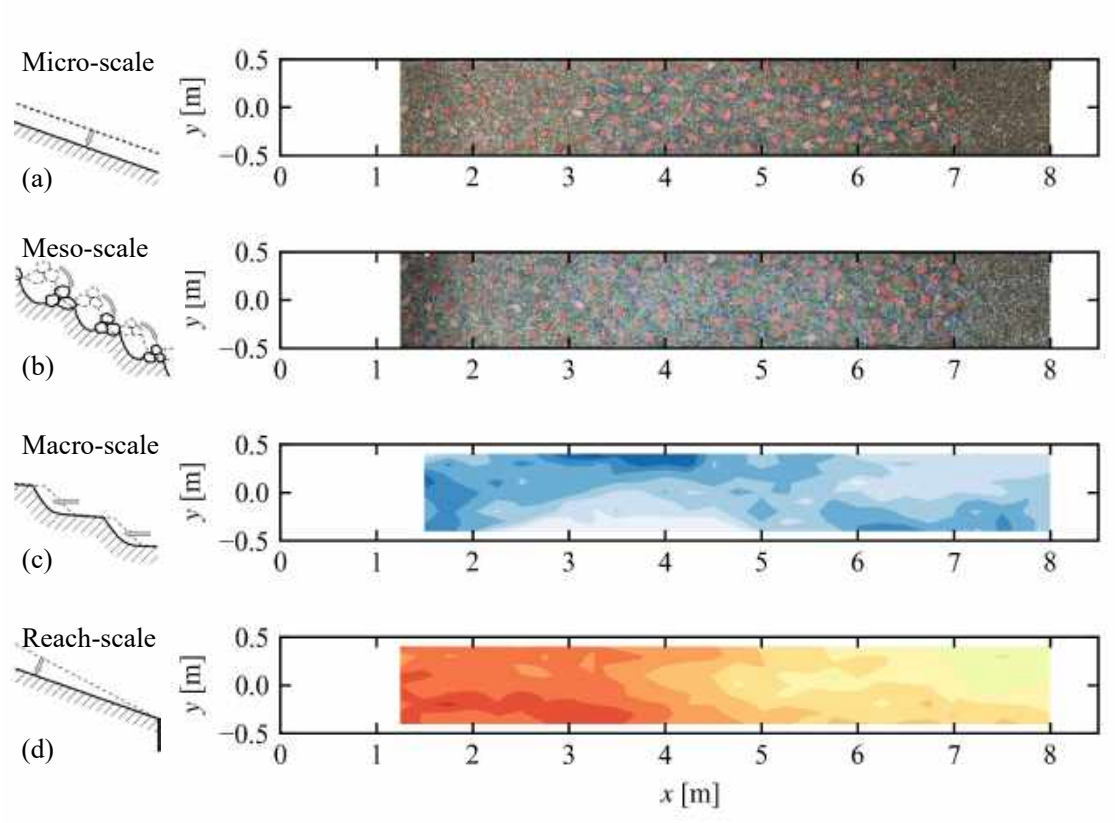

Figure 5.1: Observations of self-stabilizing mechanisms at different morphological scales. a) Armoring process revealed by visible blue blocks. b) Formation of steps and pools reflected in the clustering of the stabilizing blocks. c) Alteration of the bed-form towards an alternate-bar structure reflected in the flow depth (dark blue indicates high flow depths). d) Reduction of the bed slope due to strong erosion on the ramp head (red indicates strong erosion).

(2) Effect of LW

The objective of this part was to investigate the influence of LW on the above-mentioned structuring effects. To this end, two experiments series with stationary hydraulic loading coupled with LW loading were conducted. Of interest were both the deposition processes and the direct influences of LW deposits on bedload dynamics. In addition, the influence of LW on the stability and ecological performance of the ramp under increased hydraulic load was investigated. The key findings can be summarized as follows:

- LW was deposited around the protruding blocks. In the first runs many dispersed LW deposits formed, consisting of only one or two pieces. With increased hydraulic and

LW load, stable pieces trapped additional logs, leading to fewer but larger deposits. When the red blocks were fully submerged, deposits dissolved. Under non-plane bed conditions that formed at higher hydraulic hydraulic loads LW was not deposited.

- LW deposits can be associated with a significant alteration of the armoring process. Two consequences could be identified. (1) In the wake of LW deposits micro-scale structuring may be reduced in intensity. (2) On the channel side opposite to the LW deposits micro-scale structuring may be increased in intensity.

- On the respective side of the large LW deposits dominant bar features formed with increased hydraulic loading. The alternate bar structures were more pronounced and persistent on the beds structured under the influence of LW compared to the base case. This was reflected in a 50% higher variability of the bed elevations during three experimental runs (Figure 5.2 a)). LW might thus have a beneficial impact on flow and habitat diversity.

- In one experimental series with LW, reach-scale structuring established at lower specific discharges than in base case (Figure 5.2 b)). LW might thus lead to an acceleration of the structuring processes.

(2) Effect of the hydraulic load type

This series aimed to contextualize the effect of LW by investigating the structuring processes that develop under more realistic hydraulic conditions. A series with hydraulic loading by a flood hydrograph was carried out for this purpose. The main findings are:

- The morphological equilibrium associated with the peak discharge was not attained over the flood duration. In absolute terms, the structuring processes are therefore overestimated by stationary hydraulic loading.

- The structuring processes on all morphological scales initiated at the same at the same level of hydraulic load (q) for stationary and hydrograph loading (around $q = 35$ l/(sm) for macro- and reach-scale processes, Figure 5.2 a) and b)).

- Under the hydraulic load of a flood hydrograph the structuring process occured more gradually but also more steadily. The effect tends to vanish for very high hydraulic loads and the ramp conditions again become comparable (around $q = 60$ l/(sm), Figure 5.2).

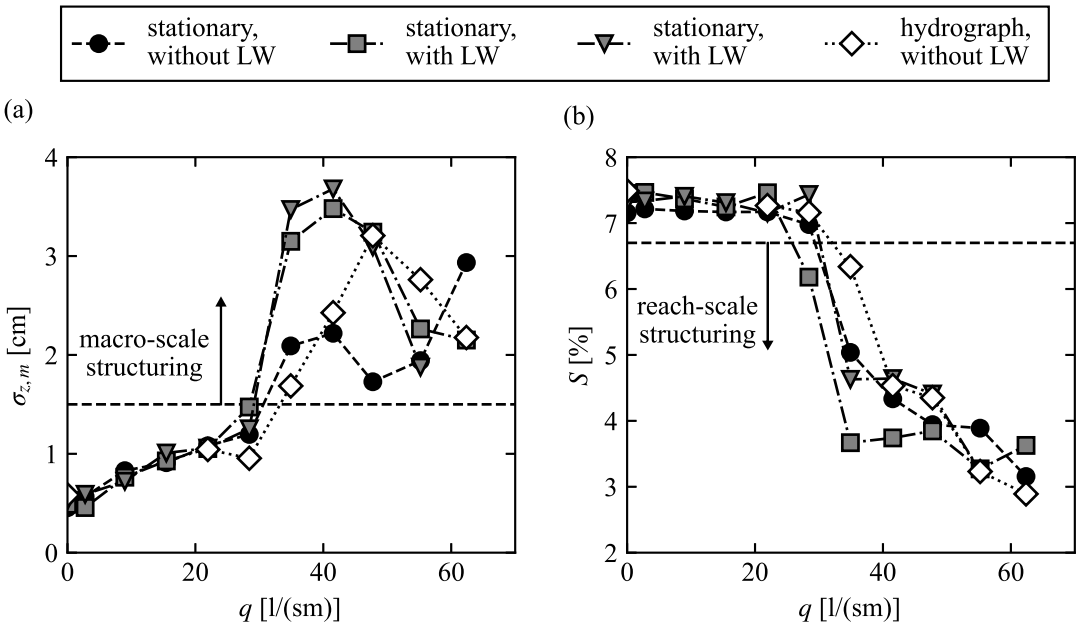

Figure 5.2: Comparison of the structuring processes developed during all four experiment series at a) macro-scale and b) reach-scale. a) Macro-scale processes are indicated by an increase of the variability in bed elevations σ, z, m. The process became prominent at the same hydraulic load for all experiment series. With respect to the base case, the intensity of the mechanism was more pronounced for the series with LW loading and increased more steadily for the series with hydraulic loading by a flood hydrograph. b) Reach scale processes are indicated by a decrease in slope. The effect initiated at the same hydraulic load, except for one series with LW, in which an acceleration of the processes was observed. With respect to the base case, the decrease in slope occurred more abruptly in the series with LW and more steadily in in the series with hydraulic loading by a flood hydrograph. The final condition of the ramp was comparable for all four series.

5.2 Outlook

LW proved to have a significant influence on the structuring processes of the dynamic ramp studied. Hybrid numerical simulations on the photogrammetrically modeled bed topographies would give further insight on the flow conditions that form on the ramp. This would allow to quantify the ecological benefit of LW by means of an ecomorphological index.

Notation

Symbols

a_i	coefficient [-]
A_c	catchment area [km^2]
$A_{c,f}$	forested catchment area [km^2]
c	Chézy coefficient [-]
CV	coefficient of variation [-]
d	grain diameter [m]
d_i	grain diameter at which i-% of the sediment sample is finer than [m]
d_0	diameter of the pipe in Darcy-Weisbach equation [m]
d_b	buoyant depth [m]
D	equivalent spherical block diameter [m]
EHQ	extreme flood [m^3/s]
f	Darcy Weisbach friction factor [-]
Fr	Froude number
g	gravitational acceleration [m/s^2]
h	flow depth [m]
h_f	friction loss height [m]
HMID	hydro-morphological index of diversity [-]
HQ_i	flood with a return period of i-years [m^3/s]
k	bed roughness height [m]
L	characteristic length [m]
L_f	forested stream length [km]
L_L	log length [m]
L_p	length of the pipe section in Darcy-Weisbach equation [m]
L_0	distance between obstacles [m]
m	mass [kg]
N_i	number in class i [-]
N_p	number of packages [-]
N_{tot}	total number [-]
N_A	number per unit area [m^{-2}]
$N_{L,tot}$	cumulative number of supplied logs [-]
$N_{L,\text{stable}}$	number of stable logs on the channel [-]
p	frequency of occurrence [-]
P	block protrusion [m]
q	specific discharge [m^2/s]
q_c	critical specific discharge [m^2/s]
q_{dim}	dimensioning specific discharge [m^2/s]
Q	discharge [m^3/s]
Q_i	discharge which is not exceeded i days per year [m^3/s]
Q_{max}	peak discharge [m^3/s]

R	hydraulic radius [m]
R_c	radius of curvature [m]
S	channel slope [-]
S_{dim}	dimensioning slope [-]
S_e	energy gradient [-]
S_0	inintial slope [-]
SL	sediment load [m^3]
t_{HQ}	flood duration [h]
t_{peak}	time of peak flow [h]
t_{tp}	time to peak [h]
T	return period [h]
U	average velocity [m/s]
U^*	shear velocity [m/s]
U_c	critical flow velocity [m/s]
V_d	discharge volume [m^3]
V_{eff}	effective large wood volume [m^3]
V_p	precipitation volume [m^3]
V_{pot}	potential large wood volume [m^3]
$V(i)$	partial diversity of a hydraulic variable i [-]
w	width [m]

Greek symbols

α	angle against the horizontal [°]
λ	scale factor [-]
Λ	proportion of the armor layer covered by blocks [-]
Λ_0	block placement density [-]
μ	mean value [-]
σ	standard deviation [-]
σ_z	standard deviation of the bed elevations [m]
$\sigma_{z,dim}$	dimensioning bed roughness [m]
$\sigma_{z,i}$	standard deviation of the bed elevations on the cross section i
$\sigma_{z,0}$	initial bed roughness [m]

Subscripts

m	mean
M	model scale
max	maximum
min	minimum
P	prototype scale

Abbreviations

GCP	ground control points
GIS	geographical information system
LW	Large wood
PIV	particle image velocimetry
VPE	variable power equation

References

Abbe, T. B., & Montgomery, D. R. (2003). Patterns and processes of wood debris accumulation in the Queets river basin, Washington. *Geomorphology*, *51*(1-3), 81–107. https://doi.org/10.1016/S0169-555X(02)00326-4

Aberle, J., & Smart, G. M. (2003). The influence of roughness structure on flow resistance on steep slopes. *Journal of Hydraulic Research*, *41*(3), 259–269. https://doi.org/10.1080/00221680309499971

Aberle, J. (2000). *Aberle, Jochen. Untersuchung der Rauheitsstruktur zur Bestimmung des Fließwiderstandes in Gebirgsbächen unter Klarwasserabfluß* (Doctoral dissertation). Institut für Wasserwirtschaft und Kulturtechnik, Universität Karlsruhe (TH).

BAFU. (2019). *Schwemmholz in Fliessgewässern*. www.bafu.admin.ch/wasser

Baillie, B. R., & Davies, T. R. (2002). Influence of large woody debris on channel morphology in native forest and pine plantation streams in the Nelson region, New Zealand. *New Zealand Journal of Marine and Freshwater Research*, *36*(4), 763–774. https://doi.org/10.1080/00288330.2002.9517129

Barbour, M. T., Gerritsen, J., Snyder, B. D., & Stribling, J. B. (1999). Rapid Bioassessment Protocols for Use in Streams and Wadeable Rivers: Periphyton, Benthic Macroinvertebrates and Fish, Second Edition.

Bathurst, J. C. (1985). Flow Resistance Estimation in Mountain Rivers. *Journal of Hydraulic Engineering*, *111*(4), 625–643. https://doi.org/10.1061/(ASCE)0733-9429(1985)111:4(625)

Bathurst, J. (2002). At-a-site variation and minimum flow resistance for mountain rivers. *Journal of Hydrology*, *269*(1-2), 11–26. https://doi.org/10.1016/S0022-1694(02)00191-9

Beckman, N. D., & Wohl, E. (2014). Carbon storage in mountainous headwater streams: The role of old-growth forest and logjams. *Water Resources Research*, *50*(3), 2376–2393. https://doi.org/10.1002/2013WR014167

Beebe, J. T. (2000). Flume Studies of the Effect of Perpendicular Log Obstructions on Flow Patterns and Bed Topography. *The Great Lakes Geographer*, *7*, 9–25.

Benda, L. E., & Sias, J. C. (2003). A quantitative framework for evaluating the mass balance of in-stream organic debris. *Forest Ecology and Management*, *172*(1), 1–16. https://doi.org/10.1016/S0378-1127(01)00576-X

Bertoldi, W., Gurnell, A., & Welber, M. (2013). Wood recruitment and retention: The fate of eroded trees on a braided river explored using a combination of field and remotely-sensed data sources. *Geomorphology*, *180-181*, 146–155. https://doi.org/10.1016/j.geomorph.2012.10.003

Bertoldi, W., Welber, M., Mao, L., Zanella, S., & Comiti, F. (2014). A flume experiment on wood storage and remobilization in braided river systems: A FLUME EXPERIMENT ON WOOD DYNAMICS IN BRAIDED RIVER SYSTEMS. *Earth Surface Processes and Landforms*, *39*(6), 804–813. https://doi.org/10.1002/esp.3537

Beschta, R. (1983). The effects of large organic debris upon channel morphology: A flume study. *Proceedings of the DB Simons Symposium on Erosion and Sedimentation, 8*, 63–78.

Bocchiola, D., Rulli, M. C., & Rosso, R. (2008). A flume experiment on the formation of wood jams in rivers: EXPERIMENT ON WOOD JAMS. *Water Resources Research, 44*(2). https://doi.org/10.1029/2006WR005846

Bocchiola, D., Rulli, M., & Rosso, R. (2006a). Flume experiments on wood entrainment in rivers. *Advances in Water Resources, 29*(8), 1182–1195. https://doi.org/10.1016/j.advwatres.2005.09.006

Bocchiola, D., Rulli, M., & Rosso, R. (2006b). Transport of large woody debris in the presence of obstacles. *Geomorphology, 76*(1-2), 166–178. https://doi.org/10.1016/j.geomorph.2005.08.016

Braudrick, C. A., & Grant, G. E. (2000). When do logs move in rivers? *Water Resources Research, 36*(2), 571–583. https://doi.org/10.1029/1999WR900290

Braudrick, C. A., & Grant, G. E. (2001). Transport and deposition of large woody debris in streams: A flume experiment. *Geomorphology, 41*(4), 263–283. https://doi.org/10.1016/S0169-555X(01)00058-7

Braudrick, C. A., Grant, G. E., Ishikawa, Y., & Ikeda, H. (1997). Dynamics of Wood Transport in Streams: A Flume Experiment. *Earth Surface Processes and Landforms, 22*(7), 669–683. https://doi.org/10.1002/(SICI)1096-9837(199707)22:7<669::AID-ESP740>3.0.CO;2-L

Bray, D. I. (1979). Estimating Average Velocity in Gravel-Bed Rivers. *Journal of the Hydraulics Division, 105*(9), 1103–1122. https://doi.org/10.1061/JYCEAJ.0005270

Chen, X., Hassan, M. A., An, C., & Fu, X. (2020). Rough Correlations: Meta-Analysis of Roughness Measures in Gravel Bed Rivers. *Water Resources Research, 56*(8). https://doi.org/10.1029/2020WR027079

Collins, B. D., Montgomery, D. R., Fetherston, K. L., & Abbe, T. B. (2012). The floodplain large-wood cycle hypothesis: A mechanism for the physical and biotic structuring of temperate forested alluvial valleys in the North Pacific coastal ecoregion. *Geomorphology, 139-140*, 460–470. https://doi.org/10.1016/j.geomorph.2011.11.011

Comiti, F., Andreoli, A., Mao, L., & Lenzi, M. A. (2008). Wood storage in three mountain streams of the Southern Andes and its hydro-morphological effects. *Earth Surface Processes and Landforms, 33*(2), 244–262. https://doi.org/10.1002/esp.1541

Davidson, S. L., & Eaton, B. C. (2013). Modeling channel morphodynamic response to variations in large wood: Implications for stream rehabilitation in degraded watersheds. *Geomorphology, 202*, 59–73. https://doi.org/10.1016/j.geomorph.2012.10.005

Dudley, S. J., Fischenich, J. C., & Abt, S. R. (1998). EFFECT OF WOODY DEBRIS ENTRAPMENT ON FLOW RESISTANCE. *Journal of the American Water Resources Association, 34*(5), 1189–1197. https://doi.org/10.1111/j.1752-1688.1998.tb04164.x

DWA, A. u. A., Deutsche Vereinigung für Wasserwirtschaft. (2009). Naturnahe Sohlengleiten. *DWA-Themen, WW-1.2-9*.

Faustini, J. M., & Jones, J. A. (2003). Influence of large woody debris on channel morphology and dynamics in steep, boulder-rich mountain streams, western Cascades, Oregon. *Geomorphology*, *51*(1-3), 187–205. https://doi.org/10.1016/S0169-555X(02)00336-7

Ferguson, R. (2007). Flow resistance equations for gravel- and boulder-bed streams. *Water Resources Research*, *43*(5). https://doi.org/10.1029/2006WR005422

Friedrich, H., Ravazzolo, D., Ruiz-Villanueva, V., Schalko, I., Spreitzer, G., Tunnicliffe, J., & Weitbrecht, V. (2022). Physical modelling of large wood (LW) processes relevant for river management: Perspectives from New Zealand and Switzerland. *Earth Surface Processes and Landforms*, *47*(1), 32–57. https://doi.org/10.1002/esp.5181

Gallisdorfer, M. S., Bennett, S. J., Atkinson, J. F., Ghaneeizad, S. M., Brooks, A. P., Simon, A., & Langendoen, E. J. (2014). Physical-scale model designs for engineered log jams in rivers. *Journal of Hydro-environment Research*, *8*(2), 115–128. https://doi.org/10.1016/j.jher.2013.10.002

Gippel, C. J. (1995). Environmental Hydraulics of Large Woody Debris in Streams and Rivers. *Journal of Environmental Engineering*, *121*(5), 388–395. https://doi.org/10.1061/(ASCE)0733-9372(1995)121:5(388)

Gostner, W., Alp, M., Schleiss, A. J., & Robinson, C. T. (2013). The hydro-morphological index of diversity: A tool for describing habitat heterogeneity in river engineering projects. *Hydrobiologia*, *712*(1), 43–60. https://doi.org/10.1007/s10750-012-1288-5

Griffiths, G. A. (1981). Flow Resistance in Coarse Gravel Bed Rivers. *Journal of the Hydraulics Division*, *107*(7), 899–918. https://doi.org/10.1061/JYCEAJ.0005699

Gurnell, A. M., Bertoldi, W., & Corenblit, D. (2012). Changing river channels: The roles of hydrological processes, plants and pioneer fluvial landforms in humid temperate, mixed load, gravel bed rivers. *Earth-Science Reviews*, *111*(1-2), 129–141. https://doi.org/10.1016/j.earscirev.2011.11.005

Guyette, R. P., Cole, W. G., Dey, D. C., & Muzika, R.-M. (2002). Perspectives on the age and distribution of large wood in riparian carbon pools. *59*, 8.

Hey, R. D. (1979). Flow Resistance in Gravel-Bed Rivers. *Journal of the Hydraulics Division*, *105*(4), 365–379. https://doi.org/10.1061/JYCEAJ.0005178

Hohermuth, B., & Weitbrecht, V. (2018). Influence of Bed-Load Transport on Flow Resistance of Step-Pool Channels. *Water Resources Research*, *54*(8), 5567–5583. https://doi.org/10.1029/2017WR021523

Huet, M. (1949). Aperçu des relations entre la pente et les populations piscicoles des eaux courants. *Schweizerische Zeitschrift für Hydrologie*, *11*, 333–351.

Keller, E. A., & Swanson, F. J. (1979). Effects of large organic material on channel form and fluvial processes. *Earth Surface Processes*, *4*(4), 361–380. https://doi.org/10.1002/esp.3290040406

Lange, D. (2007). Blockrampen - ökologische Bauwerke zur Sohlstabilisierung. *Blockrampen, Anforderungen und Bauweisen*, 5–20.

Liechti, P., Sieber, U., Blücher, U. v., & Willi, H. P. (1998). Methoden zur Untersuchung und Beurteilung der Fließgewässer: Modul-Stufen-Konzept (Bundesamt für Umwelt (BAFU), Ed.). *Mitteilungen zum Gewässerschutz*, *26*.

Maager, F., Hohermuth, B., Weitbrecht, V., & Boes, R. M. (2019). Influence of block arrangement on stability of man-made step-pool sequences in steep mountain streams. *Proceedings of the 38th IAHR World Congress*, 2110–2116. https://doi.org/10.3850/38WC092019-0646

MacFarlane, W. A., & Wohl, E. (2003). Influence of step composition on step geometry and flow resistance in step-pool streams of the Washington Cascades: Step geometry and flow resistance. *Water Resources Research, 39*(2). https://doi.org/10.1029/2001WR001238

Mao, L., Ravazzolo, D., & Bertoldi, W. (2020). The role of vegetation and large wood on the topographic characteristics of braided river systems. *Geomorphology, 367*, 107299. https://doi.org/10.1016/j.geomorph.2020.107299

Mazzorana, B., Zischg, A., Largiader, A., & Hübl, J. (2009). Hazard index maps for woody material recruitment and transport in alpine catchments. *Natural Hazards and Earth System Sciences, 9*(1), 197–209. https://doi.org/10.5194/nhess-9-197-2009

Mutz, M., Kalbus, E., & Meinecke, S. (2007). Effect of instream wood on vertical water flux in low-energy sand bed flume experiments. *Water Resources Research, 43*(10). https://doi.org/10.1029/2006WR005676

Nakamura, F., & Swanson, F. J. (1994). Distribution of coarse woody debris in a mountain stream, western Cascade Range, Oregon. *Canadian Journal of Forest Research, 24*(12), 2395–2403. https://doi.org/10.1139/x94-309

Osei, N. A., Gurnell, A. M., & Harvey, G. L. (2015). The role of large wood in retaining fine sediment, organic matter and plant propagules in a small, single-thread forest river. *Geomorphology, 235*, 77–87. https://doi.org/10.1016/j.geomorph.2015.01.031

Reeves, G. H., Burnett, K. M., & McGarry, E. V. (2003). Sources of large wood in the main stem of a fourth-order watershed in coastal Oregon. *Canadian Journal of Forest Research, 33*(8), 1363–1370. https://doi.org/10.1139/x03-095

Rickenmann, D. (1997). Schwemmholz und Hochwasser [Medium: text/html,application/pdf Publisher: Schweizerischer Wasserwirtschaftsverband]. *Wasser Energie Luft, 89*(5-6), 115–119. https://doi.org/10.5169/SEALS-940182

Rickenmann, D., & Recking, A. (2011). Evaluation of flow resistance in gravel-bed rivers through a large field data set. *Water Resources Research, 47*(7). https://doi.org/10.1029/2010WR009793

Ruiz-Villanueva, V., Díez-Herrero, A., Ballesteros, J. A., & Bodoque, J. M. (2014). Potential large woody debris recruitment due to landslides, bank erosion and floods in mountain basins: A quantitative estimation approach: Recruitable large woody debris in mountain basins. *River Research and Applications, 30*(1), 81–97. https://doi.org/10.1002/rra.2614

Ruiz-Villanueva, V., Mazzorana, B., Bladé, E., Bürkli, L., Iribarren-Anacona, P., Mao, L., Nakamura, F., Ravazzolo, D., Rickenmann, D., Sanz-Ramos, M., Stoffel, M., & Wohl, E. (2019). Characterization of wood-laden flows in rivers: Wood-laden flows. *Earth Surface Processes and Landforms, 44*(9), 1694–1709. https://doi.org/10.1002/esp.4603

Ruiz-Villanueva, V., Piégay, H., Gurnell, A. M., Marston, R. A., & Stoffel, M. (2016). Recent advances quantifying the large wood dynamics in river basins: New methods and

remaining challenges: Large Wood Dynamics. *Reviews of Geophysics, 54*(3), 611–652. https://doi.org/10.1002/2015RG000514

Ruiz-Villanueva, V., Wyżga, B., Mikuś, P., Hajdukiewicz, H., & Stoffel, M. (2016). The role of flood hydrograph in the remobilization of large wood in a wide mountain river. *Journal of Hydrology, 541*, 330–343. https://doi.org/10.1016/j.jhydrol.2016.02.060

Schalko, I. (2018). *Modeling hazards related to large wood in rivers* (PhD Thesis). ETH Zurich.

Schalko, I., Wohl, E., & Nepf, H. M. (2021). Flow and wake characteristics associated with large wood to inform river restoration. *Scientific Reports, 11*(1), 8644. https://doi.org/10.1038/s41598-021-87892-7

Shields, F. D., & Gippel, C. J. (1995). Prediction of Effects of Woody Debris Removal on Flow Resistance. *Journal of Hydraulic Engineering, 121*(4), 341–354. https://doi.org/10.1061/(ASCE)0733-9429(1995)121:4(341)

Smart, G. M., & Jaeggi, M. N. R. (1983). Sediment transport on steep slopes. *Mitteilungen der Versuchsanstalt für Wasserbau, Hydrologie und Glaziologie, 64*, 91–191.

Steeb, N., Rickenmann, D., Badoux, A., & Rickli, C. (2019). Empirische Schätzformeln. In B. für Umwelt (BAFU) (Ed.), *Schwemmholz in Fliessgewässern. Ein praxisorientiertes Forschungsprojekt*. Bundesamt für Umwelt.

Svoboda, C. D., & Russell, K. (2011). Flume Analysis of Engineered Large Wood Structures for Scour Development and Habitat. *World Environmental and Water Resources Congress 2011*, 2572–2581. https://doi.org/10.1061/41173(414)267

Tamagni, S. (2013). Unstructured block ramps. *VAW Mitteilungen, 223*.

Tamagni, S., Weitbrecht, V., & Boes, R. (2014). An Ecological and Engineering View on Unstructured Block Ramps. *River Flow*, 2453–2460.

Tamagni, S., Weitbrecht, V., & Boes, R. M. (2010). Design of unstructured block ramps: A state-of-the-art review. In A. Dittrich, K. Koll, J. Aberle, & P. Geisenhainer (Eds.), *River flow 2010* (pp. 729–736). Bundesanstalt für Wasserbau.

Thomas, R. E., Johnson, M. F., Frostick, L. E., Parsons, D. R., Bouma, T. J., Dijkstra, J. T., Eiff, O., Gobert, S., Henry, P.-Y., Kemp, P., Mclelland, S. J., Moulin, F. Y., Myrhaug, D., Neyts, A., Paul, M., Penning, W. E., Puijalon, S., Rice, S. P., Stanica, A., … Vousdoukas, M. I. (2014). Physical modelling of water, fauna and flora: Knowledge gaps, avenues for future research and infrastructural needs. *Journal of Hydraulic Research, 52*(3), 311–325. https://doi.org/10.1080/00221686.2013.876453

Tognacca, C., Catteneo, G., Rossi, V., Tamagni, S., Tognacca, S., & Gardengi, C. (2019). *Fiume Ticino: Studio sul transporto solido nel Ticino da Bedretto alla Foce - Risanamento del bilancio in materiale solido di fondo* (interner Bericht). Beffa Tognacca Sagl. Claro.

Tognacca, C., Toschini, E., & Tognacca, S. (2021). *Ponte sul Ticino sotto Ronco Bedretto: Formazione rampa dinamica - Sperimentazione su modello fisico* (interner Bericht). Laboratorium3D. Biasca.

Tognacca, S., Tognacca, C., Toschini, E., & Tamagni, S. (2021). Laboruntersuchung zum Stabilitätsverhalten eigendynamischer Rampen. *Wasserbau in Zeiten von Energiewende, Gewässerschutz und Klimawandel, Band 2*, 561–569. https://doi.org/10.3929/ethz-b-000499752

Wallerstein, N. P., Alonso, C. V., Bennett, S. J., & Thorne, C. R. (2001). Distorted Froude-scaled flume analysis of large woody debris. *Earth Surface Processes and Landforms*, *26*(12), 1265–1283. https://doi.org/10.1002/esp.271

Weichert, R. (2006). *Bed morphology and stability of steep open channels* (PhD Thesis). ETH Zurich.

Weichert, R., Bezzola, G. R., & Minor, H.-E. (2007). Stufen-Becken-Abfolgen als sohlstabilisierende Massnahme. *Wasser Energie Luft*, *99*(2), 161–166.

Weichert, R., Bezzola, G. R., & Minor, H.-E. (2009). Bed erosion in steep open channels. *Journal of Hydraulic Research*, *47*(3), 360–371. https://doi.org/10.1080/00221686.2009.9522007

Welber, M., Bertoldi, W., & Tubino, M. (2013). Wood dispersal in braided streams: Results from physical modeling: Wood Dispersal in Braided Streams. *Water Resources Research*, *49*(11), 7388–7400. https://doi.org/10.1002/2013WR014046

Wilcox, A. C., & Wohl, E. E. (2006). Flow resistance dynamics in step-pool stream channels: 1. Large woody debris and controls on total resistance: FLOW RESISTANCE DYNAMICS, 1. *Water Resources Research*, *42*(5). https://doi.org/10.1029/2005WR004277

Wohl, E., Angermeier, P. L., Bledsoe, B., Kondolf, G. M., MacDonnell, L., Merritt, D. M., Palmer, M. A., Poff, N. L., & Tarboton, D. (2005). River restoration. *Water Resources Research*, *41*(10). https://doi.org/10.1029/2005WR003985

Wohl, E., & Jaeger, K. (2009). A conceptual model for the longitudinal distribution of wood in mountain streams. *Earth Surface Processes and Landforms*, *34*(3), 329–344. https://doi.org/10.1002/esp.1722

Wohl, E., Lane, S. N., & Wilcox, A. C. (2015). The science and practice of river restoration. *Water Resources Research*, *51*(8), 5974–5997. https://doi.org/10.1002/2014WR016874

Wohl, E., & Scott, D. N. (2017). Wood and sediment storage and dynamics in river corridors: Wood and Sediment Dynamics in River Corridors. *Earth Surface Processes and Landforms*, *42*(1), 5–23. https://doi.org/10.1002/esp.3909

Zarn, B. (1992). *Lokale Gerinneaufweitungen: Eine Massnahme zur Sohlenstabilisierung der Emme bei Utzendorf* (PhD Thesis). ETH Zurich.

A Orthomosaics

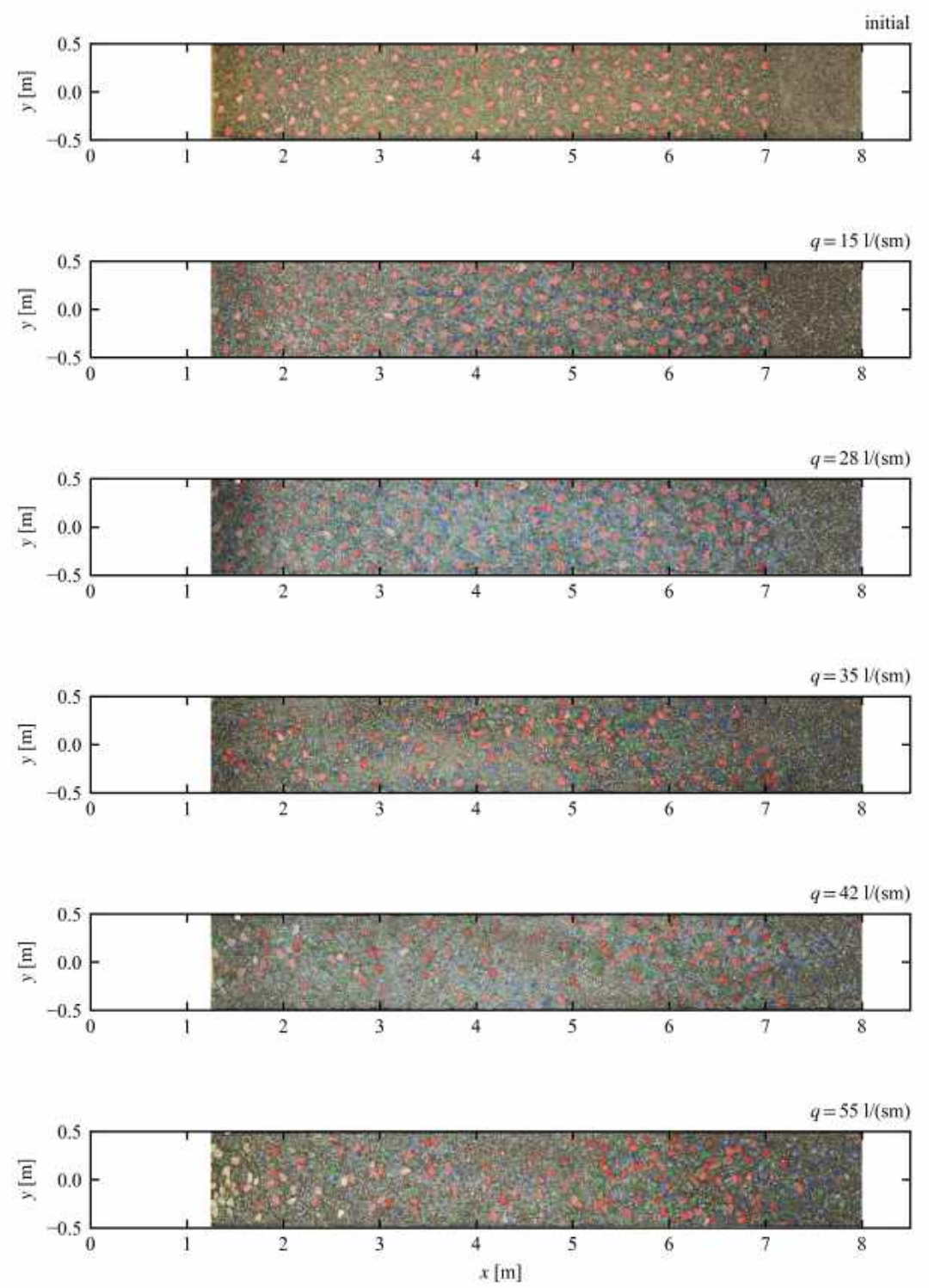

Figure A.1: Orthomosaics of series S1.

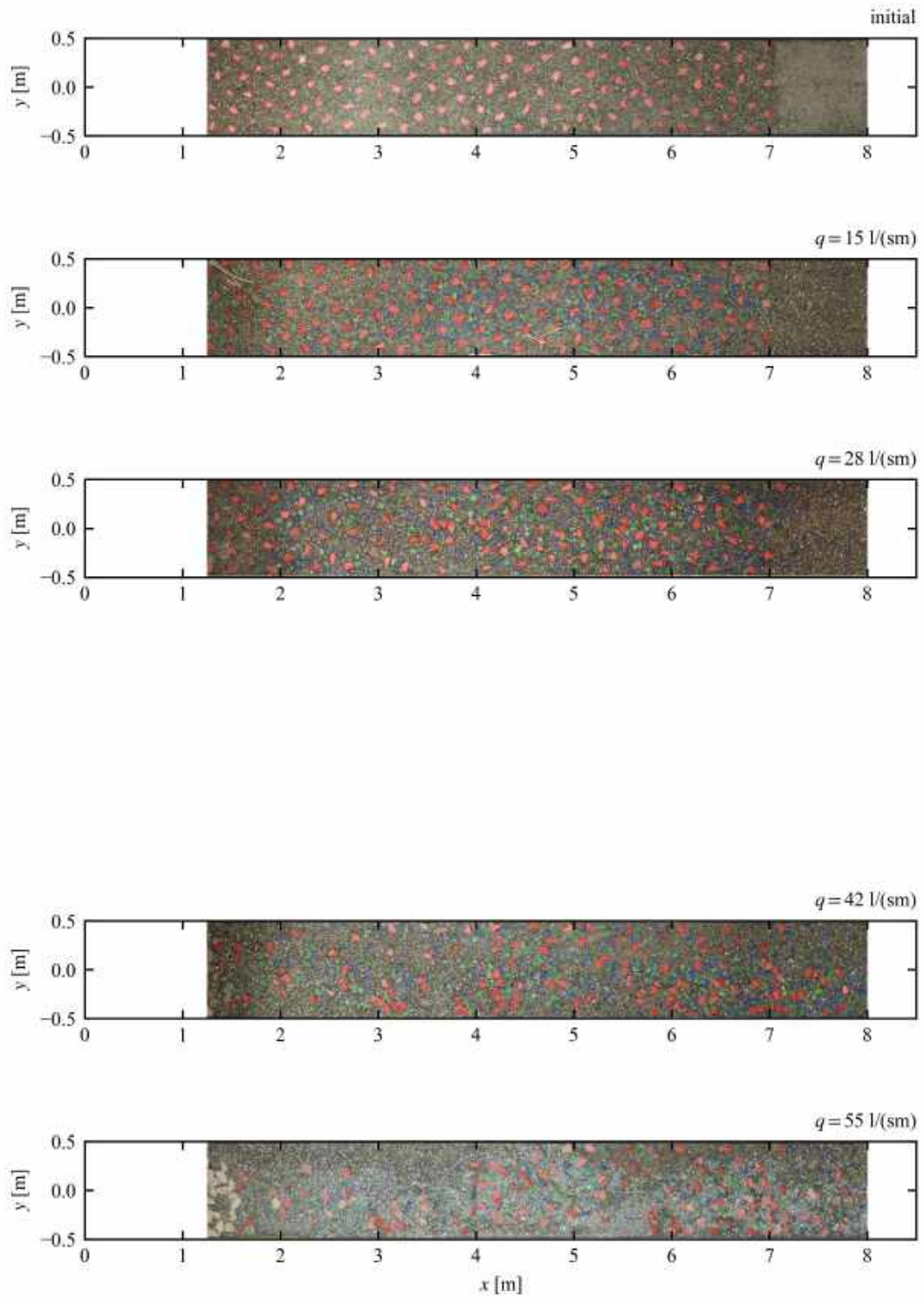

Figure A.2: Orthomosaics of series S2.

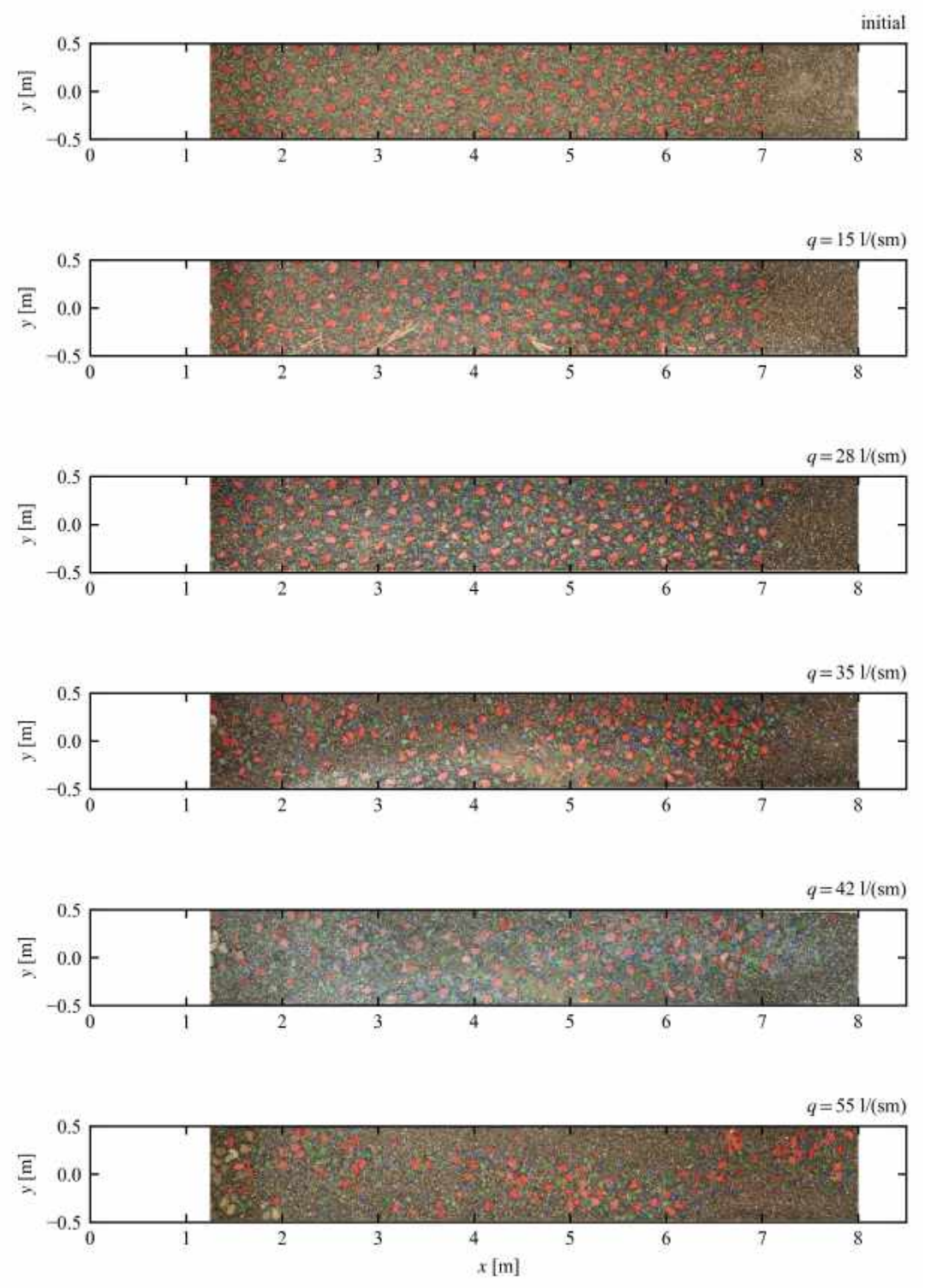

Figure A.3: Orthomosaics of series S3.

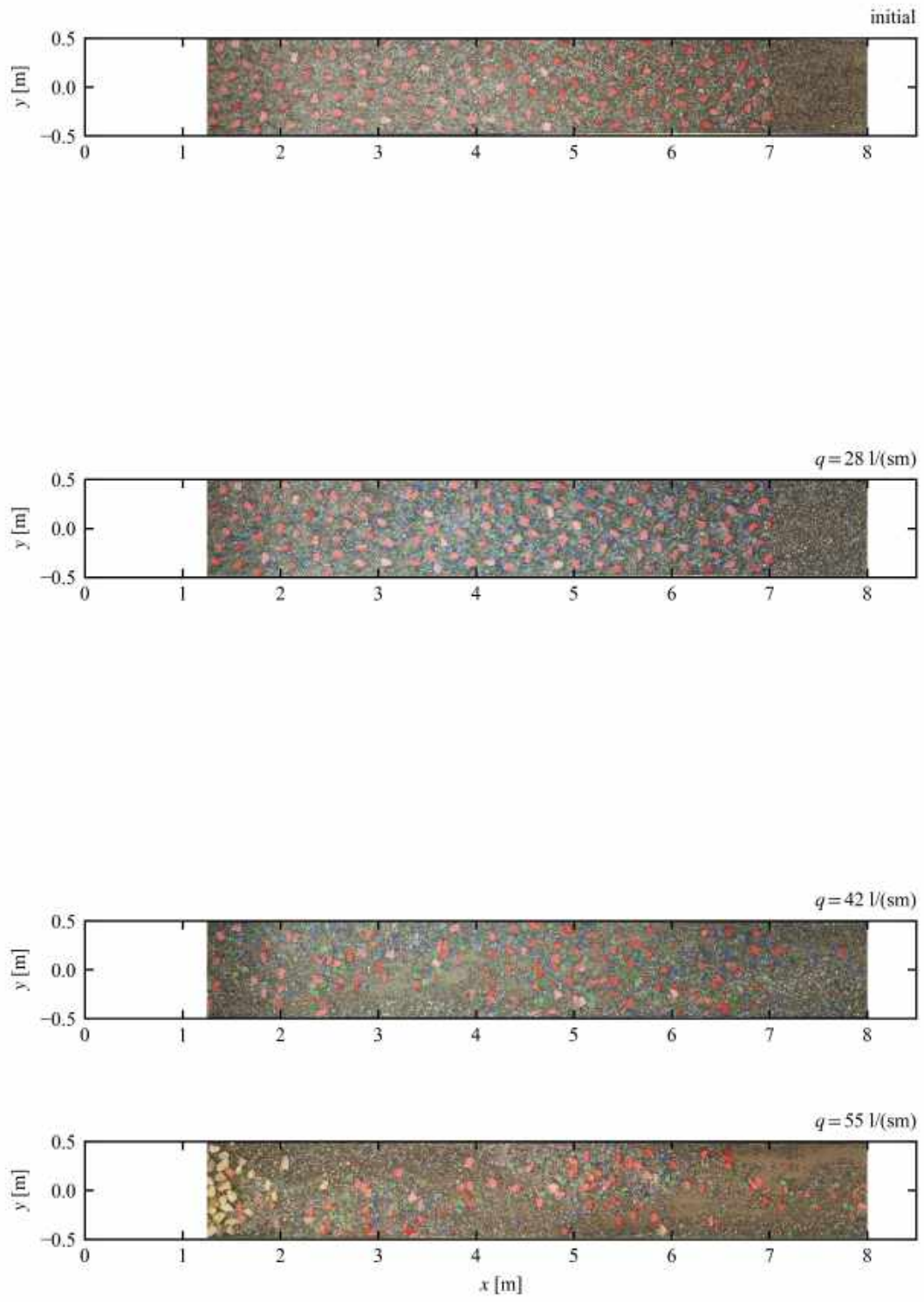

Figure A.4: Orthomosaics of series S4.

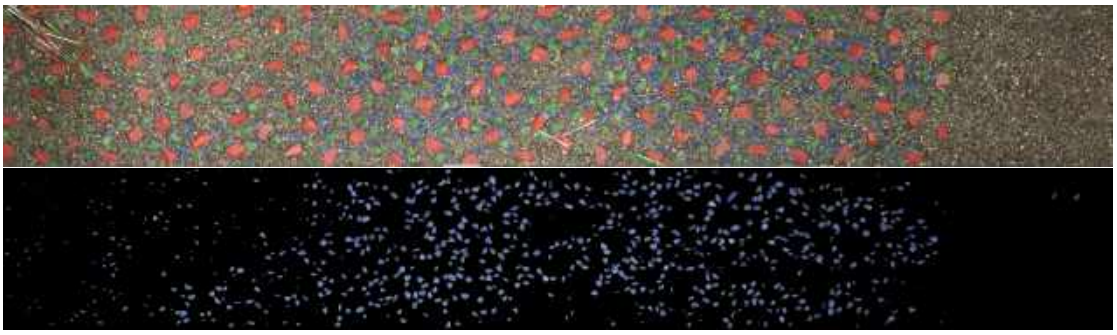

Figure A.5: Identification of the blue blocks at the example of the stable bed after q = 15 l/(sm) in series S2.

B LW deposits

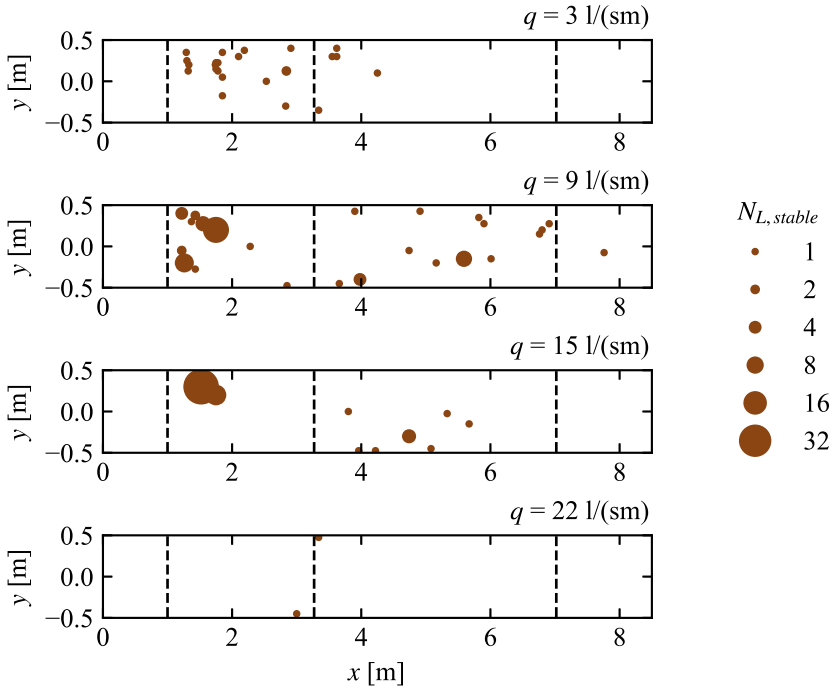

Figure B.1: Series S2: Number and position of deposited logs.

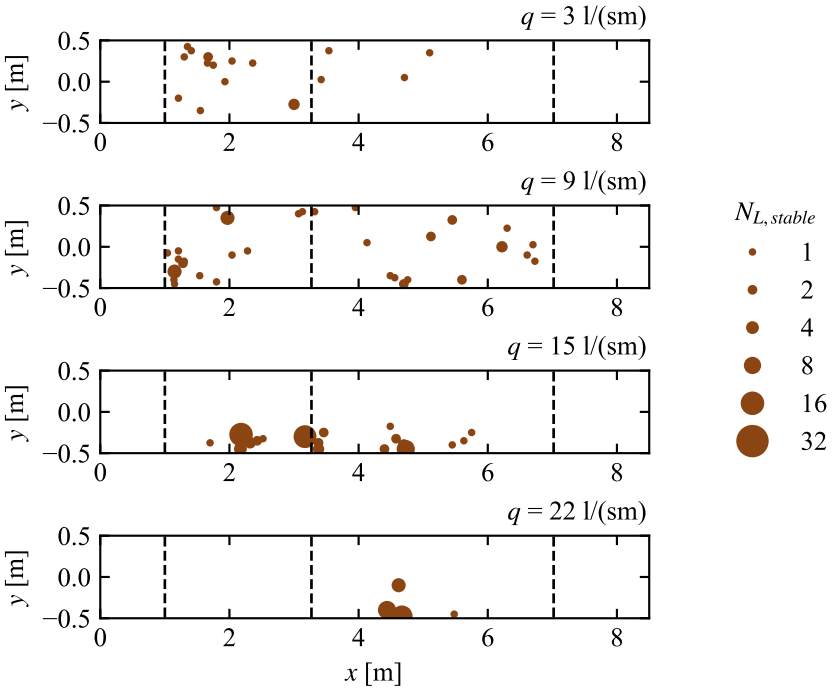

Figure B.2: Series S3: Number and position of deposited logs.

C Bed elevation

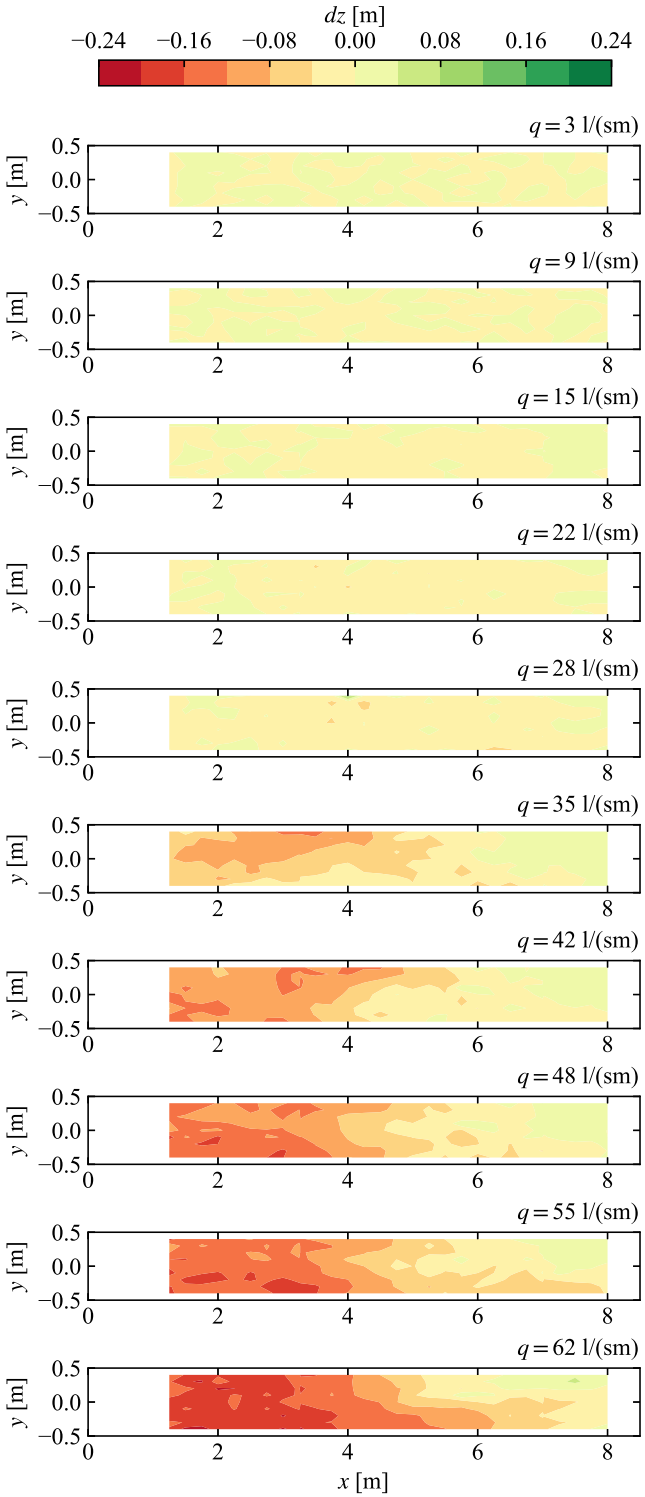

Figure C.1: Series S1: Deviation from the initial bed elevation *dz*.

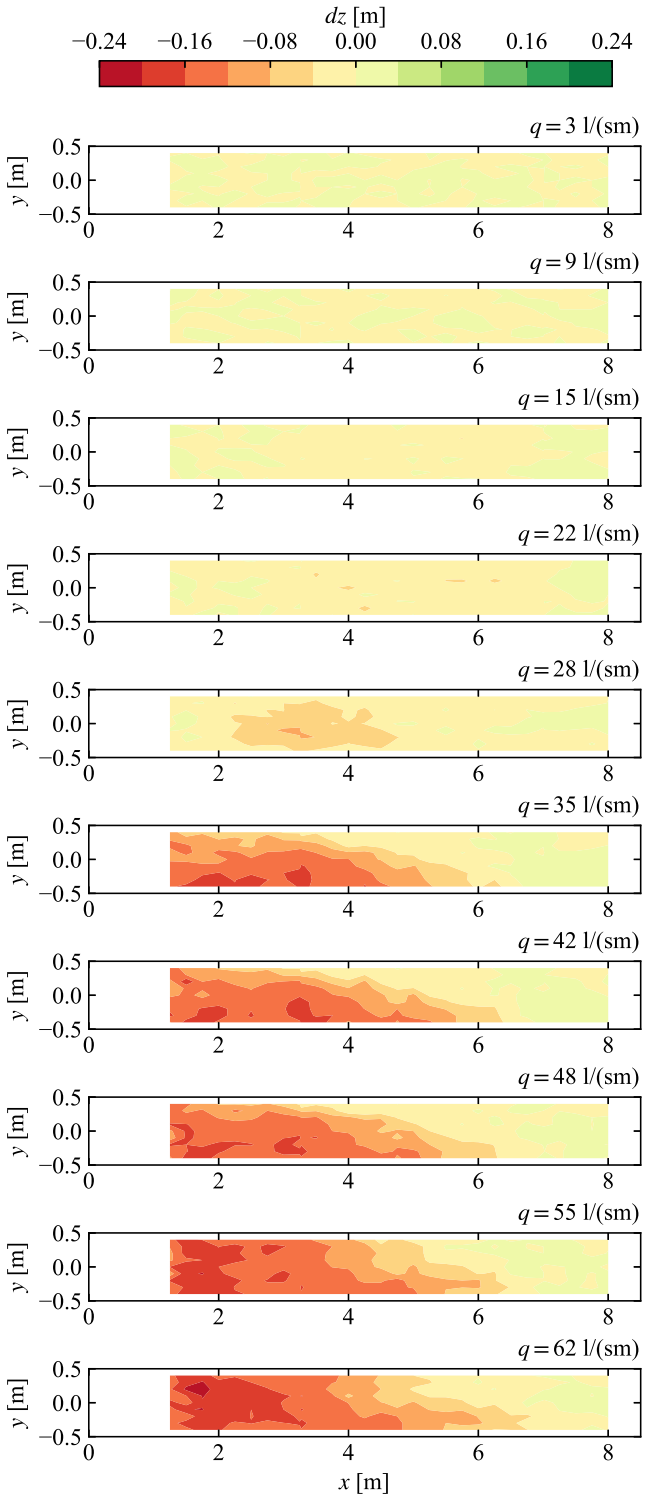

Figure C.2: Series S2: Deviation from the initial bed elevation dz.

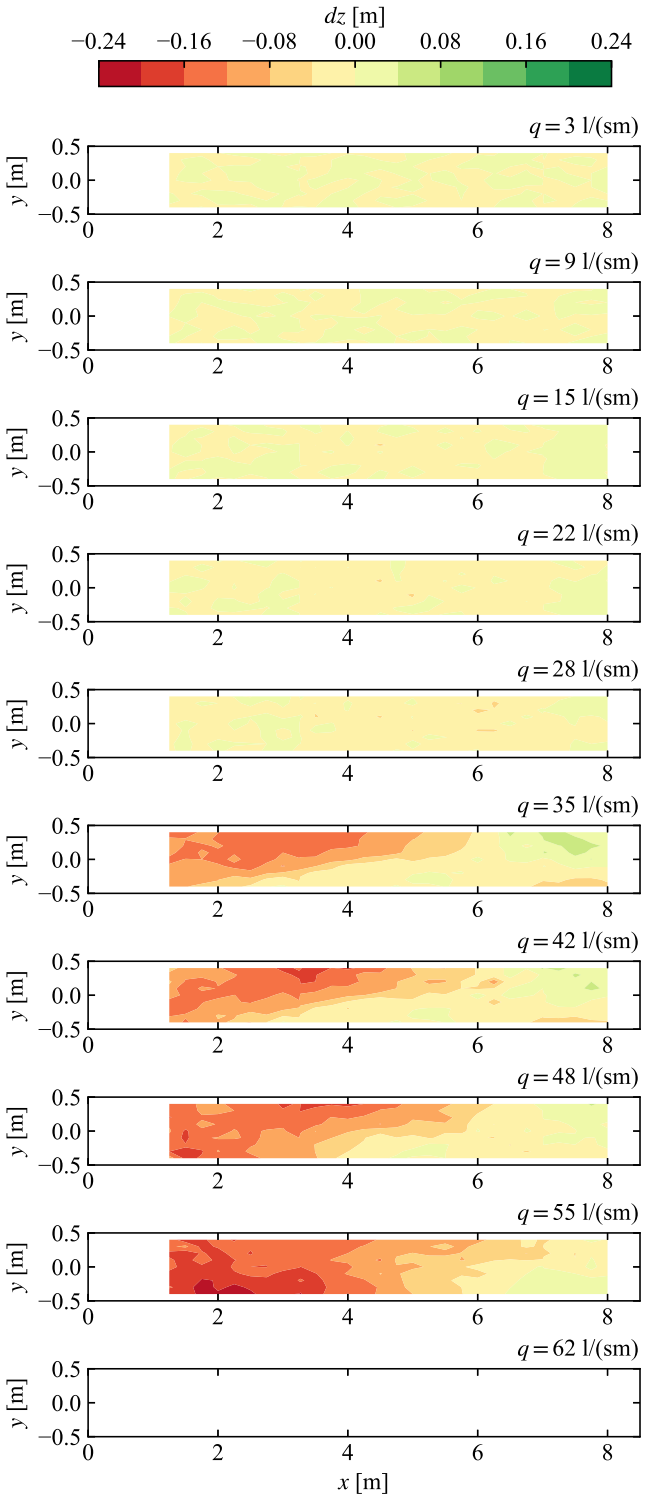

Figure C.3: Series S3: Deviation from the initial bed elevation dz. The maximum erosion of the inlet of dz = -0.15 cm was reached at q = 55 l/(sm). q = 62 l/(sm) could therefore not be tested.

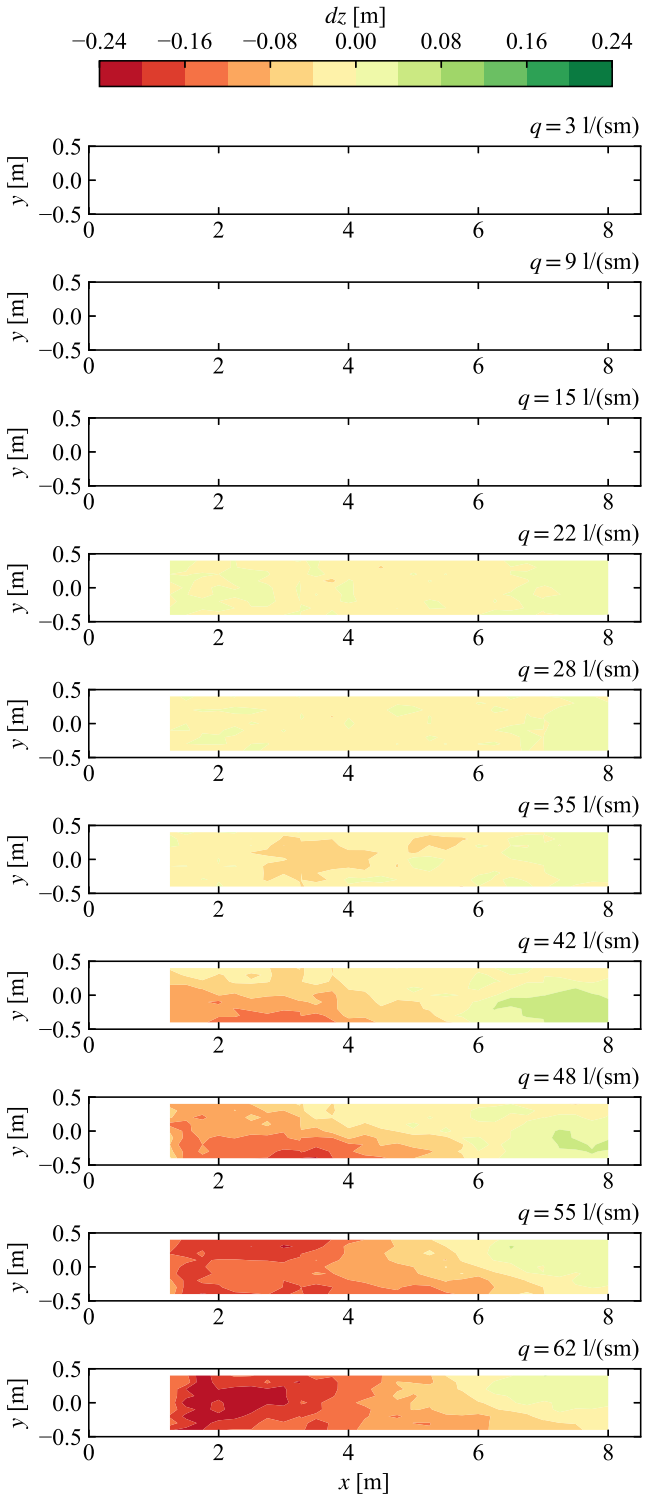

Figure C.4: Series S4: Deviation from the initial bed elevation dz.

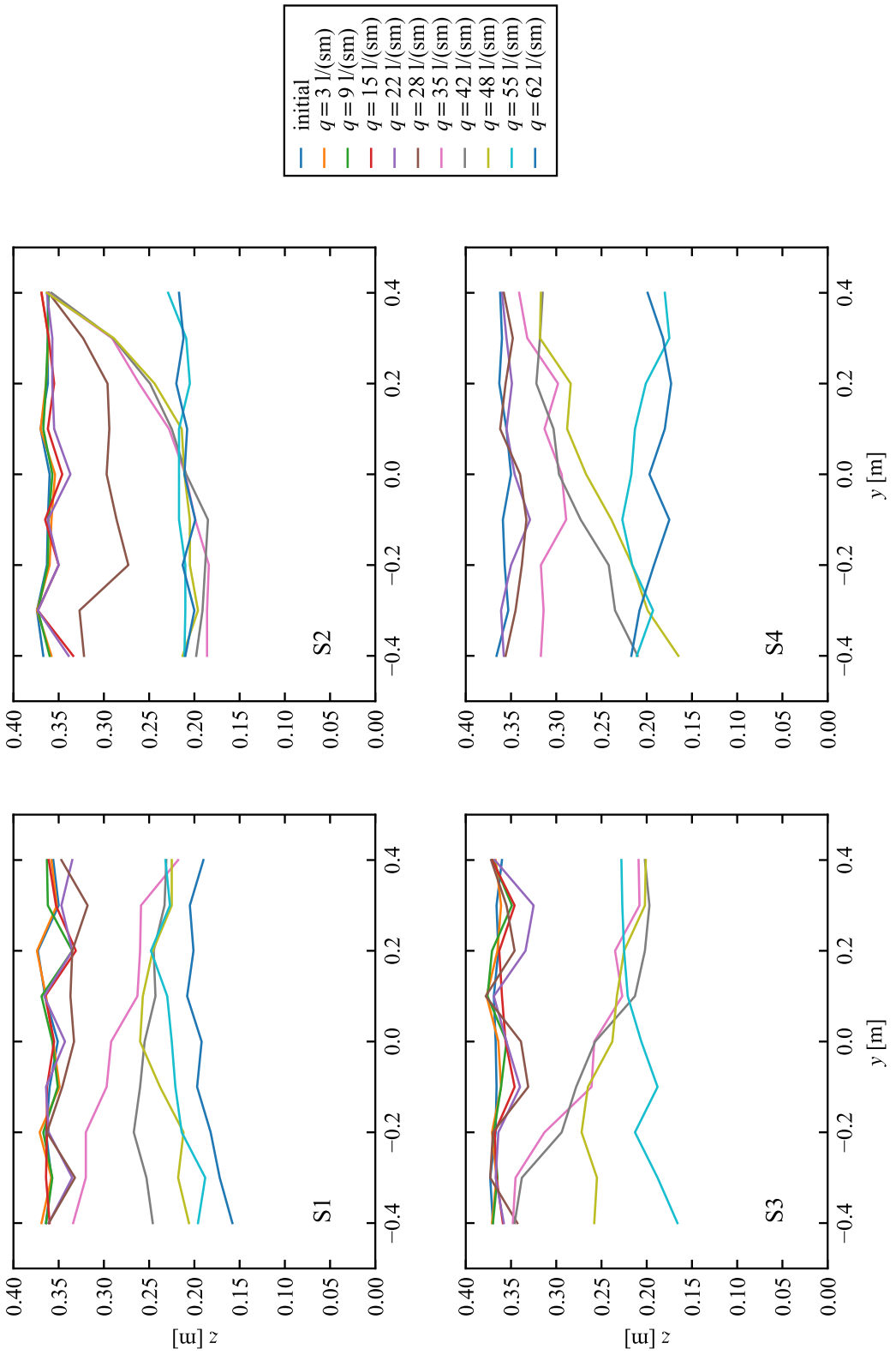

Figure C.5: Cross profiles at $x = 3.25$ m (ramp head).

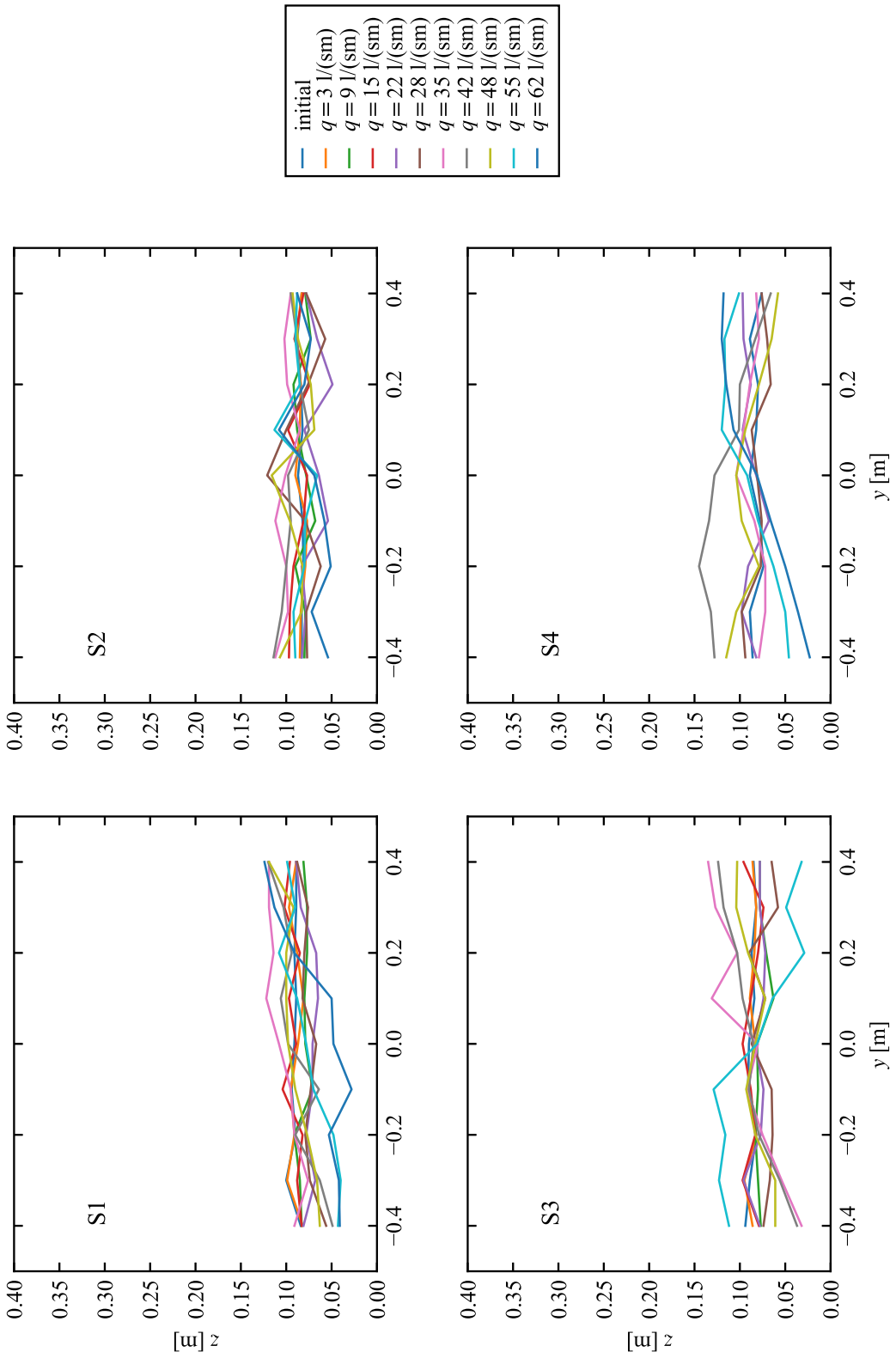

Figure C.6: Cross profiles at $x = 7.00$ m (ramp toe).

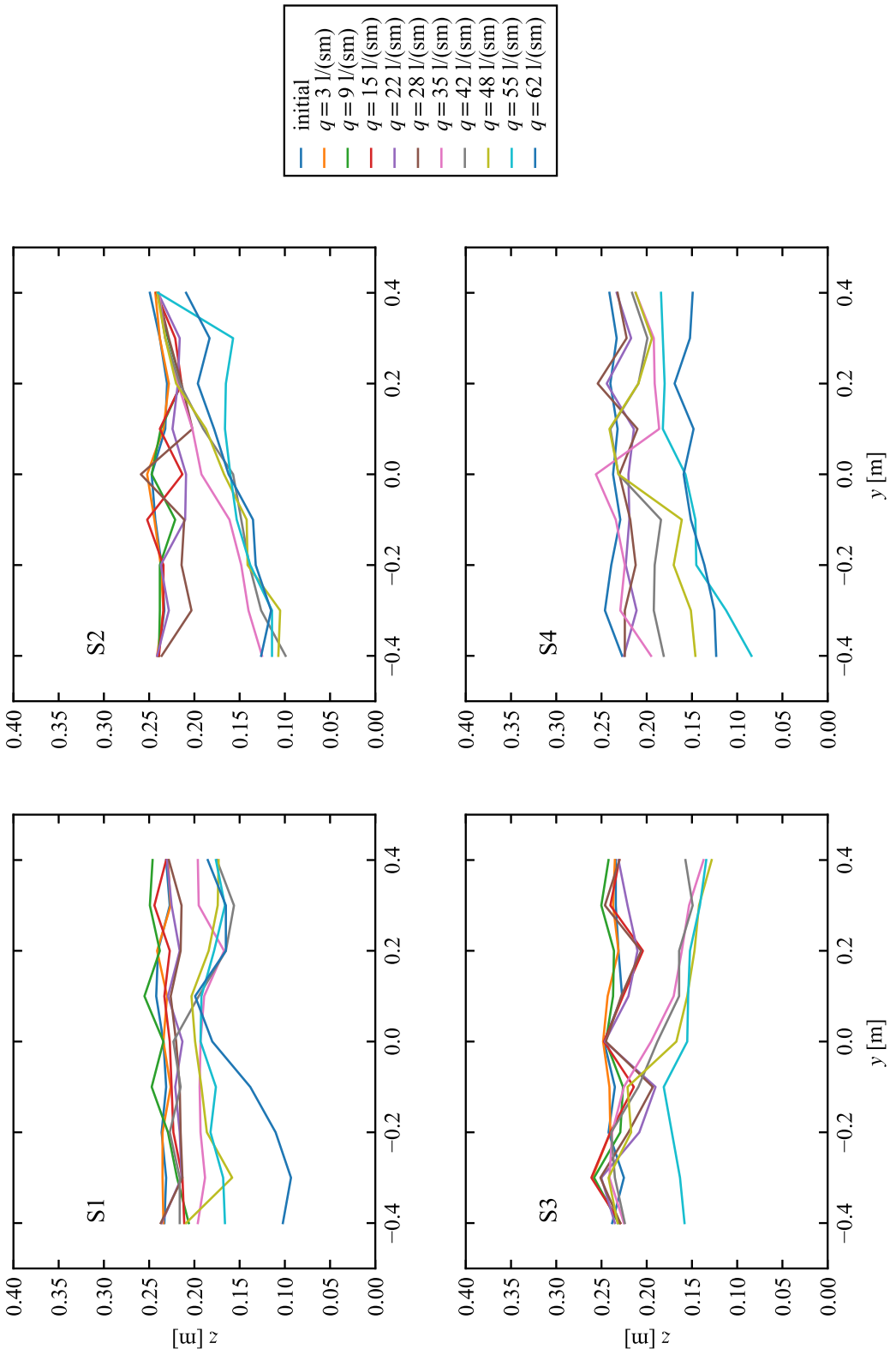

Figure C.7: Cross profiles at $x = 5.00$ m (middle of the ramp).

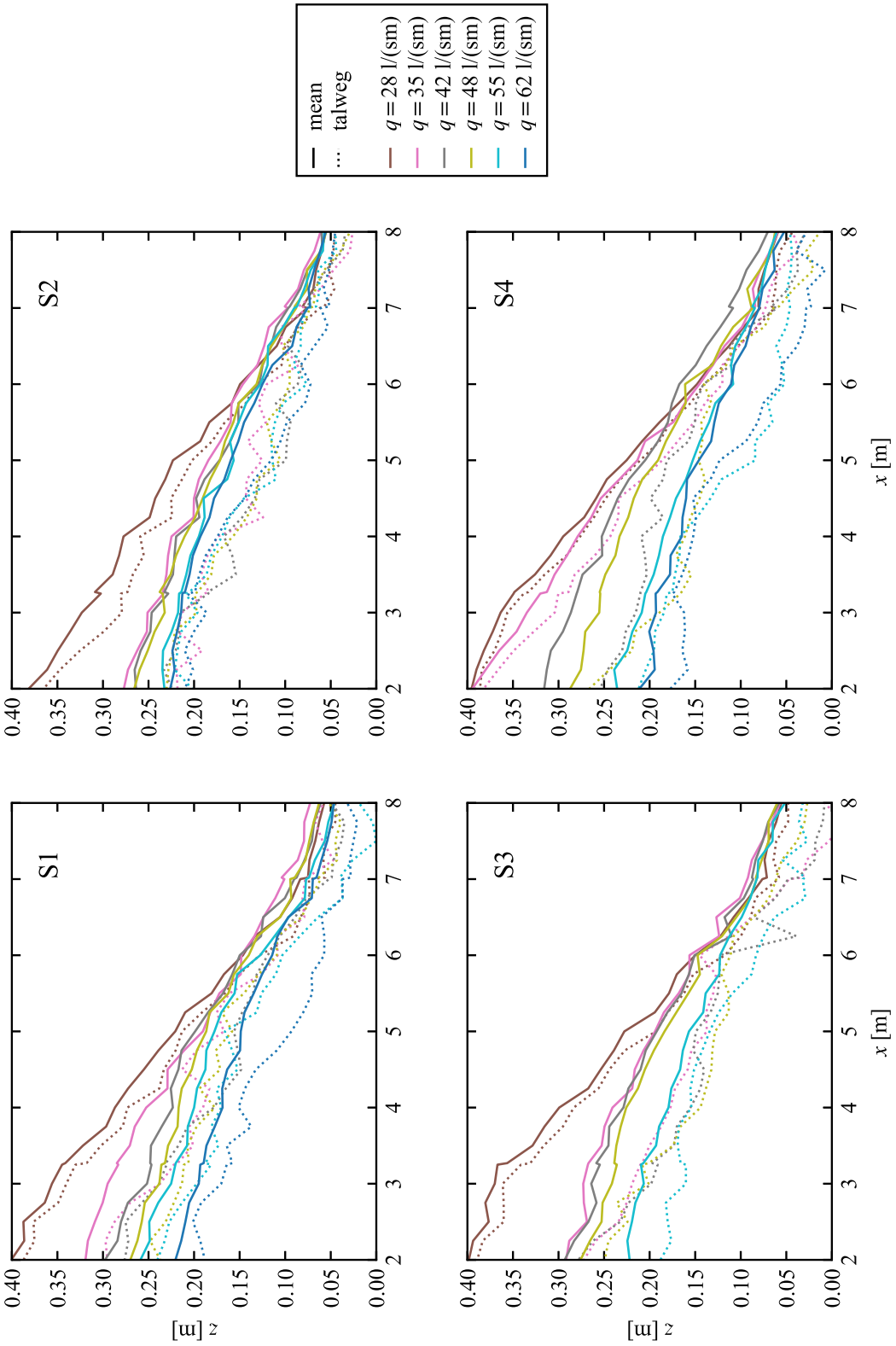

Figure C.8: Longitudinal profiles of mean bed elevation and of the talweg (minimum bed elevation).

D Flow depth

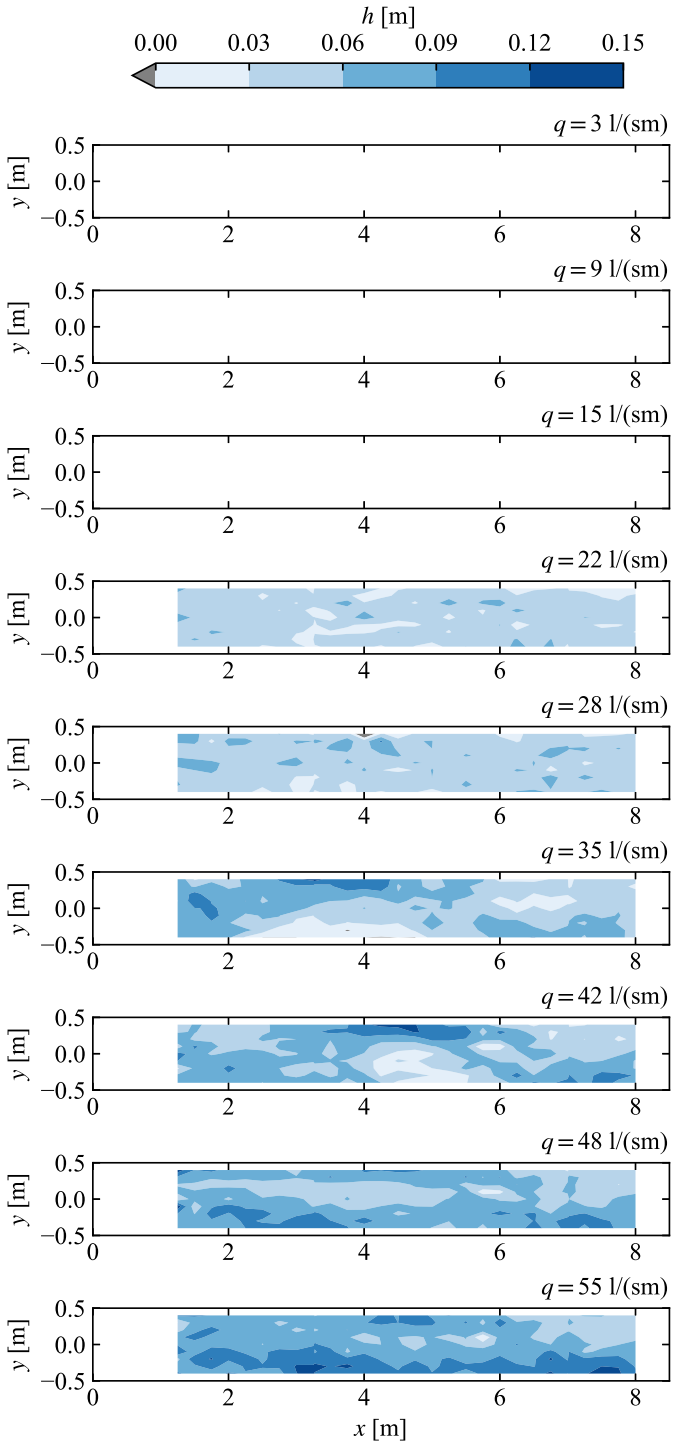

Figure D.1: Series S1: Flow depth h. The water level was not measured in the first three runs of the series. The water level of the last run (q = 62 l/(sm)) was not measured either, because the morphological equilibrium was not attained.

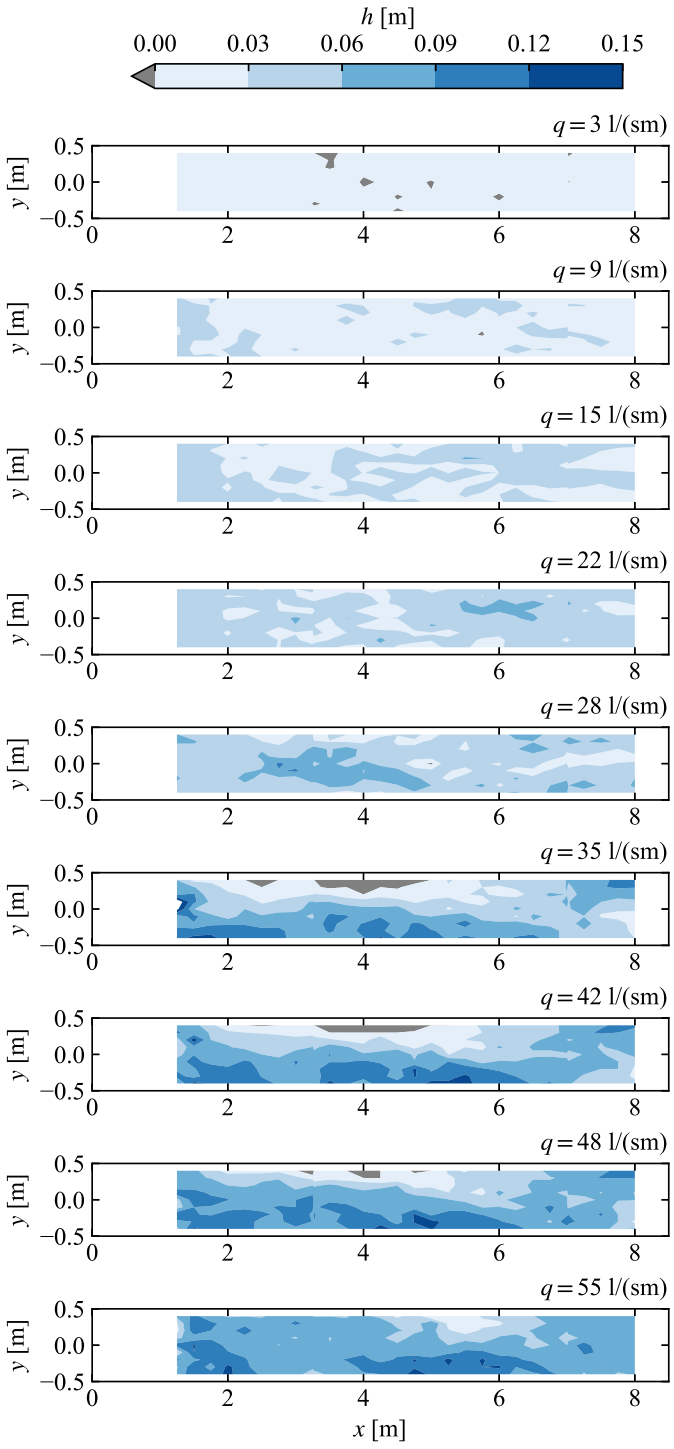

Figure D.2: Series S2: Flow depth h. The dry bed is indicated with the color grey. The water level of the last run (q = 62 l/(sm)) is not presented.

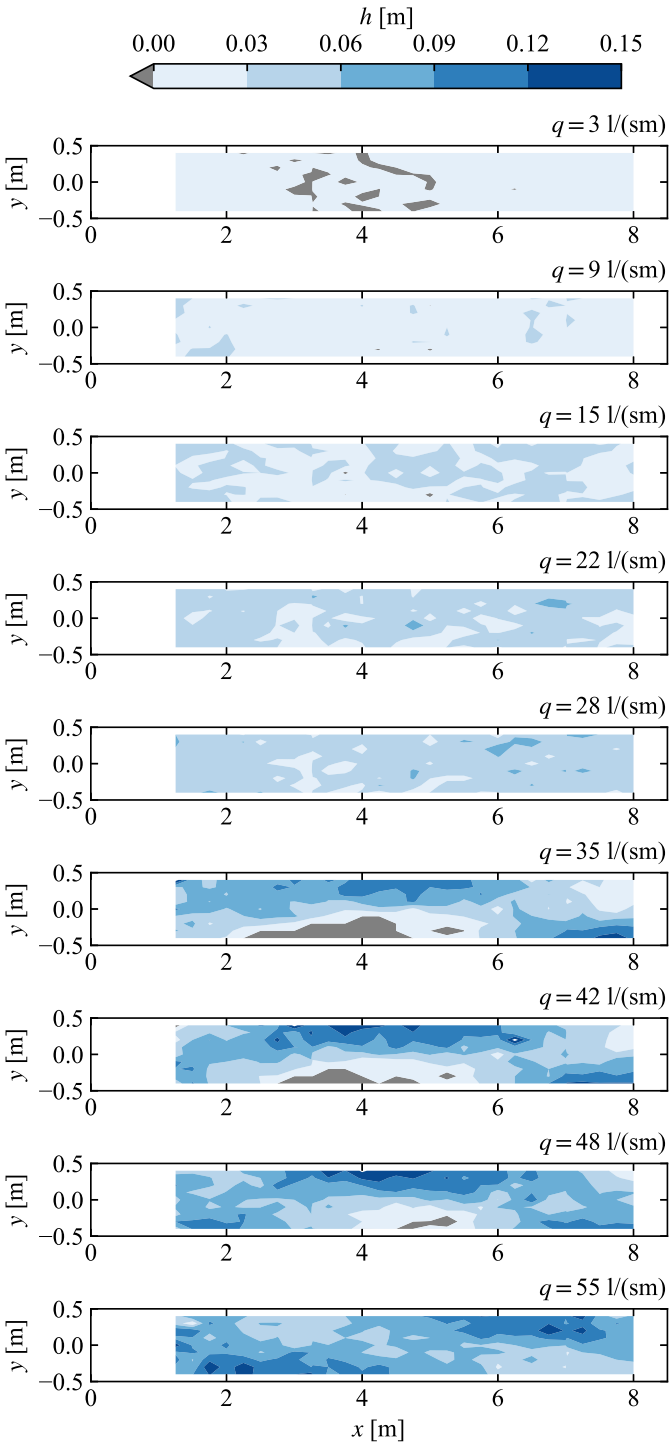

Figure D.3: Series S3: Flow depth h. The dry bed is indicated with the color grey. The last run was not executed because the maximum erosion of 15 cm at the inlet was reached in the previous run.

E Flow velocity

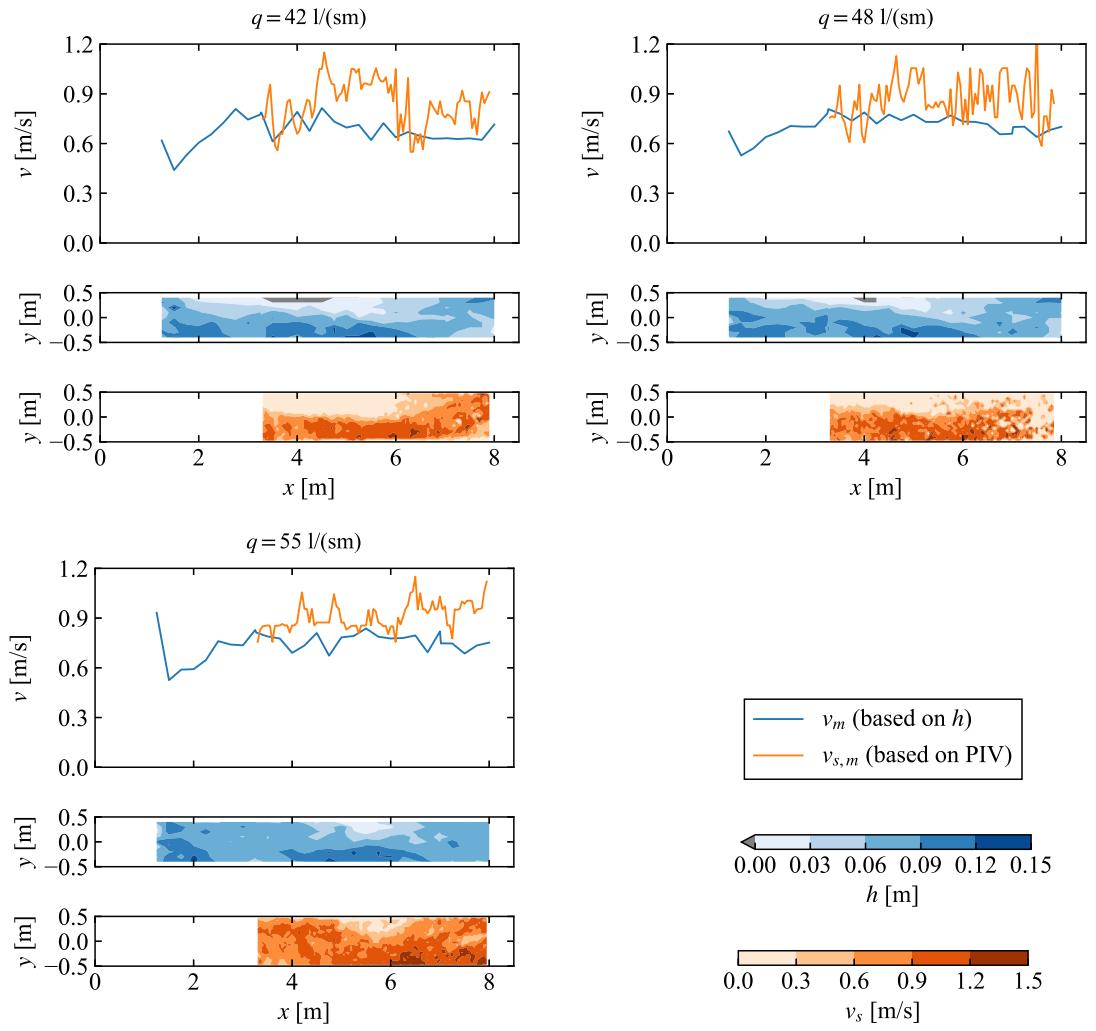

Figure E.1: Series S3: Flow depth h based on the manual survey and surface flow velocity v_s based on the PIV analysis. Based on these sizes the mean velocity v_m and the mean surface velocity $v_{s,m}$ was determined. PIV was not applied on runs with lower specific discharges.